Ollscoil na hÉireann, Corcaigh

National University of Ireland, Cork

Study of Acid Hydrolysis based Synthesis of Microcrystalline Cellulose

Thesis presented by

Conor O'Regan

for the degree of

Doctor of Philosophy

University College Cork

School of Chemistry

Head of School: Prof. Justin D. Holmes

Supervisors: Prof. Michael A. Morris, Prof. Justin D. Holmes

September 2018

Table of Contents

Declaration

This is to certify that the work I am submitting is my own and has not been submitted for another degree, either at University College Cork or elsewhere. All external references and sources are clearly acknowledged and identified within the contents. I have read and understood the regulations of University College Cork concerning plagiarism.

_____

Conor O'Regan

Abstract

A key tenet of the industrial manufacturing process of microcrystalline cellulose (MCC) is the assumption of equivalency between approved pulps, despite the natural variation in these materials. Alkali solubility, X-ray photo-spectroscopy, X-ray Diffraction and Scanning Electron Microscopy analyses of four pulps from different wood sources and delignification processes found significant differences in cellulose composition, crystallinity and morphology. Application of thermogravimetric data to three thermal decomposition kinetic models allowed for calculation of kinetic and subsequent thermodynamic parameters. Pulps delignified via an acid-sulphite process had higher activation energies when compared with the Kraft pulps (irrespective of wood source), which was correlated to higher degree of crystallinity for these pulps. Furthermore, the frequency factor for the hardwood acid-sulphite pulp was unexpectedly significantly higher than all other pulps, linking morphological characteristics to pulp degradation kinetics not given in the current literature.

Two samples of microcrystalline cellulose (Avicel® PH102 grade) produced from different starting pulps (hard and softwood) were selected for investigation. Analyses revealed that the MCC powder products showed no significant differences despite variances found in the starting pulps. For instance, the degree of polymerisation of the softwood pulp was significantly higher than the hardwood pulp. The MCC products were surprisingly found to have lower crystallinity compared to the pulps, suggesting hydrolysis of both amorphous and crystalline regions. Kinetic degradation parameters indicated lower activation energy and frequency factor for the MCC samples correlating with lower crystallinity. Importantly, there were no significant differences between the kinetic parameters of the two MCC products, indicating that differences in pulp were diminished during the MCC production hydrolysis step.

A pulp sample used in the industrial MCC process was selected for an acid hydrolysis study. Degree of polymerisation reduction curves were generated for various temperature and acid concentration conditions and differences in reaction rate and equilibrium degree of polymerisation point were observed; with increasing temperature having a greater effect on both the rate and equilibrium point when compared with increasing acid concentration impact. Scanning electron microscopy and particle size distribution analyses surprisingly showed that large quantities of material remained physically intact during the early hydrolysis stages even though the degree of polymerisation reduction was at its fastest rate, an observation not given in the current literature and significant in terms of control of the reaction industrially. Furthermore, it was observed that samples continued to reduce in both particle size and degree

of crystallinity throughout the degree of polymerisation equilibrium range, giving an important opportunity for identification of an optimum reaction end-point based on these parameters; such an end-point signal is not currently utilised in the industrial production of MCC and offers highly significant potential benefits to the commercial process.

Hydrolysis experiments were carried out on two pulp samples produced from different wood sources and delignification processes. Degree of polymerisation reduction curves were generated and Ekenstam plots used to determine the hydrolysis reaction rates. The hardwood acid-sulphite pulp was found to have a higher reaction rate compared to the softwood Kraft pulp. Kinetic parameters revealed that the hardwood pulp had a higher activation energy but also a significantly higher frequency factor, attributed to previously identified differences in crystallinity and morphology respectively. A modified version of the industry standard equation for determining hydrolysis intensity was proposed, which for the first time quantitatively accommodated differences in pulp crystallinity and morphology by inclusion of corrected activation energy and frequency factor terms, offering significant improvement in industrial reaction control.

Silicified microcrystalline cellulose (SMCC) has advantages over conventional MCC in the application of pharmaceutical tableting processes, such as improved tablet strength, retention of compressibility after wet granulation, and superior flow characteristics. Production of SMCC is achieved by addition of approximately 2% by weight of fumed silica to the MCC dispersion prior to the drying phase. Control of the silica addition in a continuous process is challenging, and in-process quality control measurement of silica content by sulphated ash method is time consuming; there is no rapid method given in the current literature. Consequently, deviations from the silica content of the SMCC dried product may not be known until hours after the material has been produced, and only then can corrective action be taken to adjust the production process. Fourier Transform - Infra Red spectroscopy studies of both SMCC and standard MCC material indicate that the silica peak at 808 cm^{-1} is not present in the MCC spectrum. Calibration curves were generated based on the area of this peak for samples of two grades of SMCC and compared against the sulphated ash results. No statistical difference was observed between the two methods. A new rapid method for determination of silica in SMCC products was, as a result, proposed, offering highly significant processing advantages industrially.

Acknowledgements

Firstly, I would like to acknowledge DuPont Nutrition and Health for their funding and support of my PhD study. I was fortunate to be able to carry out my doctorate research as an integral part of my employment at the Cork site within the Manufacturing Technology Group, and very much look forward to seeing the benefits of this study implemented in the coming months and years.

I would like to express my sincere gratitude to my supervisor Prof. Mick Morris, AMBER and Trinity College, Dublin, for his continuous support, guidance and immense knowledge throughout the time spent researching and writing this thesis. I would also like to acknowledge and thank Prof. Justin Holmes, Head of School of Chemistry, University College, Cork, and my PhD assessment committee: Dr Simon Lawrence and Dr Dave Ottway for their knowledgeable advice and support.

In addition, I would especially like to thank my manager at DuPont, Mr Brian Walsh, who fully supported and engaged in the research objectives and afforded me the time and resources to enable me to successfully complete my PhD in parallel with my working goals. I'd also like to express my gratitude to Mr Pat Comerford and Mr Greg Wilkins for their support and assistance at DuPont, Cork.

Finally, a sincere thanks to my wife Margaret, my daughters Bridget, Elizabeth and Catherine, my parents Kay and Christopher, and family and friends for their unwavering encouragement throughout these busy years spent dedicated to completing my PhD.

~~~~~~~~~~~~~~~~~~~~~~~~

"Things which we see are not by themselves what we see ... It remains completely unknown to us what the objects may be by themselves and apart from the receptivity of our senses. We know nothing but our manner of perceiving them."

Immanuel Kant, Critique of Pure Reason

"Ineluctable modality of the visible: at least that if no more, thought through my eyes."

James Joyce, Ulysses
~~~~~~~~~~~~~~~~~~~~~~~~

Glossary of Terms

α-cellulose	Long chained crystalline cellulose
β-cellulose	Short chained degraded cellulose
γ-cellulose	Amorphous and Hemicellulose
Acid-Sulphite Process	Pulp production process (delignification and bleaching)
Cuen	Cupriethylenediamene
DP	Degree of polymerisation
FT-IR	Fourier transform infrared (spectroscopy)
Kraft Process	Pulp production process (delignification and bleaching)
LODP	Level off degree of polymerisation
MCC	Microcrystalline cellulose
Pulp	Delignified and bleached cellulose
P1	Pulp of Northern Softwood (Black Spruce) origin, delignified via Acid-Sulphite process followed by oxidative elemental chlorine free bleaching. (Pulp provided courtesy of DuPont Nutrition and Health, Cork.)
P2	Pulp of Hardwood (Eucalyptus) origin, delignified via Acid-Sulphite process followed by oxidative elemental chlorine free bleaching. (Pulp provided courtesy of DuPont Nutrition and Health, Cork.)
P3	Pulp of Southern Softwood (Loblolly Pine) origin, delignified via Kraft process followed by oxidative elemental chlorine free bleaching. (Pulp provided courtesy of DuPont Nutrition and Health, Cork.)
P4	Pulp of Southern Softwood (Loblolly Pine) origin, delignified via Kraft process followed by oxidative elemental chlorine free bleaching. (Pulp provided courtesy of DuPont Nutrition and Health, Cork.)
R_{10}	Portion of pulp insoluble in 10% sodium hydroxide solution – comparable with α-cellulose
S_{10}	Portion of pulp soluble in 10% sodium hydroxide solution
S_{18}	Portion of pulp soluble in 18% sodium hydroxide solution – comparable with β-cellulose
$S_{10} - S_{18}$	Comparable with γ-cellulose
SEM	Scanning electron microscopy
SMCC	Silicified microcrystalline cellulose
TEM	Transmission electron microscopy
TGA	Thermogravimetric analysis
XPS	X-ray photoelectron spectroscopy
XRD	X-ray diffraction

Chapter 1

Introduction

1. Introduction

1.1 Cellulose

Cellulose, the most abundant natural biopolymer on Earth, is one of the most important organic compounds produced in the biosphere (Klemm, 2005). Utilised by mankind over millennia for clothing and building materials, its relatively short regeneration time ensures that the ever-increasing demands of today's consumerist world for biocompatible and environmentally friendly materials and products is still satisfied, with global annual fabrication of cellulose products estimated to be 7.5 x 10^{10} tons (Trache et al., 2016).

The word 'cellulose', used as a term in relation to the major constituent of wood, was first coined in 1839 in Paris by the Académie des Sciences who defined it as "… a compound which fills the cells and which makes up the substance of the wood itself" (Cameron, 2000). Today cellulose can be defined as macromolecule consisting of a nonbranched chain of variable length of 1-4-linked β-D-anhydroglucopyranose units as shown below (Klemm et al., 1998):

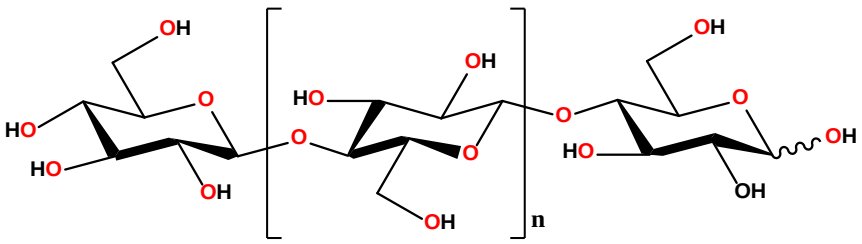

Figure 1. Cellulose Structure

Cellulose is known to exist in four different allomorphs (assigned a Roman numeral from I to IV) which differ in unit cell dimensions and chain polarity (Mittal et al., 2011). The natural form of cellulose is assigned as cellulose I which consists of I_α (triclinic form) and the more common I_β (monoclinic two-chain arrangement) (Zugenmaier, 2008). Cellulose I can be converted to the

cellulose II form by mercerization or regeneration. Cellulose III can be prepared from either cellulose I or II by treatment with anhydrous liquid ammonia or organic amines (Ciolacu, 2014). Samples of cellulose forms I, II, and III are known to always contain some amorphous content and (unless dried thoroughly) some water content. The fourth crystalline form, cellulose IV, is generated by heating of cellulose III (Goldberg et al., 1997). The allomorphs of cellulose have been studied comprehensively with additional information found in the literature: (Goldberg et al., 1997; O'Sullivan, 1997; Perez et al., 2005; Zugenmaier, 2008).

It can be seen in **Figure 1** above that the 1-4 β linkage results in alternating orientation of the glucopyranose units which allows for intramolecular hydrogen bonding. Additionally, intermolecular hydrogen bonding with neighbouring parallel chains is also thought to occur. **Figure 2** below shows the most probable hydrogen bonding within allomorphs I and II (Kroon-Batenburg et al., 1986).

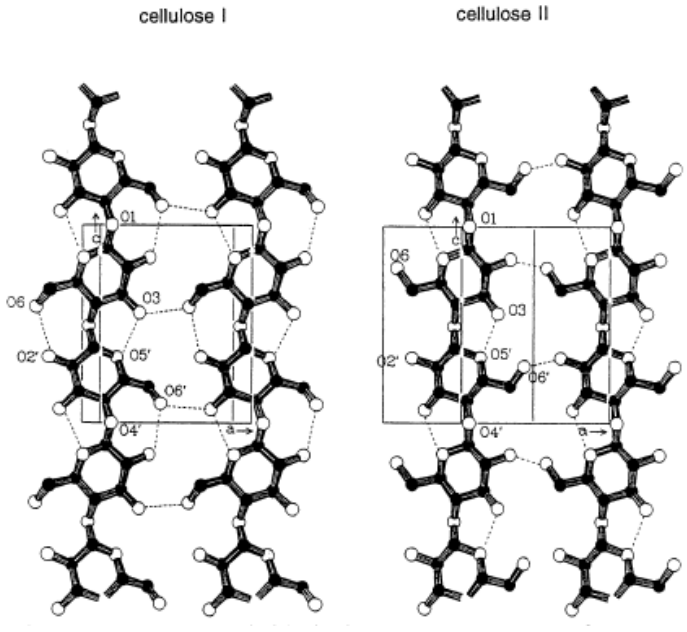

Figure 2. Hydrogen bond patterns for selected allomorphs of cellulose (Kroon-Batenburg et al., 1986), image reproduced with permission.

Hydrogen bonding is of particular importance for applications of the microcrystalline form of cellulose (MCC). During direct compression tableting with MCC as the major excipient, the formation of hydrogen bonds account almost exclusively for the strength and cohesiveness of compacts, even under low compression forces (Thoorens et al., 2014). Additional information on hydrogen bonding of MCC in relation to pharmaceutical tableting applications may be found in the literature (Carlin, 2008; Kása et al., 2009; Patel et al., 2006; Tho and Bauer-Brandl, 2011).

In natural cellulose, linear cellulose chains align to form crystalline and semi-crystalline microfibrils which are integrated with hemicelluloses and lignin of various compositions. (Kalia et al., 2011).

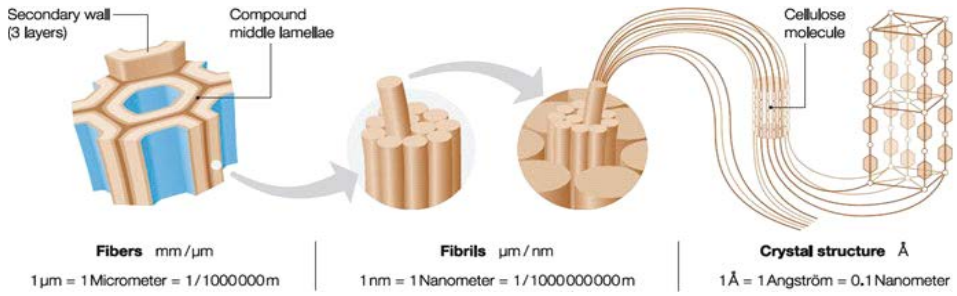

Figure 3. Arrangement of microfibrils and cellulose in the plant cell wall (Zimmermann et al., 2004), image reproduced with permission.

These microfibrils typically have a diameter of 10 to 30 nm and when grouped together are the primary constituent of the fibre cell walls. Single plant fibres are typically 1 to 50 mm in length and 10 to 50 µm in diameter (Kalia et al., 2011). **Figure 3** shows the arrangement of cellulose molecules, microfibrils and fibres in the plant cell wall. Depending on the plant / wood source, the chemical and morphological characteristics of the cellulose material can vary significantly and these variances form the basis for this current study.

Native cellulose is polydisperse, having large ranges of chain length. The degree of polymerization (DP) of cellulose can also vary largely depending on the source (Wertz et al., 2010). **Table 1** below gives typical DP ranges of various cellulose materials (Klemm et al., 1998):

Table 1. Typical DP ranges of selected celluloses

Material	**Range of DP**
Native Cotton	up to 12000
Scoured and bleached cotton linters	800 – 1800
Wood pulp (dissolving pulp)	600 – 1200
Man-made cellulose filaments and fibres	250 – 500
Cellulose powders (prepared by partial hydrolysis and mechanical disintegration)	100 – 200

1.2 Cellulose Derivatives

In the 1830's and 1840's industrial growth led to large scale generation of cellulose based products, with the first syntheses of cellulose derivatives being studied and developed (Vienken et al., 1999). Applications were focused initially on cellulose acetate fibres for clothing, home furnishings and upholstery. Use of cellulose derivatives quickly expanded in to areas such as health care (in 1846 it was discovered that nitrocellulose dissolved in organic solvents produces collodion which was subsequently used for wound dressing in the Crimean War) with the development of high absorbance surgical products, membrane filtration and diagnostic tests such as pregnancy test kits. Use of methyl cellulose grew in applications such as packaging material for products like toothpaste, detergent powders and rat poison. The viscosity adjustment properties of methyl and

ethyl cellulose, and carboxymethyl and hydroxypropal cellulose were developed as thickening agents in various food and cosmetic applications. Advances in photography led to George Eastman developing celluloid film coated with photographic emulsion for use in its Kodak still camera and subsequent imaging techniques.

1.2.1 Nitrocellulose, Cellophane, Cellulose Acetate

French chemists Henri Braconnot and Jean-Jaques Pelouze (working separately) discovered that combining nitric acid with wood fibres or starch produced an explosive material (Vienken et al., 1999). Following on shortly from this work, German-Swiss chemist Christian Friedrich Schönbein developed the first widely repeated preparation of the explosive material in Basel in 1846 and the resultant nitrocellulose product became commonly known as ‘gun-cotton’, later to be used in combination with nitro-glycerine by Alfred Nobel in the preparation of dynamite (Vienken et al., 1999). Schönbein’s preparation of nitrocellulose is based on the nitration of cellulose as follows:

$$C_6H_{10}O_5\ (s) + 3NO_2^+\ (aq) \rightarrow C_6H_7(NO_2)_3O_5\ (s) + 3H^+\ (aq) \qquad (1)$$

To generate the nitronium ion Schönbein used sulphuric acid to first protonate the nitric acid to a nitroxonium ion as follows:

$$H_2SO_4 + HNO_3 \leftrightarrow HSO_4^- + H_2NO_3 \qquad (2)$$

with the unstable nitroxonium ion readily decomposing to the nitronium ion:

$$H_2NO_3 \leftrightarrow NO_2^+ + H_2O \qquad (3)$$

In the early 20th century a type of regenerated cellulose was mass produced in Europe in clear sheet form commonly known as ‘cellophane’ which was quickly exploited as versatile packaging material for various foods. Large quantities of cellophane were exported to the United States for

sweet wrapping, leading the DuPont company to build the first US based cellophane manufacturing plant. Subsequent development of the material by DuPont, particularly in the application of nitrocellulose lacquer to cellophane which enhanced its waterproof properties, resulted in large sales and significant increase in profitability for the company (Hounshell & Kenly Smith, 1988; Winkler 1935).

Another important cellulose derivative developed around this time was an ester of cellulose called cellulose acetate. It is biodegradable, non-toxic, low cost, and has a very low flammability so use of this material is extremely widespread (with additional information in the following literature: Buchanan et al., 1993; Gaan et al., 2011; Sun Lu et al., 2013). Cellulose acetate is produced industrially in a two-step process of acetylation followed by hydrolysis; cellulose is reacted with acetic acid and acetic anhydride (in excess) in the presence of a sulphuric acid catalyst (Candidoa & Goncalves, 2016).

1.3 Microcrystalline Cellulose

Microcrystalline cellulose (MCC) is a purified and partially depolymerized form of cellulose; with pharmacopoeial MCC being defined by a DP of less than 350 glucose units (Thoorens et al., 2014). Initially developed by Batista in the late 1950's whilst working for 'American Viscose Corporation' (later acquired by FMC Corporation), MCC was first intended as a non-calorific filling agent for foodstuffs and branded in the market as Avicel®. In fact, MCC was heavily promoted as the "Food That Isn't Food" according to Life Magazine in 1961, which referred to it as forming "a miraculous gel" (Roller and Jones, 1996). However, as FMC Corporation became more familiar with the material, its excellent compaction properties became noticed, and the corporation recognised its potential for use in pharmaceutical tableting applications as an effective excipient.

In comparison to the established excipients at the time, such as lactose for example, MCC's dry binding properties more than exceeded the industry requirements and rapidly became the preferred binder for direct compression tableting (Bolhuis and Armstrong, 2006). Furthermore, MCC is self-disintegrating (Ferrari et al., 1996) and offers advantages in requiring less lubrication during tableting due to its low coefficient of friction and also due to its very low residual die wall pressure. Further information regarding MCC's tableting properties can be found in the literature (Saigal et al., 2009; Hwang and Peck, 2001; Petal et al., 2006).

MCC is prepared industrially by firstly obtaining purified α-cellulose (I_β allomorph) via delignification and bleaching of native cellulose (a process known as pulping) from various hardwood and softwood tree sources.

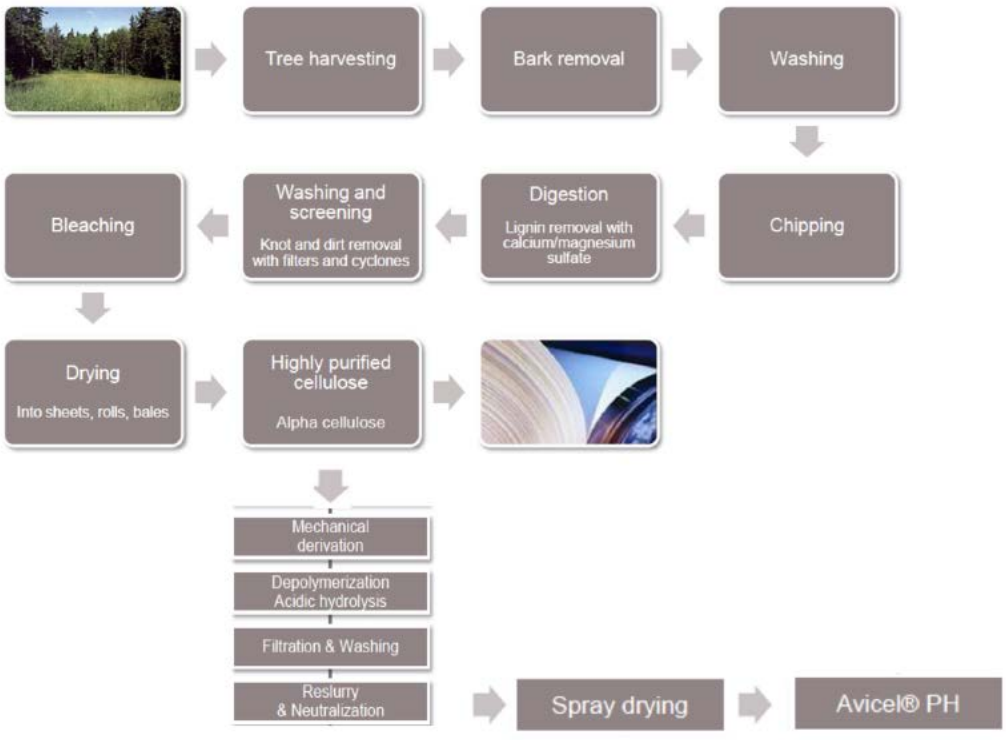

Figure 4. Schematic overview of MCC production process (Avicel® PH). Reproduced with permission from DuPont Nutrition and Health.

Subsequent controlled hydrolysis of the delignified pulp with mineral acid reduces the hemicellulose and amorphous content further, and reduces the degree of polymerization to the desired level (Fonteyne et al., 2015). A schematic overview of the production of MCC (Avicel® PH) is given above in **Figure 4**.

In addition to its use in foodstuffs and as a tablet excipient, MCC is commonly found in cosmetics as a texturiser, thickener or stabiliser. When combined with carboxymethyl cellulose (CMC), MCC and CMC colloidal mixtures are commonly used in various food and pharmaceutical applications for homogenisation and stabilisation functions.

1.3.1 Pulping Process

The objective of the pulping process is to increase the α-cellulose content (explanation of α, β, γ cellulose terminology is detailed below) by removal of lignin and reduction of hemicellulose content of natural lignocellulosic material (usually tree sources). The purified cellulose is then dried and distributed to MCC producers (or cellulose derivative producers) in the form of large pulp rolls for further processing.

Cellulose pulps are generally produced by one of two pulping processes: The acid-sulphite process or the Kraft process (Wang et al., 2014). At a high level both processes follow similar main processing steps of digestion, washing, and bleaching. **Figure 5** (reproduced with permission from 'GP Cellulose LLC') gives a schematic overview of the typical steps used in the cellulose pulping process.

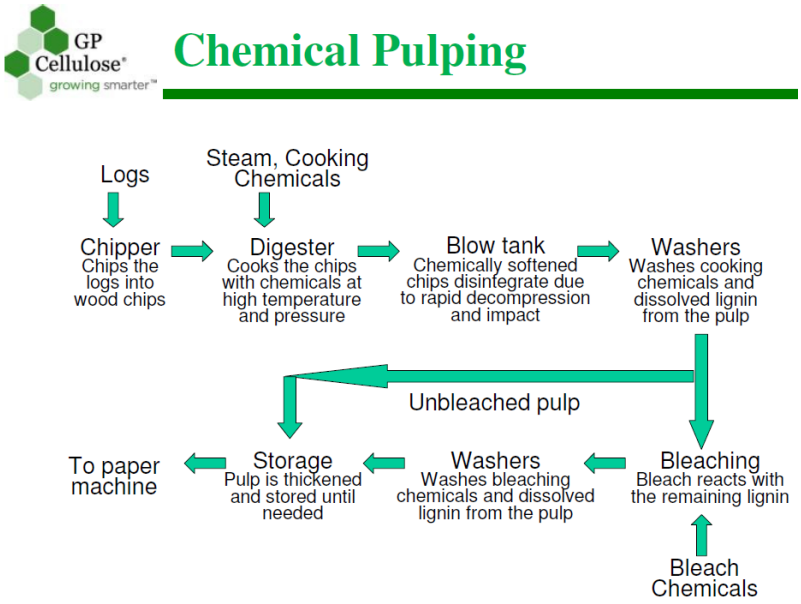

Figure 5. Chemical Pulping Process schematic overview (courtesy of GP Cellulose LLC).

The acid-sulphite digestion process uses different concentrations of aqueous solution of sulphur dioxide (SO_2) in the presence of either the sulphite ion (SO_3^{2-}) or the bisulphite ion (HSO_3^-) (Rueda et al., 2015) with the reaction proceeding in a low pH range of 1.2 to 1.5 and at high temperature (up to 160°C) (Casey, 1990). The following general reactions are implemented in the Acid-Sulphite digestion step (Hua et al., 2018):

$$R_1\text{-O-}R_2 + H^+ \rightarrow R_1^+ + R_2OH \quad (4)$$

$$R_1^+ + HSO_3^- \rightarrow R_1\text{-}SO_3\text{-H (soluble)} \quad (5)$$

As the sulphonate salt is soluble in water, if enough sulphonate groups are attached to a lignin molecule, the lignin will also become soluble and can subsequently be removed by a simple filtration separation process.

In contrast, the Kraft delignification process is an alkaline digestion method using sodium hydroxide (NaOH) and sodium sulphide (Na_2S) as the main reaction agents. The sulphide ion

reacts with the lignin by nucleophilic substitution resulting in scission of the lignin ether bonds (Sjöström, 1993) and, therefore, the lignin is not solubilised per the acid-sulphite process, but rather fragmented to a lower molecular weight to facilitate separation by washout (Aro and Fatehi, 2017). The following reactions summarise the general process (Hu et al., 2018):

$$O\text{-}R_1\text{-}O\text{-}R_2 + OH^- \rightarrow O{=}R_1OR_2 \quad (6)$$

$$O{=}R_1OR_2 + HS^- \rightarrow O\text{-}R_1S + R_2ONa \text{ (fragmented)} \quad (7)$$

Advantages and disadvantages become apparent when comparing both pulping processes. In recent times, the Kraft process has dominated the pulping industry primarily due to the ability to add a recovery step to enable regeneration of the starting reagents and a reduction in processing cost (Sixta, 2006). The acid-sulphite process however has an advantage in that the pulp is easier to bleach to full brightness (Sixta et al., 2013; Smook, 2002).

The cellulose content of commercial pulps is the primary quality factor of interest to purchasing companies. Historically, due to natural cellulose having large variances in make-up (particularly in chain length polydispersity, amorphous / paracrystalline content, and hemicellulose content) an α, β, γ terminology was developed to allow for classification of cellulosic material in pulp to three groups. Alpha-cellulose (α-cellulose) can be defined as the relatively pure and undegraded cellulose found in pulp, β-cellulose indicates shorter chain degraded cellulose content, while γ cellulose indicates short chain amorphous content usually consisting of hemicelluloses (ASTM D1696-96, 2001).

The α, β, and γ contents of pulp are typically approximated by testing their solubility in sodium hydroxide solutions (Wilson et al., 1952; Ohlsson, 1952). A 10% sodium hydroxide solution

possesses maximum dissolving power and will dissolve both degraded cellulose and hemicellulose content (Tappi, 2000). The portion of cellulose pulp that is insoluble in 10% sodium hydroxide can be designated as the 'R_{10}' number and generally corresponds to the α-cellulose content (ASTM D1696-96, 2001). The soluble portion of pulp in the 10% sodium hydroxide solution is designated as the 'S_{10}' number (it follows that $S_{10} = 100 - R_{10}$) and contains the short chain degraded cellulose and hemicellulose contents which can be correlated with the β and γ classification respectively. To determine the β / γ split, solubility tests in 18% sodium hydroxide can be used, with the 'S_{18}' number being the soluble portion and generally corresponding to the hemicellulose or γ content. The short chained degraded cellulose, or β content, is therefore, obtained by $S_{10} - S_{18}$ (Jahan, 2007). Pulp suppliers generally indicate the R_{10} number of lots supplied (approximating the α-cellulose content), however the S_{18} number and hence the breakdown between β and γ contents is generally not given.

The typical content of pulp as received by MCC manufacturers as raw material is given in **Table 2** below (courtesy of DuPont, Cork).

Table 2. Typical pulp contents as received by MCC manufacturers

R10 (~α-cellulose) %	**Lignin %**	**Ca ppm**	**Fe ppm**	**Cu ppm**	**SiO_2 ppm**
92.8	<1.5	44.0	2.7	0.1	11.0

1.3.2 MCC production from Pulp

Following generation of the cellulose pulps as described above, further refinement takes place to produce commercial grades of MCC. This process was first developed by Batista and Smith in

1955 (Thoorens et al., 2014) and in 1964 FMC Corporation marketed MCC as Avicel® PH for the pharmaceutical industry as an ingredient for direct compression tableting (Albers et al., 2006).

The industrial production of MCC from pulp is centred around the acid hydrolysis reaction to reduce the degree of polymerization to the required target. The hydrolysis reaction proceeds rapidly initially with an exponential reduction in cellulose chain length, expressed as degree of polymerisation (DP). As the reaction continues the rate of reduction in DP slows and reaches what is known as the level-off degree of polymerisation (LODP), i.e. when some sort of equilibrium is reached, with the LODP typically in the range of 180 to 210 for hardwood pulps and 210 to 250 for softwood pulps (Doelker, 1993). **Figure 6** below shows a typical reduction in DP to LODP over time for a softwood pulp.

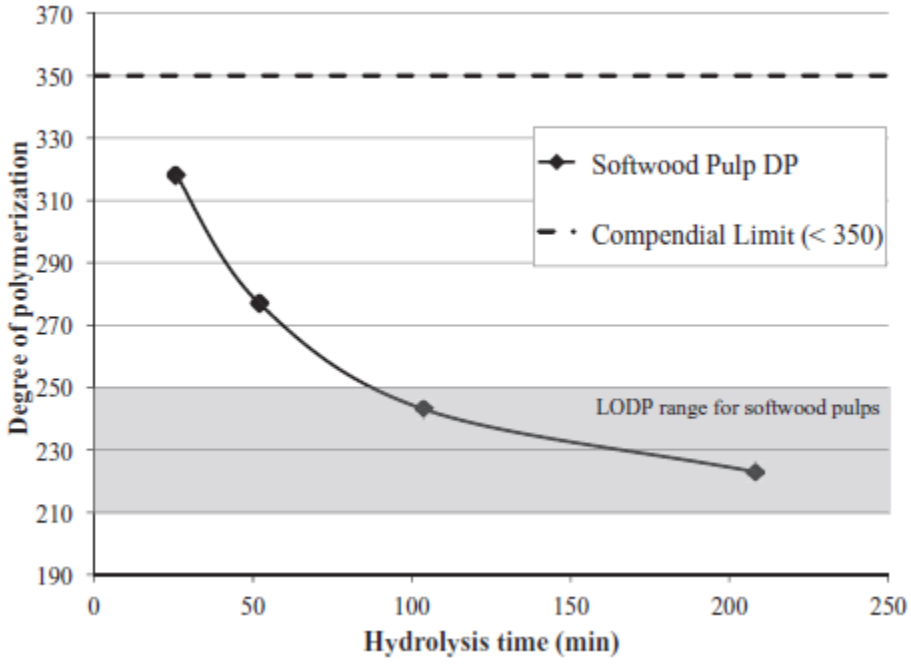

Figure 6. DP reduction (reproduced with permission from DuPont Nutrition and Health)

Full hydrolysis of pure α-cellulose to glucose is known to require high temperature (~374°C) and high pressure (~22 MPa) and/or use of a catalyst to achieve effective reaction rates (Kupiainan et al., 2014). However, during MCC production the objective is only partial depolymerization of the cellulose, and reaction with dilute mineral acids at lower temperatures (typically <150°C) allows for the amorphous content of the material to be readily hydrolysed releasing microcrystallites of MCC which remain in solid phase (Karim et al., 2014). Subsequent filtration, neutralization, and drying (typically spray drying) steps with control of moisture, particle size and bulk density parameters produce the various commercial grades of MCC.

The 'fringed fibrillar model' (developed in the 1960's) is the most widely accepted model for the arrangement of cellulose (Hearle, 1963; Frey-Wyssling and Muhlethaler, 1965) and describes cellulosic material of consisting of crystalline regions (of ordered cellulose chains) arranged in microfibrils interconnected by disordered areas. It was then later suggested (Gurnagul et al. 1992) that the mechanism for hydrolysis by dilute mineral acids involved the scission of these fibrils at the amorphous 'kinks' (structure represented below in **Figure 7**) with the crystalline regions only experiencing very slow rate hydrolysis. The LODP is, therefore, reached when the fast hydrolysed amorphous 'kinks' are reacted, resulting mainly in cellulose microcrystals remaining (Palme et al., 2016). The crystallinity of cellulose is, therefore, considered to be an important factor in the hydrolysis reaction kinetics. Tightly packed crystalline α-cellulose greatly inhibits the access of reactants (and catalysts if used) to the β-1,4-glycosidic bonds. In contrast, the rate of hydrolysis of the amorphous regions (including any hemicelluloses present) is known to be much higher (Zhao et al., 2006).

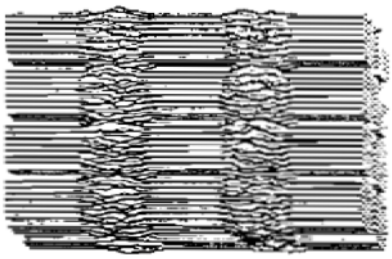

Figure 7. Representation of cellulose formation with crystalline regions connected by amorphous 'kinks'.

The 'crystallinity index' of cellulose can be estimated by a number of methods, however X-ray diffraction (XRD) used in conjunction with Segal's equation (Segal et al., 1959) provides a good estimation commonly used in cellulose analysis:

$$CI = 100\ x\ \frac{I_{002} - I_{am}}{I_{002}} \qquad (8)$$

where CI is the crystallinity index, I_{002} is the intensity of the crystalline peak (002 relection) at around 22.6° 2θ, and I_{am} is the intensity of the amorphous peak around 18° 2θ.

1.3.3 Acid Hydrolysis Reaction Mechanism

The reaction mechanism for acid hydrolysis of cellulose has been well studied (Fan et al., 1987, Tee et al., 2013; Nevell, 1976; Parikh, 1967; Szejtli, 1975) and generally proceeds by rapid protonation of the glycosidic oxygen followed by slower splitting of the glycosidic bond and the subsequent addition of a water molecule. A second pathway is also proposed whereby the cyclic oxygen is protonated (rather than the glycosidic oxygen), shifting the position of the carbonium cation formation for the scission of the glycosidic bond and water addition site. **Figure 8** describes both mechanisms.

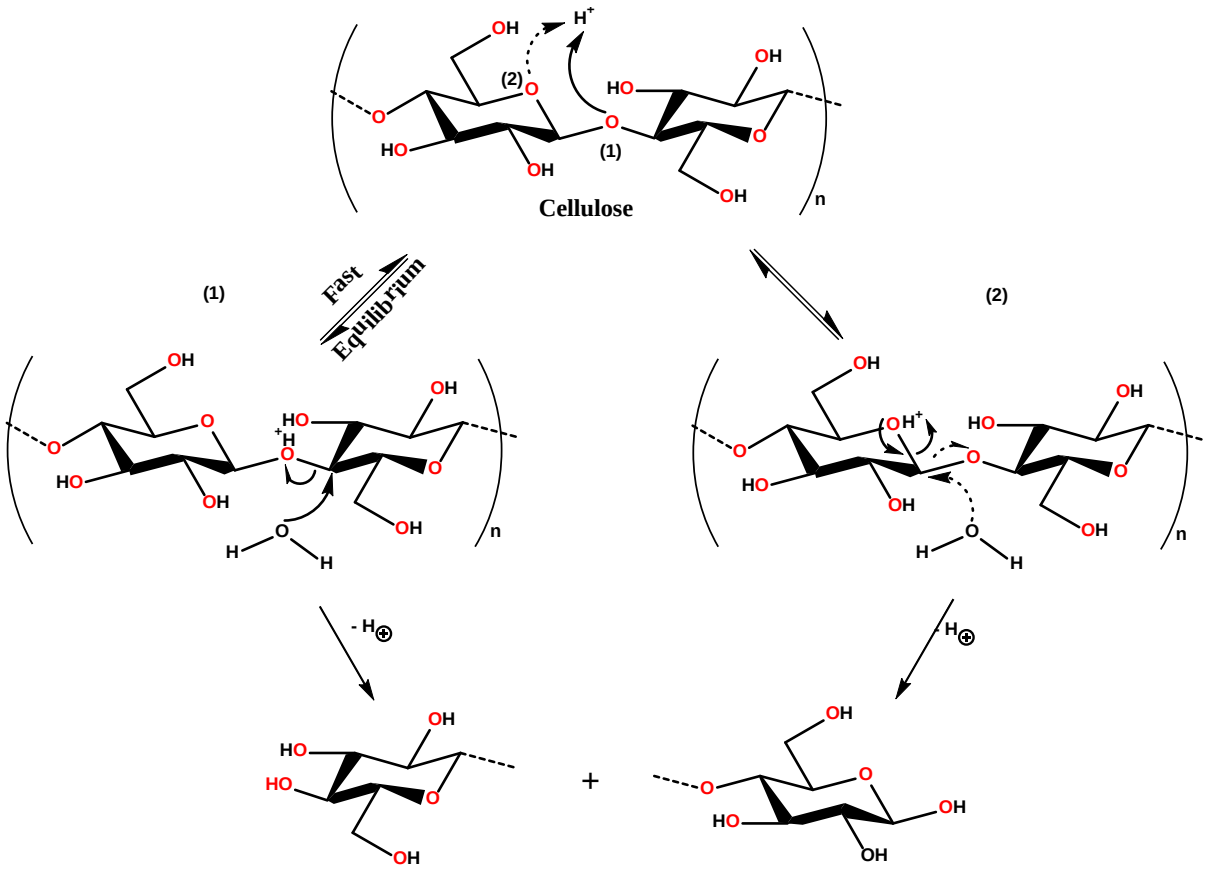

Figure 8. Reaction mechanisms for acid hydrolysis of cellulose

Additionally, it has been shown (Szejtli, 1975) that partial protonation of both oxygens (glycosidic and cyclic) can take place simultaneously. Identification of the course of the hydrolysis as being either type-1 or type-2 shown in **Figure 8** above may be possible based on the following suggested method (Whalley, 1959a; Whalley, 1959b). If the entropy of the reaction, ΔS^*, is negative, then the mechanism is most likely to be type-2, that is the mechanism proceeds via protonation of the cyclic oxygen. The probability of type-2 increases the more negative ΔS^* becomes. If ΔS^* is positive, then both type-1 and type-2 mechanisms are likely, with the probability of type-1 mechanism increasing as ΔS^* increases. This method is demonstrated experimentally in **Chapter 5** of this thesis during investigation of the hydrolysis of cellulose pulps from different origins.

1.3.4 Hydrolysis Kinetics

Kinetic parameters for the acid hydrolysis of cellulose can be calculated based on the change in DP of the cellulose as the reaction proceeds. The hydrolysis rate, *k*, is calculated based on the Ekenstam equation for a pseudo zero-order reaction as follows (Palme et al., 2016):

$$\frac{1}{DP_t} - \frac{1}{DP_0} = kt \tag{9}$$

where DP_t is the degree of polymerization at time t, DP_0 is the starting degree of polymerization, *k* is the hydrolysis rate, *t* is the hydrolysis time. DP can be determined experimentally from reactant samples via ASTM Method No. D1795-62 which relates measured intrinsic viscosity with DP. Plots of experimentally determined DPs versus time allow for calculation of the rate of hydrolysis, *k*.

Calvani et al. (2008) showed that the Ekenstam equation could be modified to describe a first order reaction, and it is found that when DP_0 is high, both pseudo zero-order and first order rate equations are equivalent. Using the Arrhenius Equation, *k* can be correlated with the activation energy, E_a, and temperature as follows:

$$k = Ae^{\left(\frac{-E_a}{RT}\right)} \tag{10}$$

where *A* is the frequency factor or pre-exponential, E_a is the activation energy, *R* is the ideal gas constant, and *T* is the hydrolysis temperature. It follows that the kinetic parameters calculated experimentally by this method can be further used to estimate thermodynamic properties of the reaction (such as enthalpy, entropy, and Gibbs Free Energy etc.).

Inclusion for acid concentration in the Arrhenius equation (Eqn 10 above) may be represented by a modified form of the equation and is shown in Eqn (11) (Zou et al., 1996):

$$k = A(a[H^+])e^{\left(\frac{-E_a}{RT}\right)} \quad (11)$$

where a is the coefficient of hydrogen ion effect, and $[H^+]$ is the hydrogen ion concentration. If the hydrolysis reaction of a given pulp type is carried out at different temperatures (but at the same acid concentration) and the hydrolysis rate k determined from Eqn (9) using measured DP values at various times as the reaction proceeds, then Arrhenius plots can be generated to determine the reaction activation energy E_a.

1.3.5 Effect of Variance in MCC Production Process

The effect of variance in the commercial MCC final product both on the pharmaceutical tableting process and on the end quality of pharmaceutical products has been extensively studied, with the following literature containing examples of such studies: Koo and Heng, 2001: Soh et al., 2008; Dumarey et al., 2011; Landin et al., 1992; Almay and Aburub, 2008. However, variance of raw material (pulp) effect in the MCC production process itself is less well understood. Given that the starting material in the overall process is wood sourced from various types of trees (hard wood / soft wood), grown in different global regions, experiencing different climates and harvesting times, and undergoing different delignification pulping processes, it is not surprising that management of both processing and final product variance represents a significant challenge for industrial MCC producers.

Control of the acid hydrolysis step in the partial depolymerisation of cellulose pulp to MCC is critical to the processing capability of the subsequent downstream steps leading to the final commercial product. It is found that quenching the hydrolysis reaction mixture too early leads to

a more viscous slurry which is difficult to process and results in inefficient spray drying at lower than target solids percentages. Conversely, quenching the reaction too late leads to the product being broken down more than desired, which is difficult to filter and risks the final product failing quality control due to high bulk density. There is, therefore, a 'sweet-spot' on the DP reduction curve (see **Figure 6** above) where the balance between under and over reacting is sought.

1.3.6 Alpha Cellulose Mass Balance

Figure 9 details a block diagram of a typical MCC industrial production process. The figure outlines the basic high-level production steps and gives a mass balance of the cellulose as it proceeds from pulp through to packaged product. It can be seen that for a packaged MCC product rate of 1,600 kg/hr, a pulp input rate of 1,780 kg/hr is required; the yield in this case is, therefore, 89.9% which is typically achieved.

The losses can be explained as follows: the 1780 kg/hr pulp contains ~91.2% α-cellulose (therefore 1,637 kg/hr) and ~8.8% β and γ cellulose (143 kg/hr). The hydrolysis reaction reduces the DP of the α-cellulose but the material remains in the solid state, whereas the hydrolysed β and γ cellulose become soluble in water. On filtration, the 143 kg/hr β and γ cellulose is captured in the filtrate, and also ~25 kg/hr α-cellulose solids is typically lost in the filtrate due to imperfect filtering. The filtrate is collected and ~20 kg of the α-cellulose is recaptured and returned to the quench tank. The remaining 5 kg α-cellulose is lost to the waste water treatment plant.

The α-cellulose filter cake solids (1,632 kg/hr) is sent to the spray dryer (following re-slurry with water) and the slurry is dried as MCC product. The product is screened to remove over-size particles, reducing the final packaged MCC product rate to 1,600 kg/hr.

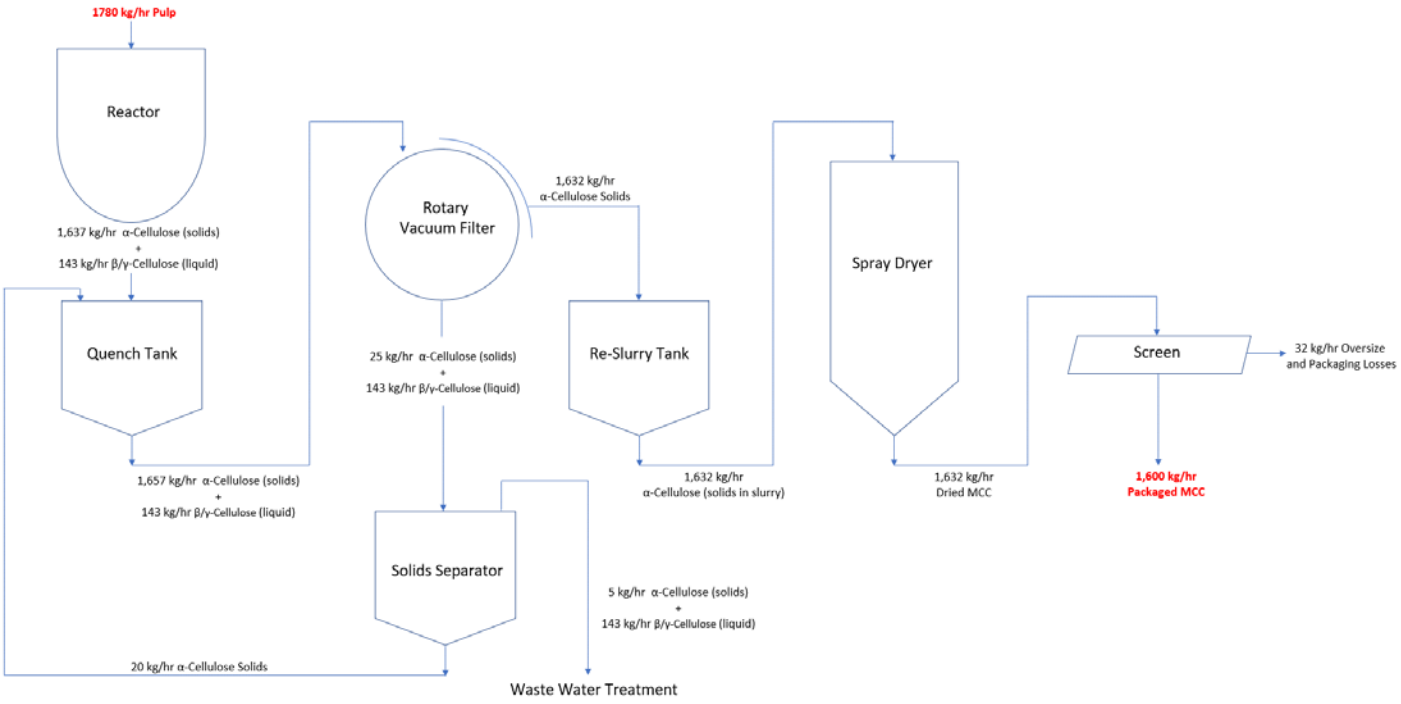

Figure 9. Industrial MCC Process α-cellulose mass balance

1.4 Silicified Microcrystalline Cellulose

Silicified microcrystalline cellulose (SMCC) is an MCC product with approximately 2% by weight of pharmaceutical grade fumed silica added. The addition of silica is known to increase the effective surface area of the MCC material, leading to tablets produced with SMCC by wet granulation having much higher tensile strength than tablets produced with standard grade MCC (Sherwood & Becker, 1998). The silica is added to the MCC slurry upstream of the drying process and the mixture is then dried as SMCC product (rather than creating a simple physical powder blend of MCC and silica post drying stage). Sherwood and Becker (1998) also showed that simple physical mixtures of MCC and silica did not achieve the same tableting tensile strength as the co-processed SMCC products.

Tight control of the addition rate of fumed silica to the MCC process is needed to achieve the specification weight percentage of silica in the end product. Therefore, it is required to carry out frequent sampling of the material during production to quantitatively test for silica content. The USP-NF (United States Pharmacopeia - National Formulary) monograph for SMCC products dictate that silica content is verified by a 'Residue on Ignition' procedure. This procedure is based on the ignition of an SMCC sample in the presence of sulphuric acid and measurement of the portion not volatized. The test requires high temperatures (~ 600°C) and is time consuming with results typically recorded around three hours from start of test. Development of a simpler and faster complimentary guidance test for silica is, therefore, of significant interest to SMCC producers.

1.5 Research Objectives and Thesis Structure

The research objectives of this doctorate project concern increasing the understanding of the chemistry of the industrial process of microcrystalline production. The research was focused particularly on the acid hydrolysis step and understanding how parameters of the starting pulp (such as crystallinity or morphology) affected the kinetics of the reaction. In addition, it was endeavoured to understand how the hydrolysis reaction conditions (such as acid concentration and reaction temperature) impacted product quality such as alpha cellulose yield. Given that there is currently no clearly defined optimum quench point for the reaction industrially, it was also desirable to explore and propose measurable parameters such as particle size distribution for such a function. Finally, the development of a rapid analytical test method for determination of silica content in silicified microcrystalline cellulose products was sought.

Chapters 2 to 6 (inclusive) of this thesis detail the research carried out over the course of the doctorate project and are presented in the format of academic research papers. However, due to

commercial sensitivity DuPont have requested that the papers remain unsubmitted for publication at this stage.

The paper given in **Chapter 2** outlines the characterisation of four commercial pulps which are used in the MCC production process to produce equivalent grade products. The pulps selected differ in source by both wood type and by delignification process. In particular, the pulps are examined for differences in composition, surface chemistry, crystallinity, morphology and thermal degradation. Three different kinetic models are applied to the thermal degradation analysis and the kinetic and thermodynamic parameters for the thermal degradation of each pulp are calculated. Differences in the kinetic and thermodynamic parameters of the pulps are correlated with the pulp characteristics explored.

Chapter 3 investigates two commercial pulp types and MCC powder products each produced exclusively from these pulps. The two MCC powder products are deemed equivalent by the MCC producer and sold commercially as such. Both the pulps and the MCC products are characterised again for differences in composition, surface chemistry, crystallinity, morphology, and thermal degradation. Kinetic modelling is used to determine thermal degradation kinetic parameters and subsequently thermodynamic parameters are also estimated. Differences in the final MCC powder products are assessed and correlated with pulp characteristics.

A study of the acid hydrolysis reaction of a selected commercial pulp is given in the paper comprising **Chapter 4**. The pulp is hydrolysed to various end points at two different temperatures and two different acid concentrations. Intrinsic viscosity and DP's are measured at each of the quench points for all conditions, DP reduction curves (similar to **Figure 6** above) are generated and differences in LODP are investigated. Particle size distribution, surface morphology analysis and crystallinity assessment (via XRD) are carried out to determine changes as the hydrolysis

reaction proceeds. Furthermore, differences in particle size distribution and crystallinity at LODP for the various reaction conditions are also investigated.

The research paper given in **Chapter 5** details a hydrolysis study of two commercial pulps from different sources. The pulps are individually hydrolysed at three different temperatures keeping a consistent starting acid concentration for all reactions. Intrinsic viscosity / DP measurements are carried out and DP reduction curves are generated. Hydrolysis rates *k* are calculated for each reaction temperature using Ekenstam's rate equation and Arrhenius plots are then used to determine activation energy values, E_a, for the acid hydrolysis reactions of both selected pulps. Thermodynamic parameters for the reaction of both pulps are also estimated and differences assessed against pulp characteristics. The likely reaction mechanism is identified from calculated entropy values. Finally, a hydrolysis intensity equation is developed to correlate hydrolysis reaction conditions at bench scale with reaction conditions at full industrial plant scale.

Chapter 6 comprises of a study of the development of a spectroscopic method for the determination of silica content (percentage by weight) in selected silicified microcrystalline cellulose grades. Samples of SMCC50 and SMCC90 grades containing various levels of silica content were obtained and their silica content determined by 'residue on ignition' (ROI) testing. FTIR analysis of the samples was carried out and a peak unique to silica (relative to non-silicified MCC) was identified and a calibration successfully developed. The ROI method is time consuming (up to three hours) and is carried out at high temperatures and high acid concentration, therefore development of an accurate FTIR method is of use to MCC producers.

A summary outlining the relevance of the research carried out for this doctorate project is given in **Chapter 7**.

References

Albers, J., Knop, K., Kleinebudde, P. (2006). Brand-to-brand and batch-to-batch uniformity of microcrystalline cellulose in direct tableting with a pneumo-hydraulic tablet press. Pharm. Ind. 68, 1420–1428.

Almaya, A., Aburub, A. (2008). Effect of particle size on compaction of materials with different deformation mechanisms with and without lubricants. AAPS PharmSciTech 9, 414–418.

Aro, T., Fatehi, P. (2017). Production and application of lignosulfonates and sulfonated lignin. ChemSusChem 10, 1861–1877.

Bolhuis, G.K., Armstrong, N.A. (2006). Excipients for direct compaction—an update. Pharm. Dev. Technol. 11, 111–124.

Buchanan, C. M., Gardner, R. M., & Komarek, R. J. (1993). Aerobic biodegradation of cellulose acetate. Journal of Applied Polymer Science, 47, 1709–1719.

Calvini, P., Gorassini, A., Merlani, A. (2008). On the kinetics of cellulose degradation: looking beyond the pseudo zero order rate equation. Cellulose, 15(2):193–203.

Cameron, J.S. (2000). Nephrology Dialysis Transplantation, Volume 15, Issue 7, Pages 1086–1091.

Candidoa, R.G., Goncalves, A.R. (2016). Synthesis of cellulose acetate and carboxymethylcellulose fromsugarcane straw, Carbohydrate Polymers 152 (2016) 679–686 2016.

Carlin, B. (2008). Direct compression and the role of filler-binders. In: Augsburger, L.L., Hoag, S.W., Hoag, S.W. (Eds.), Pharmaceutical Dosage Forms: Tablets. Informa, pp. 173–216.

Casey, J. P. (1990). Production of sulfite pulp, Producción de pulpa al sulfito. Pulpa y Papel: Química y Tecnología Química (Vol. I) Mexico: Limusa. ISBN: 968-18-2061-4.

Ciolacu, D., Chiriac, A.I., Javier Pastor, F.I., Kokol, V. (2014). The influence of supramolecular structure of cellulose allomorphs on the interactions with cellulose-binding domain, CBD3b from Paenibacillus barcinonensis, Bioresource Technology 157 14–21.

Doelker, E. (1993). Comparative compaction properties of various microcrystalline cellulose types and generic products. Drug Dev. Ind. Pharm. 19, 2399–2471.

Dumarey, M., Wikstrom, H., Fransson, M., Sparen, A., Tajarobi, P., Josefson, M., Trygg, J. (2011). Combining experimental design and orthogonal projections to latent structures to study the influence of microcrystalline cellulose properties on roll compaction. Int. J. Pharm. 416, 110–119.

Fan, L., Gharpuray, M.M., Lee, H., (1987). Cellulose Hydrolysis, ISBN-13: 978-3-642-72577-7, DOl: 10.1007/978-3-642-72575-3 Springer-Verlag.

Fonteyne, M., Correia, A., De Plecker, S., Vercruysse, J., Ili, I., Zhou, Q., Vervaet, C., Remon, J.P., Onofre, F., Bulone, V., De Beer, T. (2015). Impact of microcrystalline cellulose material attributes: A case study on continuous twin screw granulation, International Journal of Pharmaceutics 478 705–717.

Frey-Wyssling A., and Muhlethaler K. (1965). Ultrastructural Plant Cytology with an Introduction to Molecular Biology. Elsevier, Amsterdam, The Netherlands.

Gaan, S., Maucalire, L., Rupper, P., Salimova, V., Tran, T.-T., & Heuberger, M. (2011). Thermal degradation of cellulose acetate in presence of bis-phosphoramidates, Journal of Analytical and Applied Pyrolysis, 90, 33–41.

Goldberg, R.N., Schliesser, J., Mittal, A., Decker, S.R., Santos, A.F., Freitas, V.L.S., Urbas, A., Lang, B.E., Heiss, C., Ribeiro da Silva, M.D.M.C., Woodfield, B.F., Katahira, R., Wang, W., Johnson, D.K. (2015). A thermodynamic investigation of the cellulose allomorphs:

Cellulose(am), cellulose Ib(cr), cellulose II(cr), and cellulose III(cr), J. Chem. Thermodynamics 81 184–226.

Gurnagul N. (1992). The effect of cellulose degradation on the strength of wood pulp fibres. Nordic Pulp Pap. Res. J. 7(3): 152.

Hearle J.W.S. (1963). The fine structure of fibres and crystalline polymers. J. Appl. Polym. Sci. 7: 1175–1192.

Hua, J., Zhanga, Q., Lee, D.J. (2018). Kraft lignin biorefinery: A perspective, Bioresource Technology 247 (2018) 1181–1183.

Hounshell, D. A., Kenly Smith, J. (1988). Science and Corporate Strategy: Du Pont R&D, 1902–1980. Cambridge University Press. p. 170. ISBN 0-521-32767-9.

Hwang, R.-C., Peck, G.R. (2001). A systemactic evaluation of the compression and tablet characteristics of various types of microcrystalline cellulose. Pharm. Technol. 112–132.

Jahan, M.S., Al-Maruf, A, Quaiyyum, M.A. (2007). Bangladesh Journal of Scientific and Industrial Research. 1952, 01/2007; 42(4):425-434.

Kalia, S., Kaith, B.S., Kaur, I. (2011). Cellulose Fibers: Bio- and Nano-Polymer Composites Green Chemistry and Technology ISBN 978-3-642-17369-1 e-ISBN 978-3-642-17370-7 DOI 10.1007/978-3-642-17370-7 Springer, Heidelberg, Dordrecht, London, New York Library of Congress Control Number: 2011924897.

Karim, M.Z., Zaman Chowdhury, Z., Abd Hamid, S.B., Eaqub Ali, M. (2014). Statistical Optimization for Acid Hydrolysis of Microcrystalline Cellulose and Its Physiochemical Characterization by Using Metal Ion Catalyst, Materials 7, 6982-6999; doi:10.3390/ma7106982.

Kása, P., Bajdik, J., Zsigmond, Z., Pintye-Hódi, K. (2009). Study of the compaction behaviour and compressibility of binary mixtures of some pharmaceutical excipients during direct compression. Chem. Eng. Process. Process Intensifica-tion 48, 859–863.

Klemm, D., Philipp, B., Heinze, T., Heinze, U., Wagenknecht, W. (1998) Comprehensive Cellulose Chemistry; Volume 1: Fundamentals and Analytical Methods WILEY-VCH Verlag GmbH, Weinheim ISBN: 3-527-29413-9.

Klemm, D., Heublein, B., Fink, H.P., Bohn, A. (2005). Angew. Chem. Int. Ed. 44 3358–3393.

Koo, O.M.Y., Heng, P.W.S. (2001). The influence of microcrystalline cellulose grade on shape and shape distributions of pellets produced by extrusion–spheronization. Chem. Pharm. Bull. 49, 1383–1387.

Kroon-Batenburg, L.M.J., Kroon, J., Nordholt, M.G. (1986). Chain modulus and intramolecular hydrogen bonding in native and regenerated cellulose fibers, Polym. Commun. 27, 290-292.

Kupiainan, L., Ahola J., Tanskanen J. (2014). Kinetics of Formic Acid-catalysed Cellulose Hydrolysis. Bioresources 9(2), 2645-2658.

Landin, M., Vazquez, M.J., Souto, C., Concheiro, A., Gomezamoza, J.L., Martinezpacheco, R. (1992). Comparison of 2 varieties of microcrystalline cellulose as filler-binders. 1. Prednisone tablets. Drug Dev. Ind. Pharm. 18, 355–368.

Mittal, A., Katahira, R., Himmel, M.E., Johnson, D.K. (2011). Biotechnol. Biofuels 4, http://dx.doi.org/10.1186/1754-6834-4-41 (Article number 41).

Nevell, T.P., Upton, W.R. (1976), Carbohydrate Res 49:163

Ohlsson, K. E. (1952). The Alkali Solubility of Pulps. Svensk Papperstid, 55(10): 347.

O'Sullivan, A. (1997). Cellulose 4, 173–207.

Palme, A., Theliandera, H., Brelidb, H. (2016). Acid hydrolysis of cellulosic fibres: Comparison of bleached kraft pulp, dissolving pulps and cotton textile cellulose. Carbohydrate Polymers 136 1281–1287

Patel, S., Kaushal, A.M., Bansal, A.K. (2006). Compression physics in the formulation development of tablets. Crit. Rev. Ther. Drug Carrier Syst. 23, 1–65.

Parikh, R.S. (1967). Textile Res. J, ibid. 37:538

Perez, S., Mazeau, K., Dimitriu, S. (2005). Polysaccharides: Structural Diversity and Functional Versatility, Marcel Dekker, New York.

Roller, S., Jones, S.A. (1996). Handbook of Fat Replacers, CRC Press LLC, ISBN 0-8493-2512-9

Saigal, N., Baboota, S., Ahuja, A., Ali, J. (2009). Microcrystalline cellulose as a versatile excipient in drug research. J. Young Pharm. 1, 6–12.

Sherwood, B.E., Becker, J. (1998). A new class of high functionality excipients: silicified microcrystalline cellulose. Pharm. Technol. 22, 183–194.

Sixta, H. (2006). Handbook of pulp (Vol. 1) Germany: Wiley-VCH. ISBN: 3-527-30999-3.

Sixta, H., Iakovlev, M., Testova, L., Roselli, A., Hummel, M., Borrega, M. (2013). Novel concepts of dissolving pulp production. Cellulose, 20, 1547–1561.

Sjöström, E. (1993). Wood Chemistry: Fundamentals and Applications. Academic Press. ISBN 0-12-647480-X

Smook, G. A. (2002). Characteristics of pulp and wood pulp fibers. In Handbook for pulp & paper technologists. Angus Wilde Publication Inc. ISBN: 0-9694628-5-9.

Soh, J.L.P., Wang, F., Boersen, N., Pinal, R., Peck, G.E., Carvajal, M.T., Cheney, J., Valthorsson, H., Pazdan, J. (2008). Utility of multivariate analysis in modeling the effects of raw material

properties and operating parameters on granule and ribbon properties prepared in roller compaction. Drug Dev. Ind. Pharm. 34,1022–1035.

Sun, X., Lu, C., Zhang, W., Tian, D., & Zhang, X. (2013). Acetone-soluble celluloseacetate extracted from waste blended fabrics via ionic liquid catalyzedacetylation, Carbohydrate Polymers, 98, 405–411.

Szejt1i, J. (1975). Siiurehydrolyse glycosidischer Bindungen. VEB, Leipzig

Tappi, Alkali solubility of pulp, Tappi T235 OM- 60, (2000). Tappi Press, Atlanta.

Tee T.T., Sin, L.T., Gobinath, R., Bee, S.T., Hui. D., Rahmat, A.R. (2013). Investigation of nano-size montmorillonite on enhancing polyvinyl alcohol-starch blends prepared via solution cast approach. Compos Part B 47:238e47.

Tho, I., Bauer-Brandl, A. (2011). Quality by design (QbD) approaches for the compression step of tableting. Expert Opin. Drug Deliv. 8, 1631–1644.

Thoorens, G., Krier, F., Leclercq, B., Carlin, B., Evrard, B. (2014). Microcrystalline cellulose, a direct compression binder in a quality by design environment—A review, International Journal of Pharmaceutics 473 (2014) 64–72.

Trachea, D., Hazwan Hussinb, M., Tan Hui Chuinb, C., Sabarc, S., Nurul Fazitad, M.R., Taiwod, O.F.A., Hassand T.M., Mohamad Haafizd, M.K. (2016). Microcrystalline cellulose: Isolation, characterization and bio-composites application—A review, International Journal of Biological Macromolecules 93 (2016) 789–804.

Vienken J., Diamantoglu M., Henne W., Nederlof B. (1999). Artificial dialysis membranes: from concept to large scale production. Am J Nephrol, 19: 355–362.

Wang, H., Pang, B., Wu, K., Kong, F., Li, B., Mu, X. (2014) Two stages of treatments for upgrading bleached softwood paper grade pulp to dissolving pulp for viscose production. Biochem. Eng. J. 82, 183-187.

Wertz, J.L. Bédué, O., Mercier, J.P. (2010), Cellulose Science and Technology; EPFL Press: Lausanne, Switzerland, p. 21.

Whalley, E. (1959a). Can J Chern 37:788.

Whalley, E. (1959b,) Trans Faraday Soc 55:798.

Wilson, **K.**, Ringstrom, E., and Hedlund, I. (1952). The Alkali Solubility of Pulp, Svensk Papperstid. 55(2): 31

Winkler, J. K. (1935). The Dupont Dynasty. Baltimore, MD: Waverly Press, Inc. p. 271.

Zimmermann, T., Pohlerand, E., Geiger, T. (2004). Cellulose fibrils for polymer reinforcement. Adv Eng Mater 6, No. 9.

Zhao, H., Kwak, J. H., Wang, Y., Franz, J. A., White, J. M., & Holladay, J. E. (2006). Effects of crystallinity on dilute acid hydrolysis of cellulose by cellulose ball-milling study. Energy & Fuels, 20, 807–811.

Zou, X., Uesaka, T., Gurnagul, N. (1996). Prediction of paper permanence by accelerated aging I. Kinetic analysis of the aging process. Cell 3 (1), 243‑267.

Zugenmaier, P. (2008). Crystalline Cellulose and Cellulose Derivatives: Characterization and Structures, Springer-Verlag, Berlin-Heidelberg, pp. 101–174.

Chapter 2

Thermal Degradation Kinetics and Thermodynamics of Pulp: Effect of Source and Delignification Process

Thermal degradation kinetics and thermodynamics of pulp: effect of source and delignification process

Conor O'Regan[*a,b], Dipu Borah[c], John Anastasopoulos[c], John O'Connell[a], Justin D Holmes[a,c,d], and Michael A Morris[*c,d]

[a] Materials Chemistry, Department of Chemistry, University College Cork, Cork, Ireland,

[b] DuPont Nutrition and Health, Cork, Ireland

[c] AMBER, Trinity College Dublin, Dublin 2, Ireland,

[d] Tyndall National Institute, Lee Maltings, Prospect Row, Cork, Ireland,

*Corresponding author: Email: conor.o-regan@dupont.com (Conor O'Regan), morrism2@tcd.ie (Michael A Morris) Ph: +353 18963089

ABSTRACT

A key tenet of the industrial manufacturing process of microcrystalline cellulose (MCC) is the assumption of equivalency between approved pulps, despite the natural variation in these materials. Alkali solubility, X-ray photo-spectroscopy, X-ray Diffraction and Scanning Electron Microscopy analyses of four pulps from different wood sources and delignification processes found significant differences in cellulose composition, crystallinity and morphology. Application of thermogravimetric data to three thermal decomposition kinetic models allowed for calculation of kinetic and subsequent thermodynamic parameters. Pulps delignified via an acid-sulphite process had higher activation energies when compared with the Kraft pulps (irrespective of wood source), which was correlated to higher degree of crystallinity for these pulps. Furthermore, the frequency factor for the hardwood acid-sulphite pulp was unexpectedly significantly higher than all other pulps, linking morphological characteristics to pulp degradation kinetics not given in the current literature.

Keywords: Pulp; Characterization; Thermal degradation; Kinetics; Thermodynamics

1. Introduction

Speciality dissolving cellulose pulps are the primary raw material for commercially produced microcrystalline cellulose. Treatment of the speciality pulps with mineral acid allows for production of a purified and partially depolymerised microcrystalline cellulose powder that has wide applications in the pharmaceutical and food industries (**Brittain et al., 1993**). The dissolving pulps consist mainly of crystalline α-cellulose, a natural polysaccharide polymer made up of repeating (1-4)-β-D-glucopyranose units (**Krassig, 1985**) and some amorphous hemicellulose content which consists of branched polymers of various monosaccharides. In comparison to paper pulps, speciality dissolving pulps contain higher α-cellulose content (>90%), lower hemicellulose content (<4%) and trace extractives and minerals (**Ibarra et al., 2010**).

The pulps are generally produced from various wood types (both hard and soft) that have been delignified by either the acid-sulphite or the Kraft processes (**Wang et al., 2014**). Inter-lot and inter-manufacturer variances in commercially available dissolving pulp contribute to difficulties in the microcrystalline cellulose manufacturing process. The primary source of pulp variance is due to the pulp origin as cellulose is the most abundant natural polymer on earth with an annual biomass production of over 50 billion tons (**Carlin, 2008**). Factors such as wood type (hardwood or softwood), geographical origin, natural degree of polymerisation, degree of crystallinity, fibre morphology, hemicellulose make-up etc. contribute greatly to variances in dissolving pulps. Additionally, the process used in the manufacture of the pulp: acidic or alkaline, degree of degradation, bleaching sequence etc. can have a significant effect on pulp variability (**Landín et al., 1992**)

The thermal degradation of cellulose is complex and may involve many reactions (**Poletto et al., 2011**). Furthermore, degradation is known to take place at relatively low temperatures, with hemicellulose decomposition beginning at temperatures as low as 180°C (**Kim et al., 2006**). It is, therefore, important to understand the thermal stability of dissolving pulps and how this stability is affected by the pulp variances alluded to above. The objective of this study was to investigate the decomposition properties of commercially available dissolving cellulose pulps from various wood type origins and pulping processes and understand how kinetic and thermodynamic properties are affected accordingly.

Thermogravimetic analysis of selected dissolving cellulose pulps was carried out and the activation energy, frequency factor and subsequent rate constants were determined using the Coats

and Redfern integral method (**Coats and Redfern, 1964**), Freeman and Carroll differential method (**Freeman and Carroll, 1958**), and Horowitz and Metzger approximation method (**Horowitz and Metzger, 1963**). In addition, thermodynamic properties were determined. In support of the thermogravimetic analysis, the pulp characteristics were also assessed by elemental analysis, alkali solubility, FT-IR, Raman, XPS, XRD and SEM to corroborate variances observed.

2. Materials and Methods

2.1. *Materials*

Four speciality cellulose dissolving pulps were selected for study: (P1) Northern Softwood (Black Spruce) which had been delignified *via* the acid-sulphite process followed by oxidative elemental chlorine free (ECF) bleaching (**Hon and Shiraishi, 2000**), (P2) Hardwood (Eucalyptus) which had been delignified *via* the acid-sulphite process followed by oxidative ECF bleaching, (P3) Southern Softwood (Loblolly Pine) which had been delignified *via* the Kraft process followed by oxidative ECF bleaching, and (P4) A second Southern Softwood (Loblolly Pine) which had been delignified *via* the Kraft process followed by oxidative ECF bleaching. All pulps (P1 to P4) supplied courtesy of DuPont Nutrition and Health, Cork, Ireland.

2.2. *Elemental analysis of pulp*

The elemental analysis of the pulps is given in **Table 1**. Analysis of C, H and O (by difference) was performed on a Perkin Elmer 2400 Series II CHNS/O Analyzer. The four pulps show relatively similar C, H and O composition when compared to each other and marginally reduced carbon and increased oxygen when compared against theoretical composition of pure α-cellulose. Differences between the measured pulp composition and the theoretical pure α-cellulose are most likely due to amorphous hemicelluloses present in the pulps.

Table 1. Elemental analysis of selected pulp samples

Pulp	**Carbon %**	**Hydrogen %**	**Oxygen %**
P1	42.9	6.3	50.8
P2	42.8	6.2	51.0
P3	43.3	6.2	50.5
P4	43.2	6.2	50.6
α-cellulose ($C_6H_{10}O_5)_n$	44.4	6.2	49.4

2.3. *Alkali Solubility (S10 & S18)*

Alkali solubility at 10% NaOH (S10) and 18% NaOH (S18) was determined by the TAPPI 235-OM Standard Method of the Technical Association of the Pulp and Paper Industry (**Tappi, 2000**).

2.4. *Fourier transformed infrared (FTIR)*

An IR660, Varian Infrared Spectrophotometer in Attenuated Total Reflectance (ATR) mode was used to record FTIR spectra. The measurements were performed in the spectral range of 4000-500 cm^{-1}, with a resolution of 4 cm^{-1} and data averaged over 32 scans.

2.5. *Raman Spectroscopy*

Raman spectra were obtained using a HORIBA Jobin Yvon labRAM HR. The bench-top micro-Raman unit has an 800 mm focal length spectrometer giving it a resolution of < 1 cm^{-1}. Samples were excited with a Nd:YAG laser emitting at 532 nm. An objective lens of 100x was utilized and the signal was collected on a high resolution air-cooled CCD. The spectrometer was calibrated using a polished, non-oxidised silicon standard. The spectra were collected in the range 340 to 3200 cm^{-1} and the laser power was set at 100%. Spectra collection time was 30 s and 20 accumulations were taken for each sample. The samples analysed were pre-scanned to reduce auto-fluorescence and the spectra were subject to a second-order polynomial background subtraction, excluding the position of the specific peaks, to reduce the fluorescence background.

2.6. *Scanning Electron Microscopy (SEM)*

SEM images were obtained by a high resolution (< 1 nm) Field Emission Zeiss Ultra Plus-SEM with a Gemini® column operating at an accelerating voltage of 5 kV.

2.7. *X-Ray Photoelectron Spectroscopy (XPS)*

XPS was performed on Vacuum Science Workshop CLASS100 high performance hemispherical analyser using Al K_α (hν = 1486.6 eV) mono X-ray source. Spectra were obtained at a take-off angle of 15º. Samples were loaded into the vacuum chamber within 1 h after being prepared and were subjected to XPS analysis. Photoemission peak positions were corrected to a C 1s signal at a binding energy of 284.8 eV.

2.8. *X-Ray Diffraction (XRD)*

XRD spectra were recorded by a PANanalytical X'Pert PRO instrument with Ni-filtered Cu-Kα radiation (λ = 0.1542 nm) generated at 40 kV and 40 mA. The scanning was made through 2θ = 10° to 90°, and intensity data was recorded with a digital recorder. The crystallinity index (*CrI*) was calculated *via* **equation (1)**:

$$CrI = \frac{I002 - Iam}{Iam} \qquad \textbf{(1)}$$

where, I_{002} the maximum intensity of the peak corresponding to the plane in the sample with the Miller indices 002 at a 2θ angle of around 22.6°, and I_{am} is the intensity that corresponds to the non-crystalline peak at about 2θ = 18°.

The apparent crystallite size *t* was calculated using the Scherrer method as shown in **equation (2)**

$$T = \frac{K\,x\,\lambda}{\beta\,x\,cos\theta} \qquad \textbf{(2)}$$

where K is a constant of value 0.89; λ is the X-ray wavelength (0.1542 nm); β is the Full Width at Half Maximum (FWHM) of the 002 peak, and θ is the Bragg angle corresponding to the (002) plane.

2.9. *Thermogravimetric Analysis (TGA)*

TGA was carried out on Pyris 1 PerkinElmer thermogravimetric analyser. The pulps were prepared by cutting in to approximately 2 mm x 2 mm samples chips and oven dried at 70 °C for 24 hours. TGA was carried out on samples weighing around 10 mg over a temperature range from room temperature to 600 °C under nitrogen atmosphere with a flow rate of 50 ml min^{-1} and at heating rates of 5 °C min^{-1}, 10 °C min^{-1} and 20 °C min^{-1}.

3. Theory

3.1. *Coats and Redfern's Kinetics of Degradation*

The rate of decomposition of pulp under non-isothermal condition can be expressed as:

$$-\frac{dw}{dt} = kw \quad \textbf{(3)}$$

Where, w = weight of pulp; t = time and k = rate constant. Incorporation of Arrhenius equation, $k = Ae\left(-\frac{Ea}{RT}\right)$ and heating rate, $r = dT/dt$ into **equation (1)** and further rearrangement gives,

$$\frac{1}{w}\frac{dw}{dT} = \frac{A}{r}e\left(-\frac{Ea}{RT}\right) \quad \textbf{(4)}$$

Where, T = temperature; A = Arrhenius constant; r = heating rate; E_a = activation energy and R = gas constant.

The rate equation may also be expressed in terms of fractional conversion "α" and reaction order "n" as follows:

$$\alpha = \frac{wo-w}{wo-w\infty} \quad \textbf{(5)}$$

$$-\frac{d\alpha}{dt} = k\,(1-\alpha)^n \quad \textbf{(6)}$$

Where, w, w_o and w_∞ are the weight change at time t=0, t=t and t=∞, respectively.

The following equation is obtained after incorporating expressions of heating rate "r" and rate constant "k" into **equation (4)**, rearranging and integrating.

$$\int_0^\alpha \frac{d\alpha}{(1-\alpha)^n} = \frac{A}{r\int_0^T e\left(-\frac{Ea}{RT}\right)dT} \quad \textbf{(7)}$$

It should be noted that numerous approximate solutions of the above equation are available in literature. Coats and Redfern (**Coats and Redfern, 1964**) generated the following most commonly used equation considering "n= 1":

$$\ln\left[\frac{-\ln(1-\alpha)}{T2}\right] = \ln\left[\frac{AR}{rEa}\left(1-\frac{2RT}{Ea}\right)\right] - \frac{Ea}{RT} \quad \textbf{(8)}$$

The numerical values of E_a and A can be calculated from the slope and intercept, respectively, by plotting $\ln\left[\frac{-\ln(1-\alpha)}{T2}\right]$ against 1/T.

The decomposition rate constant is calculated using the Arrhenius equation mentioned above.

3.2. *Freeman and Carroll's Kinetics of Degradation*

The Freeman and Carroll equation may be written the form:

$$\frac{\Delta \log\left(\frac{dw}{dt}\right)}{\Delta \log(\alpha - w)} = -\frac{Ea}{2.303R} \cdot \frac{\Delta\left(\frac{1}{T}\right)}{\Delta \log(\alpha - w)} + n \quad \textbf{(9)}$$

Incorporation of Arrhenius equation, $k = Ae\left(-\frac{Ea}{RT}\right)$ and heating rate, $r = \frac{dT}{dt}$ into **equation (7)** for "n=1" and further rearrangement gives,

$$\log\left[\frac{\frac{dw}{dt}}{\alpha - w}\right] = \frac{Ea}{2.303RT} + \log A \quad \textbf{(10)}$$

The numerical values of E_a and A can be calculated from the slope and intercept, respectively, by plotting $\log\left[\frac{\frac{dw}{dt}}{\alpha - w}\right]$ against 1/T.

3.3. *Horowitz and Metzger's Kinetics of Degradation*

The final form of the Horowitz and Metzger equation may be expressed as:

$$\text{Ln}\left(\frac{\alpha}{\alpha - w}\right) = e\text{^}[(E\theta)/(RT_s^2)] \quad \textbf{(11)}$$

Where $\theta = T - T_s$ with T being the temperature and T_s being a reference temperature at the point of inflection, defined by the authors. This equation can be used for "n=1", where a plot of $\frac{\log\log\alpha}{\alpha - w}$ against θ gives a straight line with slope $E/2.303RT_s^2$.

3.4. *Thermodynamics of Degradation*

The thermodynamic parameters of degradation can be calculated from the following equations (**Straszko et al., 1997; Humienik, and Mozejko, 2000**):

$$\Delta H = Ea - RT \quad \textbf{(12)}$$

$$Ae^{\frac{-Ea}{RT}} = \frac{KBT}{h} e^{\frac{-\Delta G}{RT}} \quad \textbf{(13)}$$

$$\Delta G = \Delta H - T\Delta S \quad \textbf{(14)}$$

where, ΔG, ΔH and ΔS are free energy, enthalpy and entropy, receptivity. K_B and h are the Boltzmann and Plank constants respectively.

4. Results and Discussion

4.1. *Alkali Solubility (S10 & S18)*

The solubility of cellulose pulps in sodium hydroxide solutions can provide indicative information on the amount of lower molecular weight carbohydrates (degraded short chained cellulose and hemicellulose) content remaining in the pulp following the delignification process (**Wilson et al., 1952; Ohlsson, 1952**). A 10% sodium hydroxide solution possesses maximum

dissolving power and will dissolve both degraded cellulose and hemicellulose content (**Tappi, 2000**). The weight percentage extracted by the 10% sodium hydroxide solution (S10) was determined by the TAPPI 235-OM Standard Method, and the insoluble content retained (R10) can be considered a good approximation of the long chained α-cellulose percentage, (R10 = 100 - S10). Furthermore, an 18% sodium hydroxide solution will generally dissolve only the hemicellulose contents (S18 via TAPPI 235-OM)) and the remaining short chained degraded cellulose with a degree of polymerization between approximately 50 and 150 can be determined by S10 – S18 (Jahan et al., 2007).

Table 2. Alkali Solubility of Selected Pulps

Pulp	R10,%	S10,%	S18,%	S10-S18, %
P1	90.5	9.5	5.1	4.4
P2	87.6	12.4	6.4	6.0
P3	85.3	14.7	13.7	1.0
P4	85.5	14.5	11.7	2.8

The alkali solubility results are detailed in **Table 2** above. It can been seen that the two Kraft softwood pulps P3 and P4 had the highest S10 values (14.7% and 14.5% respectively) and, therefore, lowest long chained α-cellulose content (R10). The two acid-sulphite pulps P1 (eucalyptus hardwood) and P2 (northern softwood) showed lower S10 values than P3 and P4 indicating higher α-cellulose content. Comparing the S18 value to the S10 gives an indication of the make-up of the non-α-cellulose content. The acid-sulfite pulps P1 and P2 have an approximately equal split between short chained degraded cellulose and hemicelluloses, while the Kraft pulps P3 and P4 showed S18 values close to the S10, indicating their non-α-cellulose content being made up largely of hemicellulose content only and very little degraded cellulose.

4.2. *FT-IR analysis of pulps*

The FT-IR spectra of pulp samples are shown in **Figure 1**. The four pulp samples exhibited similar spectra. The broad band at 3347 cm^{-1} is from the stretching of –O-H groups and the lower wave-number peak at 3309 cm^{-1} is assigned to intra-molecular hydrogen bonding (**Maréchal, and Chanzy, 2000**). The peak at 2908 cm^{-1} is assigned to C-H stretching. The band at 1650 cm^{-1} is due to absorbed water. The band at 1434 cm^{-1} is attributed to C-O-H bending while the band at 1326 cm^{-1} is assigned to C-H bending. The strong band at 1033 cm^{-1} is attributed to the C–O stretching of primary alcohols characteristic of cellulose, including a satellite at 998 cm^{-1} indicating alternative conformations of the primary alcohols. Peaks at 1110 cm^{-1} and 1160 cm^{-1} just visible off the main 1033 cm^{-1} band are likely to be C-O-C cellulose ring modes (**Maréchal, and Chanzy, 2000**). The peaks identified in the spectra that can be attributed to those characteristic of cellulose, while it can also be noted that peaks associated with hemicelluloses (**Kačuráková et al., 2000**) are not distinguishable indicating a relative high degree of α-cellulose purity.

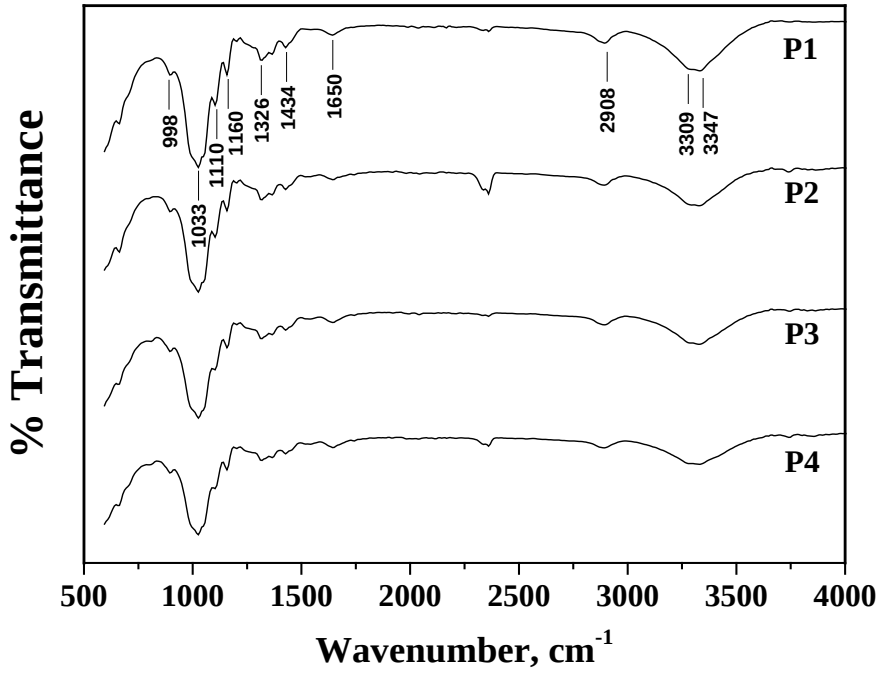

Figure 1. FT-IR spectra of selected pulp samples (labelled in the figure).

4.3. *Raman analysis of pulps*

Figure 2 compares the Raman spectra of the pulps under investigation. All four spectra are similar with peaks occurring at 380, 436, 493, 517, 897, 971, 996, 1094, 1119, 1336, 1378, 1472 and 2894 cm^{-1} attributed to cellulose (**Gierlinger et al., 2013**) Position and assignment of the Raman bands are presented in **Table 3**.

The peak at 380 cm^{-1} is known to be characteristic of crystalline cellulose and it is speculated to originate from one torsion or bending modes of the six-membered ring with respect to the glycosidic bonds (**Lee at al., 2016; Agarwal et al., 2010; Schenzel et al., 2005**). Generally, hemicelluloses do not exhibit a peak at 380 cm^{-1} while they can show broad peaks in the CH_2 bending vibration region (**Lee et al., 2016**). Agarwal et al. studied the effect of changes in crystallinity on the shape cellulose Raman bands and resulted that amorphous cellulose shows significant decline in band heights accompanied by band broadening (**Agarwal and Ralph, 1997**). It is worth noting that pulp samples 3 and 4 exhibited differentiations regarding the shape and height of the Raman peaks (e.g 493 cm^{-1}) as observed in the spectra that might be attributed to the existence of a higher amount of amorphous cellulose.

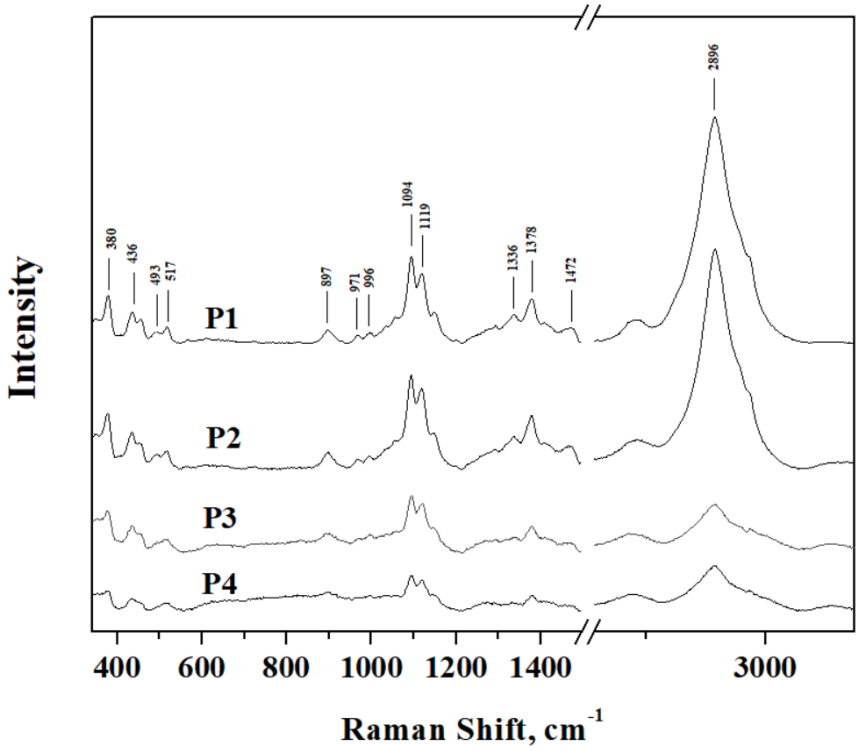

Figure 2. Raman spectra of selected pulp samples (labelled in the figure).

Table 3: Position and assignment of the Raman bands of the pulp samples

Raman bands (cm^{-1})	Assignment
380	δ (CCC) ring
436	Γ (COC) def
493	ν (COC) glycosidic
517	δ (COC) glycosidic
897	υ (COC) in plane, sym
971	ρ (CH_2)
996	ρ (CH_2)
1094	υ (COC) glycosidic, asym
1119	υ (COC) glycosidic, sym
1336	ω (CH_2)
1378	δ (CH_2)
1472	δ (CH_2), δ (COH)
2896	υ (CH)

(*def:* deformation, *sym:* symmetric, *asym:* antisymmetric)

4.4. *XPS analysis of pulps*

XPS spectra for the four pulps showed significant carbon C_{1S} and oxygen O_{1S} peaks observed around 287 – 288 eV and 533 to 535 eV respectively. The relative surface carbon and oxygen percentages are given in **Table 4**. The C_{1S} spectrum of cellulose can be separated in to three categories (**Dorris and Gray, 1978**): (1) C_1 is carbon-carbon or carbon-hydrogen bonding, (2) C_2 is carbon having a single bond with one oxygen, (3) C_3 is carbon bonded to one oxygen atom of a carbonyl group or carbon bonded to two oxygen atoms of a non-carbonyl group. **Figure 3** shows the 'C_{1S}' XPS spectra for the four pulps and **Table 4** details the binding energy and relative percentages of each carbon category for the four pulps being investigated.

It can be seen that for all four pulps the C_2 carbon category dominates. Hydroxyl groups on the 1, 3 and 6 carbons of the β-D-glucopyranose rings of the cellulose structure are known to take part in intra and inter molecular hydrogen bonding resulting in a strong hydroxyl domain in the inner cellulose structure and the associated dominance of the C_2 category (**Zhang et al., 2009**). The P1 and P2 acid-sulphite pulps showed similar spectra with the C_2 category accounting for over 90%, whereas the southern softwood P3 and P4 pulps showed just over 50% C_2 suggesting higher amorphous content (as observed by the alkali extraction and Raman analysis) and, therefore, lower crystallinity due to the lower α-cellulose content. Furthermore, both P3 and P4 pulps showed

greater C_3 area than the P1 and P2 (P2 had no C_3 detected), which may be due to some oxidized groups in the exposed surface cellulose chain as a result of the Kraft delignification and bleaching process common to the two southern softwood pulps (**Gustafsson, 2007**). The higher C_3 area associated with these pulps correlates with the higher oxygen ratio as indicated in **Table 1**. Additionally, P3 also showed higher C_1 content than the other three pulps and this is generally associated with possible lignin presence (**Johansson et al., 1999**).

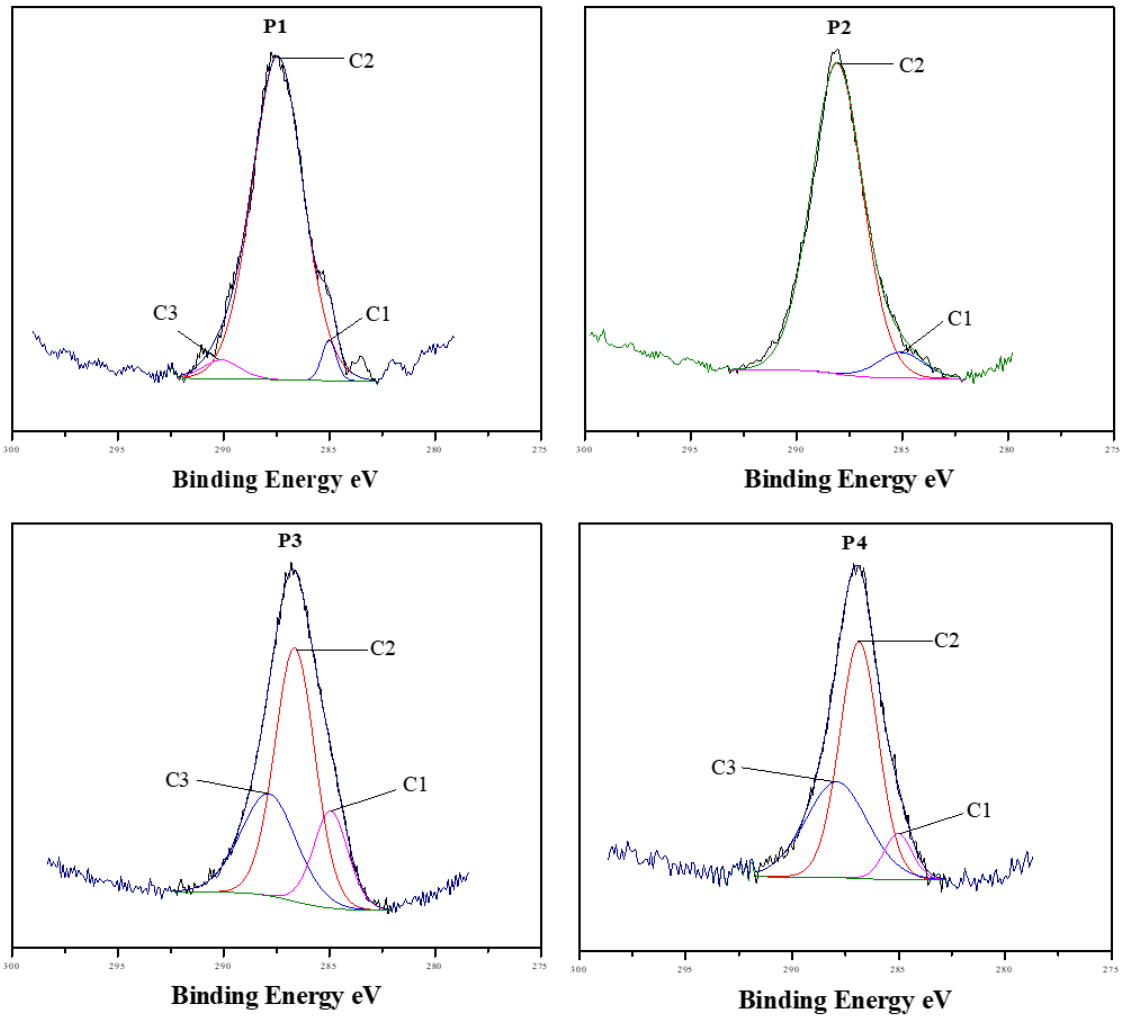

Figure 3 High resolution XPS C 1s spectra of selected pulp samples (labelled in the figures).

Table 4. C_{1S} categories binding energy and relative areas for selected pulps

Pulp	Survey Spectra		Deconvolution Spectra					
			C_1		C_2		C_3	
	Carbon (%)	Oxygen (%)	Binding Energy (eV)	Area (%)	Binding Energy (eV)	Area (%)	Binding Energy (eV)	Area (%)
P1	60.14	39.86	285.01	3.29	287.44	92.87	290.12	3.83
P2	73.61	26.39	285.07	6.86	288.07	93.14	-	-
P3	55.78	44.22	284.93	17.59	286.63	52.97	287.86	29.44
P4	60.63	39.37	285.02	7.93	286.86	56.00	287.90	36.07

4.5. *XRD analysis of pulps*

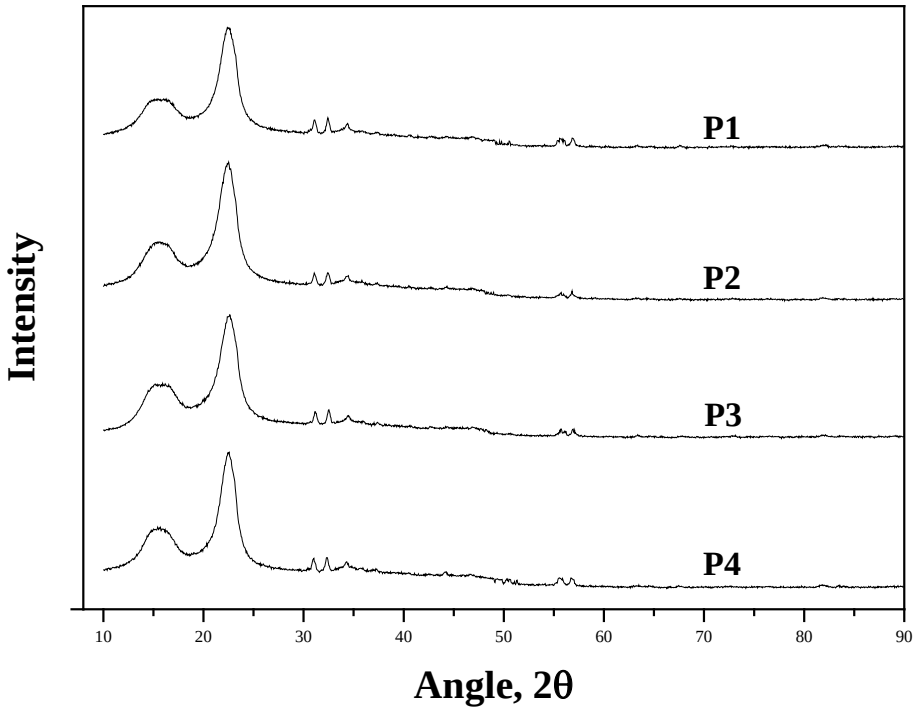

Figure 4. XRD diffractograms of selected pulp samples (labelled in the figure).

The crystallinity of the pulp samples was investigated by X-ray diffraction and the resulting scans are shown in **Figure 4**. The characteristic cellulose I_{002} peak at around 22.6° 2θ as assigned by Segal et. al (1959) is observed in all pulps in addition to the amorphous peak at around 18° 2θ.

The relative intensity of the I_{002} and amorphous peaks was used to determine the degree of crystallinity and the Scherrer equation was used to estimate the crystallite size for each pulp sample (**Mohkami and Talaeipour, 2011**); results are given in **Table 5**. It can be seen that the southern softwood Kraft pulps (P3 and P4) showed slightly reduced crystallinity when compared to the acid-sulphite pulps P1 and P2. The difference in crystallinity is relatively small and likely to be attributed to the lower α-cellulose content as determined in the S10 alkali analysis above and also correlates with the XPS surface analysis.

Table 5. Crystallinity index and crystallite size of selected pulps

Pulp	**Crystallinity index (%)**	**Crystallite size (nm)**
P1	50.2	3.81
P2	50.7	3.34
P3	48.1	3.64
P4	47.6	4.00

4.6. *SEM*

The surface morphology of the pulp samples was analysed by SEM and the resulting micrographs are shown in **Figure 5**. It can be seen that the fibres of all four pulps are relatively smooth and free from debris. The wood species origin of the pulp is the primary factor affecting morphology and large variations exist between different woods, for instance hardwood pulps are known to consist of shorter fibres and smaller in diameter than pulps derived from softwoods (**Browning, 1963**). P2 pulp, which is derived from eucalyptus hardwood, has the shortest fibre length and also the smallest average diameter.

Furthermore, morphology variations within the two classes of woods (hard and soft) also exist (**Browning, 1963**). Southern softwood pines (such as the P3 and P4 pulps) are known to have thick walls and larger diameter fibres when compared to pulps that originate from spruce softwood (such as the P1 pulp) which have thinner walled slender fibres (**Browning, 1963**). It can be seen in **Figure 5** that the fibres of the P3 and P4 pulps are slightly larger in diameter than the P1 fibres, while also appearing to be more rounded due to the thicker walls.

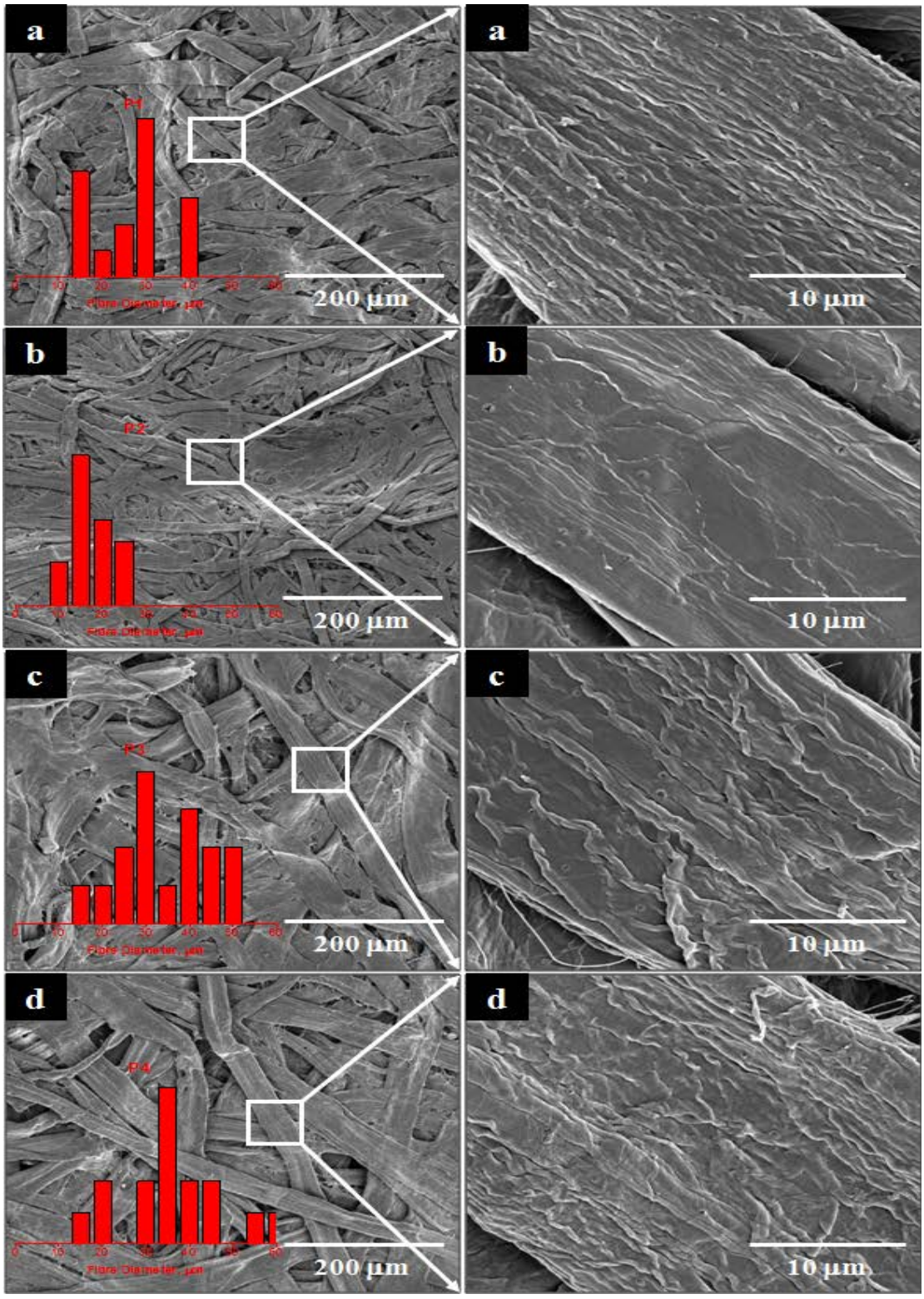

Figure 5. Top-down low resolution (left side) and high resolution (right side) SEM images of selected pulp samples: **(a)** P1, **(b)** P2, **(c)** P3, and **(d)** P4. Insets, are the fibre diameter distribution diagrams.

Analysis of fibre diameter size distribution as indicated in **Figure 5** confirms that the P2 eucalyptus hardwood pulp has the smallest average diameter fibres and a narrow distribution range. The northern softwood P1 pulp has larger diameters than the P2 pulp, while the southern softwoods P3 and P4 have the largest fibre diameters and widest distribution range. Southern pine pulps do not develop as much inter-fibre bonding relative to both spruce softwood and eucalyptus hardwood which both have higher number of fibres in a given weight than the pine; this can be seen in **Figure 5** where the P3 and P4 pulps appear to have less surface area and fewer inter-fibre connections.

4.7. *TGA analysis of pulps*

Figure 6 shows the thermogravimetric analysis carried out on dissolving cellulose wood pulps P1 at a heating rate of 5 °C min^{-1}. A minor weight loss region is observed from around 40°C to 120°C which can be attributed to water loss. A major thermal degradation stage takes place around 250°C to 340°C temperature range and corresponds to the decomposition of cellulose and hemicellulose (**Poletto et al., 2011**). The depolymerisation of both the crystalline α-cellulose and the various hemicelluloses occurs *via* random cleavage of the glycosidic linkages and subsequent rapid decomposition, with the hemicellulose content degrading first in the 150 °C to 350 °C range while the α-cellulose decomposition occurs from 275 °C (**Kim et al., 2006**).

The chemical structure of hemicellulose is amorphous with random branching and is easily hydrolyzed; it is this structural property that may result in higher thermal activity than the α-cellulose (**Poletto et al., 2011**). The α-cellulose structure is highly organized consisting of long chained polymers of glucose units arranged in a crystalline manner, with free hydroxyl groups likely to be involved in intramolecular and intermolecular hydrogen bonding (consistent with the FT-IR peak observed at 3309 cm^{-1}). High crystallinity coupled with hydrogen bonding is likely to be the reason for the increased thermal stability of cellulose relative to hemicellulose (**Ouajai and Shanks, 2005)**. A third significant degradation step occurs from around 350°C to 500°C and this is attributed to ash formation. Lignin present on the pulp is also likely to contribute to the char formation (**Sonia and Pryia Dasan, 2012**).

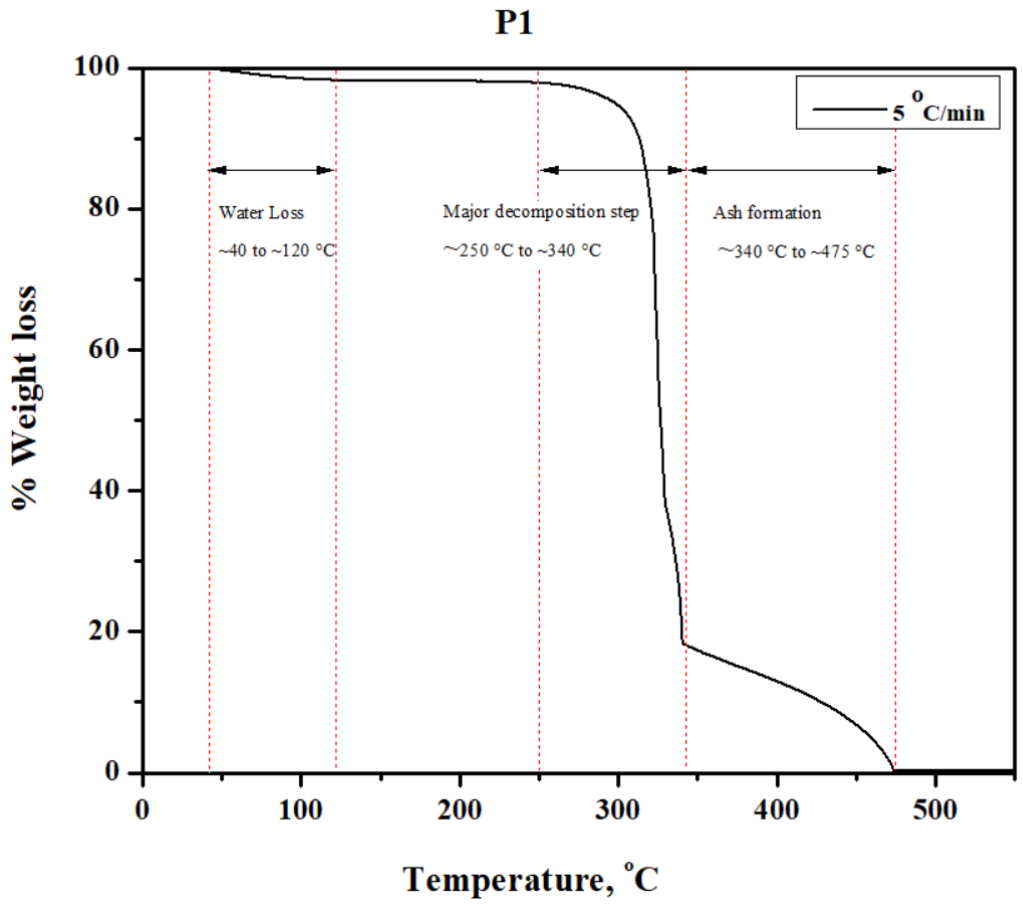

Figure 6. TGA thermogram example for a pulp sample.

Figure 7 shows the TGA analysis for all four cellulose pulps at heating rates of 5, 10 and 20 °C min^{-1}. The onset temperature of the major degradation step is increased with increasing heating rate as expected (heat transfer limitation results in the sample spending less time at each temperature and therefore the decomposition onset is pushed out to higher temperatures). As the temperature intervals of the hemicellulose and cellulose decomposition steps partially overlap (**Poletto et al., 2011**), noticeable separation of the decomposition steps will only be possible when the hemicellulose content is relatively high (alkali solubility analysis shows hemicelluloses content in the region of 1 to 6%).

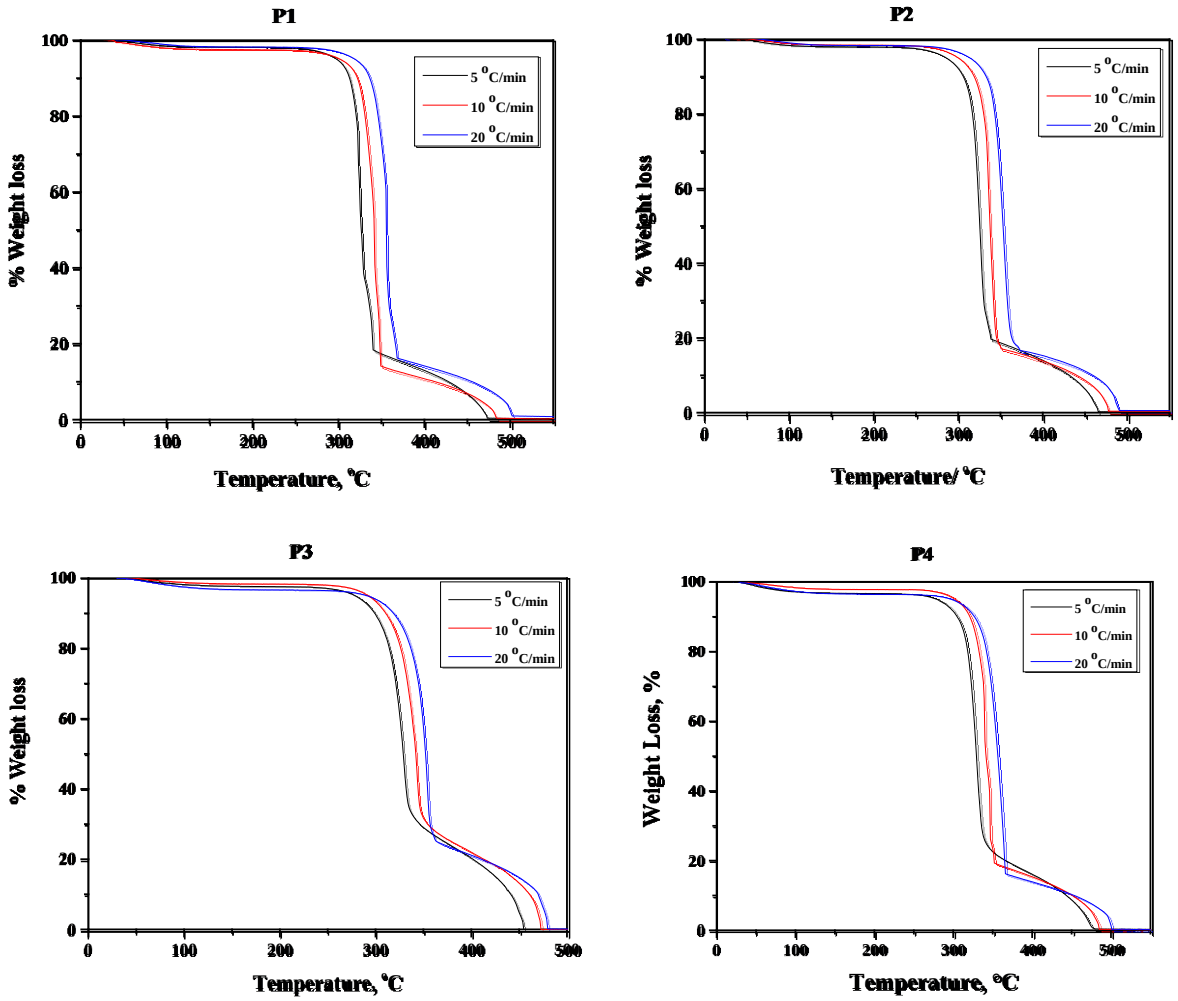

Figure 7. TGA thermograms of selected pulp samples (labelled in the figures).

Table 6 shows the temperature range and weight loss percentage for the minor and major decomposition steps for each pulp at each of the three heating rates. The results show that the temperature interval and weight loss percentage associated with the major cellulose degradation step for both P1 and P2 pulps are comparable.

Table 6. Weight loss data from TG analysis of selected pulps

Pulp	Heating Rate (°C min^{-1})	Weight Loss Temperature Range (°C)		Weight Loss (%)	
		Minor	**Major**	**Minor**	**Major**
P1	5	38 – 120	319 – 340	1.7	64.1
P1	10	38 – 126	331 – 350	2.3	65.3
P1	20	55 – 130	342 – 373	1.7	69.3
P2	5	50 – 125	313 – 338	1.9	64.9
P2	10	57 – 130	326 – 350	1.4	67.4
P2	20	67 – 136	338 – 374	1.5	69.9
P3	5	36 – 126	310 – 343	2.2	52.7
P3	10	49 – 129	323 – 351	1.5	51.4
P3	20	41 – 134	338 – 365	3.1	53.4
P4	5	36 – 115	290 – 342	2.9	68.9
P4	10	36 – 121	295 – 353	2.0	76.7
P4	20	37 – 126	315 – 368	3.0	76.8

The respective results for the P3 and P4 major degradation step show a slight reduction in the onset temperature. The lower onset temperatures for these pulps may be attributed to lower crystallinity (**Ouajai and Shanks, 2005**) as also observed during the Raman and XRD analysis and lower α-cellulose content as determined by the alkali solubility and XPS analysis. Furthermore, P3 pulp showed higher thermal stability during the major degradation step with just over 50% weight loss as opposed to ~65-75% for the other pulps. This may be due to higher lignin levels present (**Sonia and Pryia Dasan, 2012)** consistent with the XPS observations.

4.8. *Kinetic analysis of pulps*

Kinetic parameters for the thermal decomposition of the speciality cellulose dissolving pulps under investigation were determined by application of the Coats and Redfern integral model (**Coats and Redfern, 1964**) equation. The pulp degradation was assumed to follow first order reaction kinetics (n = 1) and a plot of $\log[(-\log(1-\alpha))/T^2]$ against 1/T in all were pseudo-linear across the greater region of the major decomposition step as can be seen in **Figure 8**. **Table 7** details the following calculated kinetic parameters for the thermal decomposition of the pulps: specific rate constant, activation energy and frequency factor.

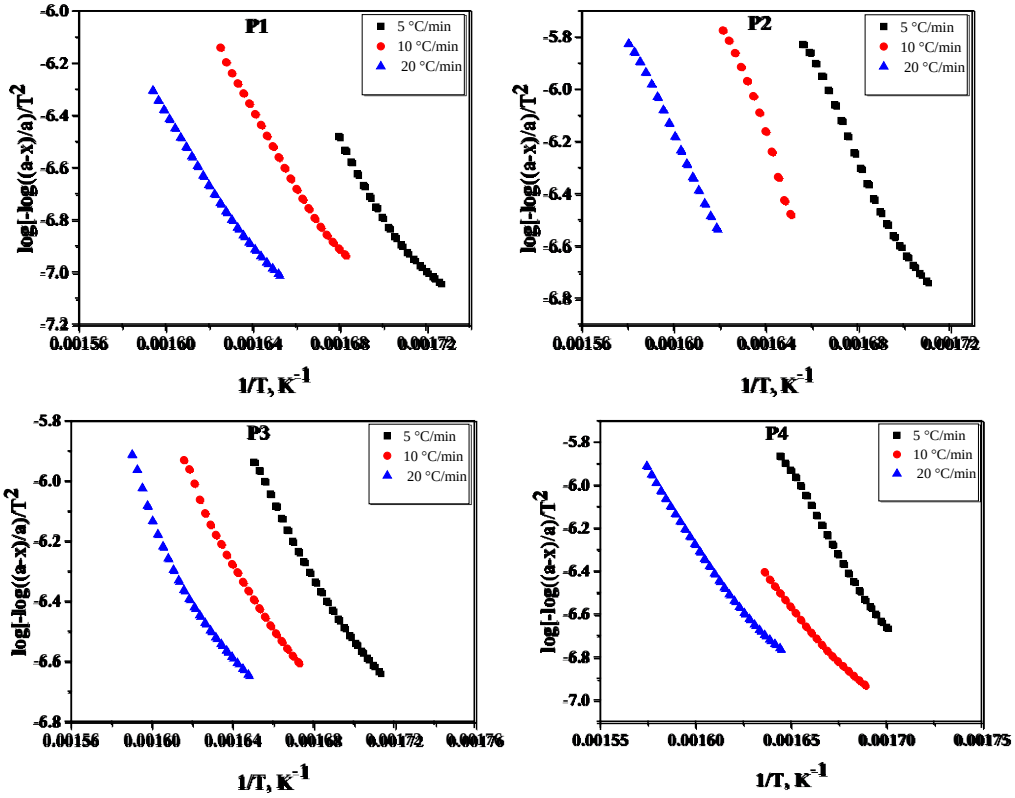

Figure 8. Coats and Redfern kinetic plots for the selected pulps (labelled in the figure).

Table 7. Kinetic and thermodynamic parameter for the non-isothermal degradation of selected pulps using the Coats and Redfern kinetic model.

		Kinetic parameters			Thermodynamic parameters		
Pulp	**Heating rate ($^{\circ}C\ min^{-1}$)**	**Specific rate constant (s^{-1})**	**Activation energy (kJ mol^{-1})**	**Frequency factor (s^{-1})**	**ΔH (kJ mol^{-1})**	**ΔS (J mol^{-1} k^{-1})**	**ΔG (kJ mol^{-1})**
P1	5	2.40×10^{-22}	231	7.49×10^{18}	229	108	196
P1	10	5.36×10^{-26}	269	7.14×10^{21}	266	165	217
P1	20	9.81×10^{-24}	237	4.00×10^{18}	235	103	204
P2	5	5.81×10^{-32}	346	2.50×10^{29}	343	310	251
P2	10	8.52×10^{-54}	471	3.44×10^{29}	469	312	376
P2	20	3.50×10^{-33}	364	4.01×10^{29}	362	314	268
P3	5	4.39×10^{-21}	219	1.06×10^{18}	217	92	189
P3	10	5.73×10^{-22}	224	1.24×10^{18}	222	93	194
P3	20	3.73×10^{-23}	234	3.65×10^{18}	231	102	201
P4	5	3.07×10^{-25}	287	1.00×10^{24}	285	206	223
P4	10	3.49×10^{-16}	176	4.31×10^{13}	174	8	171
P4	20	1.66×10^{-23}	236	4.46×10^{18}	234	103	203

Application of the Freeman and Carroll's (**Freeman and Carroll, 1958**) differential kinetic model can be seen in **Figure 9** below, where for "n=1" plotting $\log[(dw/dt)/(\alpha - w)]$ against 1/T gives pseudo-straight lines and numerical values of E_a and A were calculated from the slope and intercept, respectively. While plots of $\log\log \alpha/(\alpha - w)$ against θ for the "n=1" case of Horowitz and Metzger's kinetic model (**Horowitz and Metzger, 1963**) also gave pseudo-straight lines as can be seen in **Figure 10** below. The resultant kinetic parameters are given in **Tables 8 and 9.**

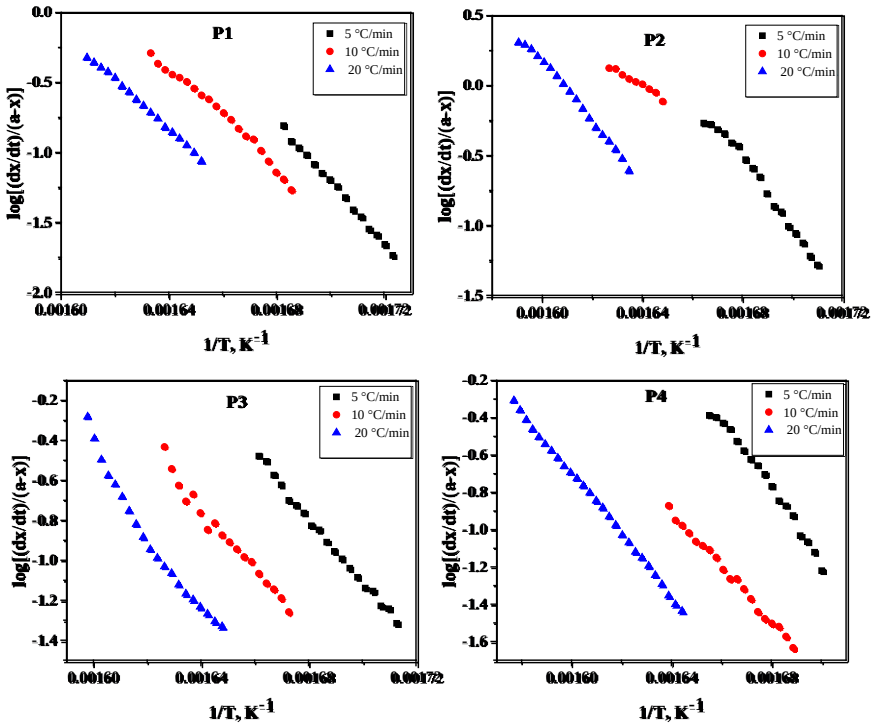

Figure 9. Freeman and Carroll kinetic plots for the selected pulps (labelled in the figure).

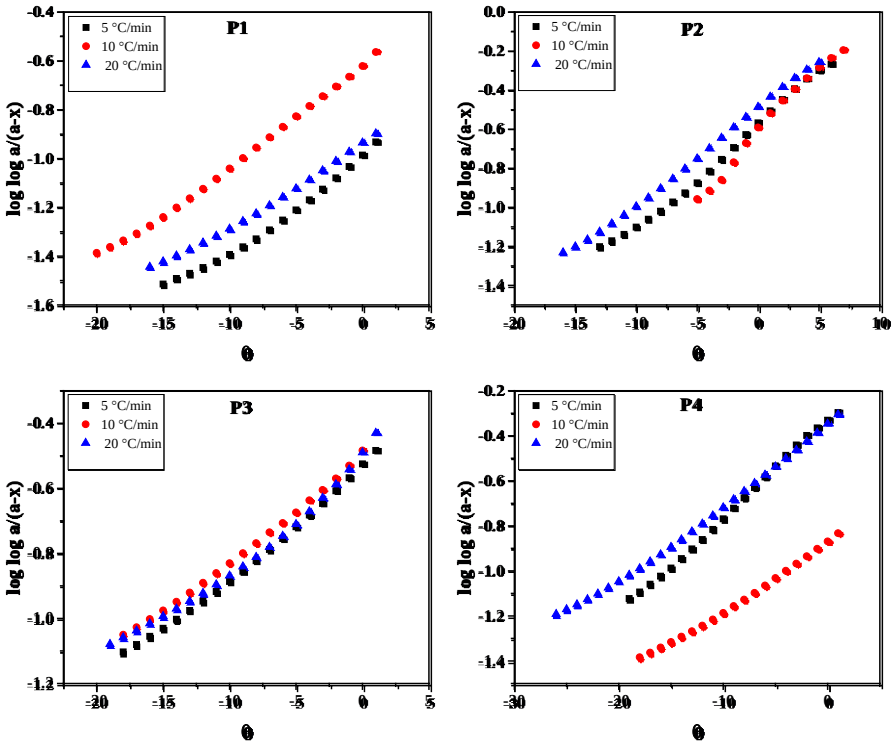

Figure 10. Horowitz and Metzger kinetic plots for the selected pulps (labelled in the figure).

Table 8. Kinetic and thermodynamic parameter for the non-isothermal degradation of selected pulps using the Freeman and Carroll kinetic model.

		Kinetic parameters			Thermodynamic parameters		
Pulp	**Heating rate ($^{\circ}C\ min^{-1}$)**	**Specific rate constant (s^{-1})**	**Activation energy (kJ mol^{-1})**	**Frequency factor (s^{-1})**	**ΔH (kJ mol^{-1})**	**ΔS (J mol^{-1} k^{-1})**	**ΔG (kJ mol^{-1})**
P1	5	1.67×10^{-38}	423	2.14×10^{36}	420	442	289
P1	10	1.03×10^{-31}	341	7.16×10^{28}	339	299	250
P1	20	9.97×10^{-32}	337	1.00×10^{28}	334	283	250
P2	5	2.16×10^{-41}	459	4.97×10^{39}	456	507	305
P2	10	4.55×10^{-39}	427	3.27×10^{36}	425	446	292
P2	20	6.54×10^{-38}	407	1.61×10^{34}	405	402	285
P3	5	1.79×10^{-28}	308	1.73×10^{26}	306	249	231
P3	10	2.19×10^{-28}	300	1.00×10^{25}	298	225	231
P3	20	1.54×10^{-36}	385	5.90×10^{31}	383	355	277
P4	5	8.53×10^{-33}	357	3.73×10^{30}	355	332	256
P4	10	7.10×10^{-27}	282	1.67×10^{23}	279	191	222
P4	20	4.26×10^{-30}	313	2.70×10^{25}	310	834	241

P1 and P2 acid-sulphite pulps showed higher values of activation energy than the Kraft P3 and P4 pulps for each of the three kinetic models (with the Coats and Redfern and Horowitz and Metzger model results matching closely). A possible reason for this may be due to the pulping delignification processes associated with the pulps; the Kraft process is known to have a greater effect on the crystallinity, thermal stability and cell structure than the acid-sulphite process (**Poletto et al., 2011**), correlating with the reduced α-cellulose content (and therefore reduced crystallinity) observed by the alkali solubility, Raman and XRD analyses.

Table 9. Kinetic and thermodynamic parameters for the non-isothermal degradation of selected pulps using the Horowitz and Metzger kinetic model.

		Kinetic parameters			Thermodynamic parameters		
Pulp	**Heating rate ($^{\circ}C\ min^{-1}$)**	**Specific rate constant (s^{-1})**	**Activation energy (kJ mol^{-1})**	**Frequency factor (s^{-1})**	**ΔH (kJ mol^{-1})**	**ΔS (J mol^{-1} k^{-1})**	**ΔG (kJ mol^{-1})**
P1	5	1.92×10^{-24}	247	3.47×10^{19}	244	121	208
P1	10	9.99×10^{-29}	287	2.28×10^{22}	285	175	233
P1	20	6.73×10^{-25}	241	1.13×10^{18}	238	92	211
P2	5	2.12×10^{-34}	361	3.24×10^{29}	358	312	265
P2	10	2.50×10^{-36}	375	1.39×10^{30}	373	324	276
P2	20	2.78×10^{-36}	365	2.35×10^{28}	362	290	276
P3	5	6.24×10^{-23}	226	2.36×10^{17}	224	79	200
P3	10	4.49×10^{-23}	226	1.71×10^{17}	223	77	201
P3	20	7.79×10^{-24}	234	8.11×10^{17}	232	90	205
P4	5	3.88×10^{-30}	306	1.89×10^{24}	304	212	241
P4	10	2.46×10^{-21}	208	7.40×10^{15}	206	51	191
P4	20	3.03×10^{-23}	257	3.92×10^{19}	255	122	218

The XPS analysis also suggested that the Kraft pulps showed more surface degradation again supporting the observed lower activation energies for the thermal decomposition of these pulps when compared with the acid-sulphite pulps. The activation energy for P2 pulp was significantly higher than the other acid-sulphite P1 pulp and a reason for this may be due to the relative fibre size. As demonstrated by the SEM analysis, the average fibre diameter for the P2 hardwood pulp was significantly lower than for the P1 pulp. The tight packing of the cellulose chains of the P2 pulp (which also had the highest crystallinity level) may contribute to the higher activation energy required for thermal decomposition.

The frequency factor for the P2 pulp was also significantly higher than the other three pulps and this was observed for all three kinetic models. This is again likely to be due to the relative differences in the pulp morphologies. As can be seen from the SEM analysis, the P2 pulp has more fibres per given weight and will therefore tend to have more collisions during the decomposition stage.

4.9. *Thermodynamic analysis of pulps*

Application of the activated complex theory to the thermal degradation of speciality dissolving cellulose pulps enable determination of thermodynamic parameters; results for enthalpy (ΔH), entropy (ΔS) and Gibb's free energy (ΔG) are given in **Table 7, 8, 9** for the respective kinetic models applied. The positive value of ΔH indicates the endothermic nature of cellulosic pulp degradation. The larger value for ΔH for the P2 pulp (observed by all three models) relative to the other pulps at a particular temperature indicates that thermal decomposition requires greater heat input, corresponding to the higher activation energies calculated for this pulp.

The entropy for the decomposition of the pulps at a particular temperature is calculated by using **equation (14)**. It is evident that the ΔS values for all four pulps are positive indicating that thermal decomposition leads to an increase in disorder. The relative magnitude of the positive value of ΔS can be correlated to the frequency factor whereby higher frequency of collisions leads to greater disorder and this trend can be seen in **Tables 7, 8, 9**.

The non-spontaneous nature of the decomposition of cellulose pulp is evident from the positive value of Gibb's free energy, ΔG. The higher value of ΔG for the P2 pulp indicates that the decomposition is less spontaneous relative to other pulps.

5. Conclusions

Manufacturers of microcrystalline cellulose (MCC) use a wide range of speciality dissolving pulps from different wood sources and delignification processes primarily for commercial reasons. However, the assumption of equivalency of pulps is challenged in this paper following identification of significant differences between the selected pulps. Acid-sulphite pulps contained higher amounts of α-cellulose and β-cellulose in comparison to the Kraft pulps which contained higher γ-cellulose levels; higher α and β content represent opportunity for a higher yield of MCC product which is highly significant for commercial producers in a competitive market. Correlating

with higher α-cellulose content, the crystallinity indices for the acid-sulphite pulps, as measured by XRD, were also higher than those measured for the Kraft pulps, suggesting that the delignification process had impact on crystallinity, in alignment with current literature.

However, detailed kinetic modelling of the thermal degradation of the pulps (following thermogravimetric analysis) indicated significant differences between the two acid-sulphite pulps (P1 and P2). Pulp P2 was found to have higher activation energy values than pulp P1 and unexpectedly significantly higher frequency factor values. SEM analysis clearly showed morphological differences between the softwood pulp P1 and hardwood pulp P2, with the hardwood pulp having significantly smaller fibres tightly packed across a narrower distribution range. The large difference in frequency factor and activation energy between to the two acid-sulphite pulps during the thermal degradation process may, therefore, be attributed to morphological differences linked with wood source, an observation not given in the current literature. Pulp morphology and its potential impact is rarely if ever assessed by MCC producers during pulp qualification.

The results of the present investigation, therefore, indicate large differences in pulp samples attributed to both delignification process *and* wood type, which is of particular importance to MCC producers who are challenged with processing pulps that were deemed ‘equivalent’.

Acknowledgements

The authors wish to acknowledge AMBER Centre, Trinity College Dublin for providing financial support to carry out the research, and DuPont Nutrition and Health for pulp supply and onsite laboratory access.

References

Agarwal, U.P., Reiner, R.S., Ralph, S.A. (2010). Cellulose I crystallinity determination using FT-Raman spectroscopy: univariate and multivariate methods. Cellulose 17(4), 721-733.

Agarwal, U.P., Ralph, S.A. (1997). FT-Raman spectroscopy of wood: Identifying contributions of lignin and carbohydrate polymers in the spectrum of Black Spruce (Picea mariana). Appl. Spec. 51, 1648-1655.

Brittain, H.C., Lewen, G., Newman, W., Fiorelli, K., Bogdanowich, S. (1993). Changes in material properties accompanying the national formulary (NF) identity test for microcrystalline cellulose. Pharm. Res. 10, 61-67.

Browning, B.L. (1963) The Chemistry of Wood. Interscience (Wiley), New York.

Carlin, B. (2008). Direct compression and the role of filler-binders. In: Augsburger, L.L., Hoag, S.W. (Eds.), Pharmaceutical Dosage Forms: Tablets. Informa, 173-216.

Coats, A.W. and Redfern, J.P. (1964). Kinetic Parameters from Thermogravimetric Data. Nature, 201, 68-69

Dorris, G.M., Gray, D.G. (1978) The surface analysis of paper and wood fibres by ESCA. II. Surface composition of mechanical pulps. Cell. Chem. Technol. 12, 721-734.

Freeman, E. S. and Carroll, B. J. (1958). Phys. Chem., 62, 394

Gierlinger, N., Keplinger, T., Harrington, M., Schwanninger, M. (2013). Raman imaging of lignocellulosic feedstock, Cellulose - Biomass Conversion. Prof. John Kadla. InTech, DOI: 10.5772/50878.

Gustafsson, J., Ciovica, L., Peltonen J. (2002). The ultrastructure of spruce kraft pulps studied by atomic force microscopy (AFM) and X-ray photoelectron spectroscopy (XPS). Polymer 44, 661-670.

Hon, D. N.-S., Shiraishi, N. (2000). Wood and Cellulosic Chemistry, Second Edition, Revised, and Expanded (2000-11-08). 1786. ISBN: 9780824741358

Horowitz, H. H. and Metzger G. (1963). Anal. Chem., 35, 1464.

Humienik, M.O., Mozejko, J. (2000) Thermodynamic functions of activated complexes created in thermal decomposition processes of sulphates. Thermochim. Acta 344, 73-79.

Ibarra, D., Köpcke, V., Larsson, P.T., Jääskeläinen, A.S., Ek, M. (2010). Combination of alkaline and enzymatic treatments as a process for upgrading sisal paper-grade pulp to dissolving-grade pulp. Bioresour. Technol. 101, 7416-7423.

Jahan, M.S., Al-Maruf, A, Quaiyyum, M.A. (2007). Bangladesh Journal of Scientific and Industrial Research. 1952, 01/2007; 42(4):425-434

Johansson, L.S., Campbell, J.M., Koljonen, K., Stenius, P. (1999). Evaluation of surface lignin on cellulose fibers with XPS. Appl. Surf. Sci. 144-145, 92-95.

Kačuráková, M., Capek, P., Sasinková, V., Wellner, N., Ebringerová, A. (2000). FT-IR study of plant cell wall model compounds: pectic polysaccharides and hemicelluloses. Carbohyd. Polym. 43, 195-203.

Kim, H.-S., Kim, S., Kim, H.-J., Yang, H.-S. (2006). Thermal properties of bio-flour-filled polyolefin composites with different compatibilizing agent type and content. Thermochim. Acta 451, 181-188.

Krassig, H. (1985). Cellulose and its derivatives: Chemistry, biochemistry and applications, J.F. Kennedy, G.O. Phillips, D.J. Wedlock, P.A. Williams (eds), Ellis Horwood Limited Publishers, Chichester, UK.

Landín, M., Martínez-Pacheco, R., Gómez-Amoza, J.L., Souto, C., Concheiro, A., Rowe, R.C. (1992). Effect of batch variation and source of pulp on the properties of microcrystalline cellulose. Int. J. Pharm. 91, 133-141.

Lee, C., Dazen, K., Kafle, K., Moore, A., Johnson, D.K., Park, S., Kim, S.H. (2016). Correlations of apparent cellulose crystallinity determined by XRD, NMR, IR, Raman, and SFG methods. Adv. Pol. Sci. 271, 115-132.

Maréchal, Y., Chanzy, H. (2000). The hydrogen bond network in Iβ cellulose as observed by infrared spectrometry. J. Mol. Struct. 523, 183-196.

Mohkami, M., Talaeipour. M. (2011). Investigation of the chemical structure of carboxylated and carboxymethylated fibers from waste paper *via* XRD and FTIR analysis. 2011, Bioresources 6, 1988-2003.

Ohlsson, K. E. (1952). The Alkali Solubility of Pulps. Svensk Papperstid. 55(10): 347.

Ouajai, S., Shanks, R. A. (2005). Morphology and structure of bioscouring hemp fibre. J. Macromol. Biosci. 5, 124-134.

Poletto, M., Pistor, V., Zeni, M., Zattera, A.J. (2011). Crystalline properties and decomposition kinetics of cellulose fibers in wood pulp obtained by two pulping process. Polym. Degrad. Stab. 96, 679-685.

Poletto, M., Zattera, A.J., Forte, M.M.C., Santa, R.M.C. (2011). Thermal decomposition of wood: Influence of wood components and cellulose crystallite size. Bioresource Technol. 109, 148-153.

Schenzel, K., Fischer, S., Brendler, E. (2005). New method for determining the degree of cellulose I crystallinity by means of FT-Raman spectroscopy. Cellulose 12(3), 223-231.

Segal L., Creely, J.J., Martin Jr., A.E., and Conrad, C.M. (1959). An empirical method for estimating the degree of crystallinity of native cellulose using X-ray diffractometer, Textile Research Journal 29, 786-794,

Sonia, A., Priya Dasan, K. (2013). Chemical, morphology and thermal evaluation of cellulose microfibers obtained from Hibiscus sabdariffa. Carbohyd. Polym. 92, 668-674.

Straszko, J., Humienik, M.O., Mozejko, J. (1997). Kinetics of thermal decomposition of $ZnSO_4 \cdot 7H_2O$. Thermochim. Acta 292, 145-150.

Tappi, (2000)**.** Alkali solubility of pulp, Tappi T235 OM- 60, Tappi Press, Atlanta.

Wang, H., Pang, B., Wu, K., Kong, F., Li, B., Mu, X. (2014). Two stages of treatments for upgrading bleached softwood paper grade pulp to dissolving pulp for viscose production. Biochem. Eng. J. 82, 183-187.

Wilson, K., Ringstrom, E., and Hedlund, I. (1952). The Alkali Solubility of Pulp, Svensk Papperstid. 55(2): 31

Zhang, J., Zhang, J., Lin, L., Chen, T., Zhang, J., Liu, S., Li, Z., Ouyang, P. (2009). Dissolution of microcrystalline cellulose in phosphoric acid- molecular changes and kinetics. Molecules 14, 5027-5041.

Chapter 3

Study of Variance in Microcrystalline Cellulose Thermal Degradation Kinetics and Thermodynamics due to Pulp Source

Study of variance in Microcrystalline Cellulose thermal degradation kinetics and thermodynamics due to pulp source

Conor O'Regan[*a,b], Dipu Borah[c], John Anastasopoulos[c], John O'Connell[a], Justin D Holmes[a,c,d], and Michael A Morris[*c,d]

[a] Materials Chemistry, Department of Chemistry, University College Cork, Cork, Ireland,

[b] DuPont Nutrition and Health, Cork, Ireland

[c] AMBER, Trinity College Dublin, Dublin 2, Ireland,

[d] Tyndall National Institute, Lee Maltings, Prospect Row, Cork, Ireland,

*Corresponding author: Email: conor.o-regan@dupont.com (Conor O'Regan), morrism2@tcd.ie (Michael A Morris) Ph: +353 18963089

ABSTRACT

Two samples of microcrystalline cellulose (Avicel® PH102 grade) produced from different starting pulps (hard and softwood) were selected for investigation. Analyses revealed that the MCC powder products showed no significant differences despite variances found in the starting pulps. For instance, the degree of polymerisation of the softwood pulp was significantly higher than the hardwood pulp. The MCC products were surprisingly found to have lower crystallinity compared to the pulps, suggesting hydrolysis of both amorphous and crystalline regions. Kinetic degradation parameters indicated lower activation energy and frequency factor for the MCC samples correlating with lower crystallinity. Importantly, there were no significant differences between the kinetic parameters of the two MCC products, indicating that differences in pulp were diminished during the MCC production hydrolysis step.

Keywords: MCC; Pulp; Cellulose; Thermal degradation; Kinetics; Thermodynamics

1. Introduction

Microcrystalline cellulose (MCC) is manufactured commercially by the controlled hydrolysis of speciality cellulose pulps with mineral acid, which allows for production of a purified and partially depolymerised microcrystalline cellulose powder that has wide applications in the pharmaceutical and food industries. It is differentiated from native / natural cellulose by measurement of its degree of polymerisation (DP), with pharmacopoeial MCC being defined by a DP of less than 350 glucose units (**Thoorens et al., 2014**).

Commercial production of MCC is challenging; the raw material in the overall process is wood sourced from various types of trees (hard wood / soft wood), grown in different global regions, experiencing different climates and harvesting times, and undergoing different delignification pulping processes. The effect of variance in commercial MCC final product both on the pharmaceutical tableting process and on the end quality of pharmaceutical products has been extensively studied, (**Koo and Heng, 2001; Soh et al., 2008; Dumarey et al., 2011; Landin et al., 1992; Almay and Aburub, 2008**). Therefore, MCC manufactures are required to negate the effects of raw material variance to produce MCC products from different sources but with equivalent specifications and functionality acceptable to the end user.

In this study, two samples of MCC powder products (Avicel® PH102 grade) produced from different starting pulps were characterised and their thermal degradation kinetics and thermodynamics investigated to understand variances between the two samples. Additionally, the powder MCC samples were compared against the starting pulp materials which were also characterised and decomposition properties investigated accordingly.

The objective of this study was to investigate the decomposition properties of two samples of the same grade of commercially available MCC powder product which were produced from pulps of different wood type and understand how kinetic and thermodynamic properties are affected.

Thermogravimetic analyses of the MCC powder product samples and selected dissolving cellulose pulp raw materials were carried out and the activation energy, frequency factor and subsequent rate constants were determined using three established methods: the Coats and Redfern integral method (**Coats and Redfern, 1964**), Freeman and Carroll differential method (**Freeman and Carroll, 1958**), and Horowitz and Metzger approximation method (**Horowitz and Metzger, 1963**).

2. Materials and Methods

2.1. *Materials*

Two microcrystalline cellulose samples of Avicel® PH102 grade, identified as 'F1' and 'F2' in this paper, were selected for study. Sample F1 was produced from a pulp (P1) derived from northern softwood (Black Spruce), while sample F2 was produced from pulp (P2) which was derived from a hardwood source (Eucalyptus). Both pulps were originally delignified *via* the acid-sulphite process followed by oxidative elemental chlorine free (ECF) bleaching (**Hon and Shiraishi, 2000**). All materials were supplied courtesy of DuPont Nutrition and Health, Cork, Ireland.

2.2. *Elemental analysis of pulp and MCC samples*

The elemental analysis of the pulp and MCC samples is given in **Table 1**. Analysis of C, H and O (by difference) was performed on a Perkin Elmer 2400 Series II CHNS/O Analyzer. The four samples show relatively similar C, H and O composition when compared to each other with the two pulp samples (P1 and P2) showing marginally reduced carbon and increased oxygen when compared against the MCC powder samples (F1 and F2) and the theoretical composition of pure α-cellulose. Differences between the measured pulp composition and the MCC samples are likely due to increased hemicelluloses and amorphous content present in the pulps which were subsequently hydrolysed out during the MCC production process.

Table 1. Elemental analysis of selected pulp samples

Pulp	Carbon %	Hydrogen %	Oxygen %
P1	42.89	6.31	50.80
P2	42.79	6.18	51.03
F1	43.43	6.24	50.34
F2	43.34	6.23	50.44
α-cellulose $(C_6H_{10}O_5)_n$	44.44	6.17	49.38

2.3. *Degree of Polymerisation*

The degree of polymerisation (DP) for each sample was determined by ASTM D1795 standard method, using cupriethylenediamene (CUEN) solution to measure intrinsic viscosity and subsequent relation to average DP. The aqueous solvent CUEN is a copper complex with an amine hydroxide and chemical formula: $[Cu(H_2N.(CH_2)_2.NH_2)_2](OH)_2$.

2.4. *Alkali Solubility (S10 & S18)*

Alkali solubility at 10% NaOH (S10) and 18% NaOH (S18) was determined by the TAPPI 235-OM Standard Method of the Technical Association of the Pulp and Paper Industry (**Tappi, 2000**).

2.5. *Fourier transformed infrared (FTIR)*

An IR660, Varian Infrared Spectrophotometer in Attenuated Total Reflectance (ATR) mode was used to record FTIR spectra. The measurements were performed in the spectral range of 4000-500 cm^{-1}, with a resolution of 4 cm^{-1} and data averaged over 32 scans.

2.6. *Raman Spectroscopy*

Raman spectra were obtained using a HORIBA Jobin Yvon labRAM HR. The bench-top micro-Raman unit has an 800 mm focal length spectrometer giving it a resolution of < 1 cm^{-1}. Samples were excited with a Nd:YAG laser emitting at 532 nm. An objective lens of 100x was utilized and the signal was collected on a high resolution air-cooled CCD. The spectrometer was calibrated using a polished, non-oxidised silicon standard. The spectra were collected in the range 340 to 3200 cm^{-1} and the laser power was set at 100%. Spectra collection time was 30 s and 20 accumulations were taken for each sample. The samples analysed were pre-scanned to reduce auto-fluorescence and the spectra were subject to a second-order polynomial background subtraction, excluding the position of the specific peaks, to reduce the fluorescence background.

2.7. *Scanning Electron Microscopy (SEM)*

SEM images were obtained by a high resolution (< 1 nm) Field Emission Zeiss Ultra Plus-SEM with a Gemini® column operating at an accelerating voltage of 5 kV.

2.8. *Transmission Electron Spectroscopy (TEM)*

TEM images were obtained from JEOL Transmission Electron Microscope (TEM) JEM 2000FXII (Jeol Ltd., Tokyo, Japan).

2.9. *X-Ray Photoelectron Spectroscopy (XPS)*

XPS was performed on Vacuum Science Workshop CLASS100 high performance hemispherical analyser using Al K_α (hν = 1486.6 eV) mono X-ray source. Spectra were obtained at a take-off angle of 15°. Samples were loaded into the vacuum chamber within 1 h after being prepared and were subjected to XPS analysis. Photoemission peak positions were corrected to a C 1s signal at a binding energy of 284.8 eV.

2.10. *X-Ray Diffraction (XRD)*

XRD spectra were recorded by a PANanalytical X'Pert PRO instrument with Ni-filtered Cu-Kα radiation (λ = 0.1542 nm) generated at 40 kV and 40 mA. The scanning was made through 2θ = 10° to 90°, and intensity data was recorded with a digital recorder. The crystallinity index (*CrI*) was calculated *via* **equation (1)**:

$$CrI = \frac{I_{002} - Iam}{Iam} \quad \textbf{(1)}$$

where, I_{002} the maximum intensity of the peak corresponding to the plane in the sample with the Miller indices 002 at a 2θ angle of around 22.6°, and I_{am} is the intensity that corresponds to the non-crystalline peak at about 2θ = 18°.

2.11. *Thermogravimetric Analysis (TGA)*

TGA was carried out on **Pyris 1 PerkinElmer** thermogravimetric analyser. The pulps were prepared by cutting in to approximately 2 mm x 2 mm samples chips, and both pulps and MCC powder samples were oven dried at 70 °C for 24 hours. TGA was carried out on samples weighing around 10 mg over a temperature range from room temperature to 600 °C under nitrogen atmosphere with a flow rate of 50 ml min^{-1} and at heating rates of 5 °C min^{-1}, 10 °C min^{-1} and 20 °C min^{-1}.

3. Theory

3.1. *Coats and Redfern's Kinetics of Degradation*

The rate of decomposition of pulp under non-isothermal condition can be expressed as:

$$-\frac{dw}{dt} = kw \quad \textbf{(2)}$$

Where, w = weight of pulp; t = time and k = rate constant. Incorporation of Arrhenius equation, $k = Ae\left(-\frac{Ea}{RT}\right)$ and heating rate, $r = dT/dt$ into **equation (1)** and further rearrangement gives,

$$\frac{1}{w}\frac{dw}{dT} = \frac{A}{r}e\left(-\frac{Ea}{RT}\right) \quad \textbf{(3)}$$

Where, T = temperature; A = Arrhenius constant; r = heating rate; E_a = activation energy and R = gas constant.

The rate equation may also be expressed in terms of fractional conversion "α" and reaction order "n" as follows:

$$\alpha = \frac{wo-w}{wo-w\infty} \quad \textbf{(4)}$$

$$-\frac{d\alpha}{dt} = k\,(1-\alpha)^n \quad \textbf{(5)}$$

Where, w, w_o and w_∞ are the weight change at time t = 0, t = t and t = ∞, respectively.

The following equation is obtained after incorporating expressions of heating rate "r" and rate constant "k" into **equation (4)**, rearranging and integrating.

$$\int_0^\alpha \frac{d\alpha}{(1-\alpha)^n} = \frac{A}{r\int_0^T e\left(-\frac{Ea}{RT}\right)dT} \quad \textbf{(6)}$$

It should be noted that numerous approximate solutions of the above equation are available in literature. Coats and Redfern (**Coats and Redfern, 1964**) generated the following most commonly used equation considering "n = 1":

$$\ln\left[\frac{-\ln(1-\alpha)}{T2}\right] = \ln\left[\frac{AR}{rEa}\left(1-\frac{2RT}{Ea}\right)\right] - \frac{Ea}{RT} \quad \textbf{(7)}$$

The numerical values of E_a and A can be calculated from the slope and intercept, respectively, by plotting $\ln\left[\frac{-\ln(1-\alpha)}{T2}\right]$ against 1/T.

The decomposition rate constant is calculated using the Arrhenius equation mentioned above.

3.2. *Freeman and Carroll's Kinetics of Degradation*

The Freeman and Carroll equation may be written the form:

$$\frac{\Delta\log\left(\frac{dw}{dt}\right)}{\Delta\log(\alpha-w)} = -\frac{Ea}{2.303R}.\frac{\Delta\left(\frac{1}{T}\right)}{\Delta\log(\alpha-w)} + n \quad \textbf{(8)}$$

Incorporation of Arrhenius equation, $k = Ae\left(-\frac{Ea}{RT}\right)$ and heating rate, $r = \frac{dT}{dt}$ into **equation (6)** for "n=1" and further rearrangement gives,

$$\log\left[\frac{\frac{dw}{dt}}{\alpha-w}\right] = \frac{Ea}{2.303RT} + \log A \quad \textbf{(9)}$$

The numerical values of E_a and A can be calculated from the slope and intercept, respectively, by plotting$\log\left[\frac{\frac{dw}{dt}}{\alpha-w}\right]$ against 1/T.

3.3. *Horowitz and Metzger's Kinetics of Degradation*

The final form of the Horowitz and Metzger equation may be expressed as:

$$\text{Ln}\left(\frac{\alpha}{\alpha - w}\right) = e\text{^}[(E\theta)/(RT_s^2)] \quad \textbf{(10)}$$

Where $\theta = T - T_s$ with T being the temperature and T_s being a reference temperature at the point of inflection, defined by the authors. This equation can be used for "n = 1", where a plot of $\frac{\log\log\alpha}{\alpha - w}$ against θ gives a straight line with slope $E/2.303RT_s^2$.

3.4. *Thermodynamics of Degradation*

The thermodynamic parameters of degradation can be calculated from the following equations (**Straszko et al., 1997; Humienik, and Mozejko, 2000**):

$$\Delta H = Ea - RT \quad \textbf{(11)}$$

$$Ae^{\frac{-Ea}{RT}} = \frac{KBT}{h} e^{\frac{-\Delta G}{RT}} \quad \textbf{(12)}$$

$$\Delta G = \Delta H - T\Delta S \quad \textbf{(13)}$$

where, *ΔG*, *ΔH* and *ΔS* are free energy, enthalpy and entropy, receptivity. K_B and h are the Boltzmann and Plank constant, respectively.

4. Results and Discussion

4.1. *Degree of Polymerisation*

The degree of polymerisation (DP) of both the starting pulps (P1 and P2) and their respective finished microcrystalline cellulose powder products (F1 and F2) were estimated using the standard method according to ASTM D1795 which is based on intrinsic viscosity measurement of the samples in cupriethylenediamene (CUEN) solution. The results are shown below in **Table 2.**

Table 2. Degree of polymerisation of starting pulps and finished MCC powder samples

Sample	Degree of Polymerisation
P1	1161
P2	770
F1	221
F2	215

The difference in DP between the pulps P1 and P2 can be attributed to the origin of wood source in generating the pulps; P1 is manufactured from northern softwood Spruce while P2 is generated from eucalyptus hardwood; hardwood pulps generally exhibit lower DPs compared to softwood pulps (**Chen et al., 2017**). However, post hydrolysis it can be seen that both MCC powder products have a similar degree of polymerisation indicating a controlled hydrolysis step to a specific "Levelling off Degree of Polymerisation" (LODP) target during the conversion of the two pulps to MCC.

4.2. *Alkali Solubility (S10 & S18)*

The solubility of cellulose pulps in sodium hydroxide solutions can provide information as to the amount of lower molecular weight carbohydrates (degraded short chained cellulose and hemicellulose) content remaining in the pulp following the delignification process (**Wilson t al., 1952; Ohlsson, 1952**). A 10% sodium hydroxide solution possesses maximum dissolving power and will dissolve both degraded cellulose and hemicellulose content (**Tappi, 2000**). The weight percentage extracted by the 10% sodium hydroxide solution (S10) was determined by the TAPPI 235-OM Standard Method, and the insoluble content retained (R10) can be considered a good approximation of the long chained α-cellulose percentage, (R10 = 100 - S10). Furthermore, an 18% sodium hydroxide solution will generally dissolve only the hemicellulose contents (S18 via TAPPI 235-OM)) and the remaining short chained degraded cellulose with a degree of polymerization between approximately 50 and 150 can be determined by S10 – S18 (**Jahan et al., 2007**).

Table 3. Alkali Solubility of Selected Pulps

Pulp	R10,%	S10,%	S18,%	S10-S18, %
P1	90.5	9.5	5.1	4.4
P2	87.6	12.4	6.4	6.0

The alkali solubility results given in **Table 3** above show that the spruce softwood pulp P1 has a marginally higher R10 value than the eucalyptus hardwood pulp indicating a higher α-cellulose content. Both pulps show relatively similar breakdown between the hemicellulose content (S18) and the degraded short chained content (S10-S18). The relative constituents of the two pulps (α-cellulose vs short chained cellulose vs hemicelluloses) can be said to be similar despite the large differences in degree of polymerisation as outlined above, suggesting that the

delignification process (acid sulphite for both pulps) is the key determinant in the pulp constituents, and therefore differences in degree of polymerization as shown above in **Table 2** are due largely to pulp wood source.

4.3. *FT-IR analysis of pulp and MCC samples*

The FT-IR spectra of the pulp and MCC product samples are shown in **Figure 1**. The four samples exhibited similar spectra. The broad band at 3347 cm^{-1} is from the stretching of –O-H groups and the lower wave-number peak at 3309 cm^{-1} is assigned to intra-molecular hydrogen bonding (**Maréchal, and Chanzy, 2000**). The peak at 2908 cm^{-1} is assigned to C-H stretching. The band at 1650 cm^{-1} is due to absorbed water. The band at 1434 cm^{-1} is attributed to C-O-H bending while the band at 1326 cm^{-1} is assigned to C-H bending. The strong band at 1033 cm^{-1} is attributed to the C–O stretching of primary alcohols characteristic of cellulose, including a satellite at 998 cm^{-1} indicating alternative conformations of the primary alcohols. Peaks at 1110 cm^{-1} and 1160 cm^{-1} just visible off the main 1033 cm^{-1} band are likely to be C-O-C cellulose ring modes (**Maréchal, and Chanzy, 2000**). The peaks identified in the spectra that can be attributed to those characteristic of cellulose, while it can also be noted that peaks associated with hemicelluloses (**Kačuráková et al., 2000**) are not distinguishable indicating a relative high degree of α-cellulose purity.

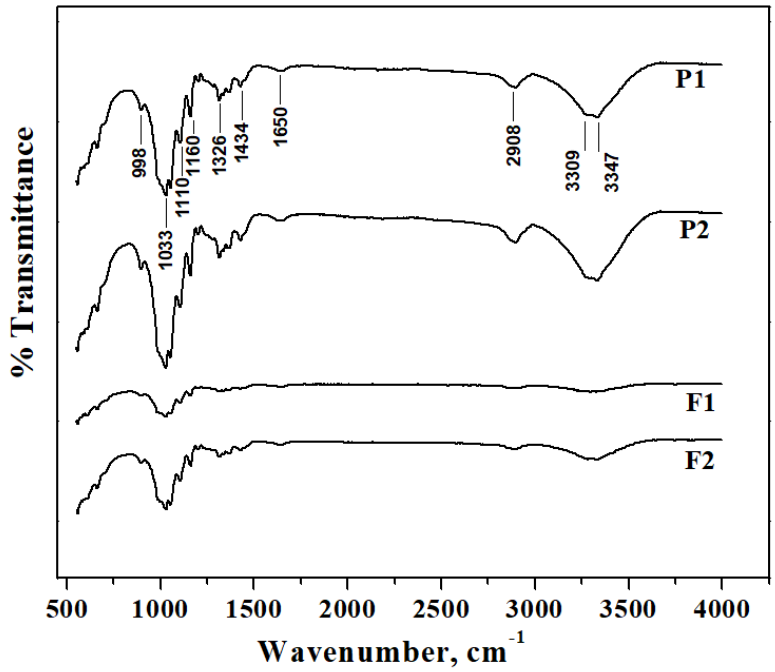

Figure 1. FT-IR spectra of selected pulp samples (labelled in the figure).

4.4. *Raman analysis of pulps*

Figure 2 compares the Raman spectra of the pulps under investigation. All four spectra are similar with peaks occurring at 380, 436, 493, 517, 897, 971, 996, 1094, 1119, 1336, 1378, 1472 and 2894 cm^{-1} attributed to cellulose (**Gierlinger et al., 2013**) Position and assignment of the Raman bands are presented in **Table 4**.

The peak at 380 cm^{-1} is known to be characteristic of crystalline cellulose and it is speculated to originate from one torsion or bending modes of the six-membered ring with respect to the glycosidic bonds (**Lee at al., 2016; Agarwal et al., 2010; Schenzel et al., 2005**). Generally, hemicelluloses do not exhibit a peak at 380 cm^{-1} while they can show broad peaks in the CH_2 bending vibration region (**Lee et al., 2016**). Agarwal et al. studied the effect of changes in crystallinity on the shape cellulose Raman bands and resulted that amorphous cellulose shows significant decline in band heights accompanied by band broadening (**Agarwal and Ralph, 1997**). It is noted that some peaks for the finished product MCC are different in shape and intensity relative to the two pulps, for instance at 436 cm^{-1} and 493 cm^{-1} which is likely due to differences in amorphous content.

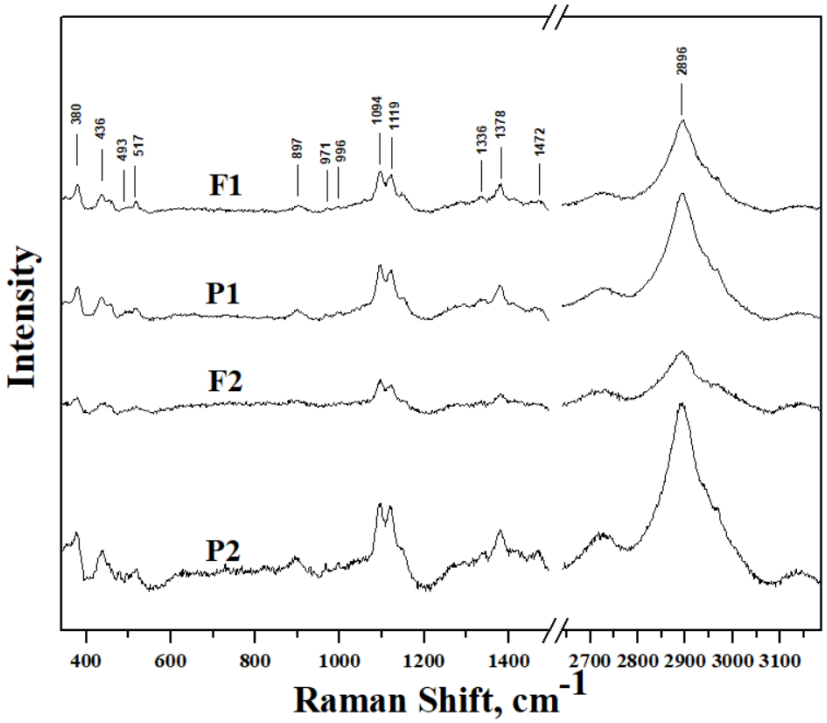

Figure 2. Raman spectra of selected pulp samples (labelled in the figure).

Table 4: Position and assignment of the Raman bands of the pulp samples (**Gierlinger et al., 2013)**

Raman bands (cm^{-1})	Assignment
380	δ (CCC) ring
436	Γ (COC) def
493	ν (COC) glycosidic
517	δ (COC) glycosidic
897	υ (COC) in plane, sym
971	ρ (CH_2)
996	ρ (CH_2)
1094	υ (COC) glycosidic, asym
1119	υ (COC) glycosidic, sym
1336	ω (CH_2)
1378	δ (CH_2)
1472	δ (CH_2), δ (COH)
2896	υ (CH)

(*def:* deformation, *sym:* symmetric, *asym:* antisymmetric)

4.5. *XPS analysis of pulps and MCC powder products*

The XPS spectra for the two MCC powder products and their respective raw material pulps are given in **Figure 3** below. Significant carbon C_{1S} and oxygen O_{1S} peaks were observed around 287 – 288 eV and 533 to 535 eV respectively. The relative surface carbon and oxygen percentages are given in **Table 5**. The C_{1S} spectrum of cellulose can be separated in to three categories (**Dorris and Gray, 1978**): (1) C_1 is carbon-carbon or carbon-hydrogen bonding, (2) C_2 is carbon having a single bond with one oxygen, (3) C_3 is carbon bonded to one oxygen atom of a carbonyl group or carbon bonded to two oxygen atoms of a non-carbonyl group. **Figure 3** shows the 'C_{1S}' XPS spectra for the four samples and **Table 5** details the binding energy and relative percentages of each carbon category for the four pulps being investigated.

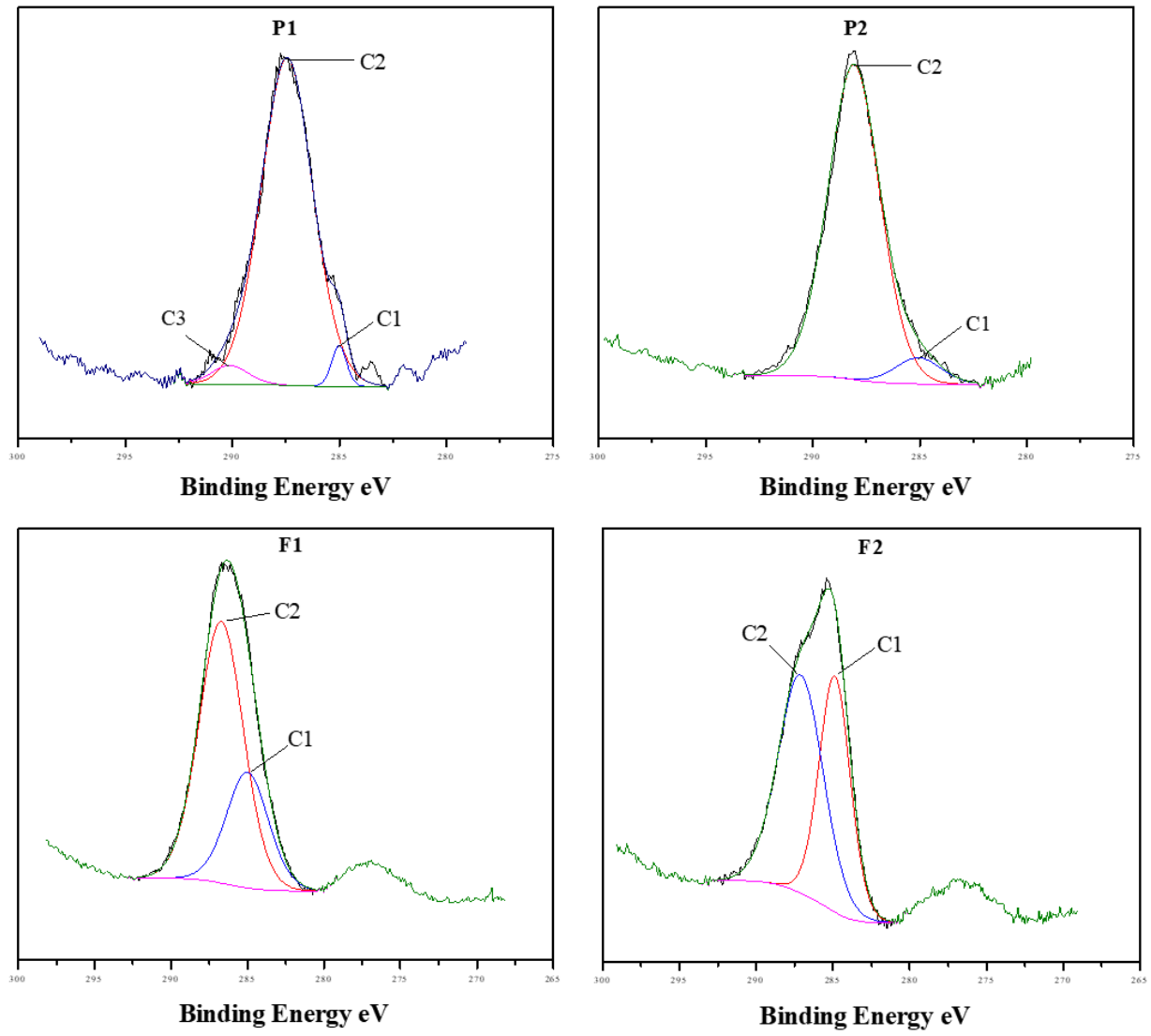

Figure 3. High-resolution XPS C 1s spectra of selected pulp and MCC samples (labelled in the figures).

Hydroxyl groups on the 1, 3 and 6 carbons of the β-D-glucopyranose rings of the cellulose and hemicellulose structure are known to take part in intra and inter molecular hydrogen bonding resulting in a strong hydroxyl domain in the inner cellulose structure and the associated dominance of the C_2 category (**Zhang et al., 2009**). The P1 and P2 pulps showed similar spectra with the C_2 category accounting for over 90%, whereas their respective MCC powder products, F1 and F2, showed reduced C_2 area suggesting lower hemicellulose content and possible a reduction in crystallinity following the hydrolysis process (correlating with the XRD analysis below). Pulp P1

exhibited a small C_3 area which may be due to some oxidized groups in the exposed surface cellulose chain resulting from the delignification and bleaching process (**Gustafsson, 2007**). When comparing the MCC samples, F1 had a higher C_2 area than F2 (70.54% vs 57.34%) and this relative difference in C_2 area is not noticed when comparing their corresponding pulps.

Table 5. C_{1S} categories binding energy and relative areas for selected pulps

	Survey Spectra		**Deconvolution Spectra**					
			C_1		**C_2**		**C_3**	
Pulp	**Carbon (%)**	**Oxygen (%)**	**Binding Energy (eV)**	**Area (%)**	**Binding Energy (eV)**	**Area (%)**	**Binding Energy (eV)**	**Area (%)**
P1	60.14	39.86	285.01	3.29	287.44	92.87	290.12	3.83
P2	73.61	26.39	285.07	6.86	288.07	93.14	-	-
F1	67.39	32.61	285.00	29.46	286.72	70.54	-	-
F2	69.79	30.21	284.88	42.66	287.10	57.34	-	-

4.6. *XRD analysis of pulps and MCC powder products*

Figure 4 below shows the X-ray diffraction scans for the two selected pulps and their corresponding MCC powder products. The characteristic cellulose I_{002} peak at around 22.6° 2θ as assigned by Segal et. al (1959) is observed in all samples in addition to the amorphous peak at around 18° 2θ. The relative intensity of the I_{002} and amorphous peaks was used to determine the degree of crystallinity and the Scherrer equation was used to estimate the crystallite size for each pulp sample (**Mohkami and Talaeipour, 2011**); results are given in **Table 6**. It is worth noting that the pulp samples and their respective MCC powder products did not show significant differences in crystallinity, with the MCC powder products surprisingly showing a slight reduction over the pulps. Similar results have been found by **Vanhatalo and Dahl (2014)** and also **Tolonen et al., (2011)**. An explanation for this is proposed by **Vanhatalo and Dahl (2014)** whereby two counter-mechanisms may be at operation: firstly, the hydrolysis of the amorphous content releasing individual crystallites and therefore increasing crystallinity, and secondly, damage to crystalline regions (by swelling and hydrolysis) leading to a reduction in crystallinity. This conclusion is also proposed by **Sun et al., (2008)**, and is consistent with the XPS analysis above.

The crystallinity index values given in **Table 6** are within the range for typical crystallinity index measurements for commercial Avicel® MCC (**Park et al., 2010**). It should also be noted that

Park et al., (2010) reviewed extensive literature on measurement of the crystallinity index of commercial Avicel® MCC products and concluded that the results depend greatly on the specific XRD instruments and on the computation method used. Therefore, it is generally accepted that relative crystallinity values are useful in comparing within a given study rather than the absolute values.

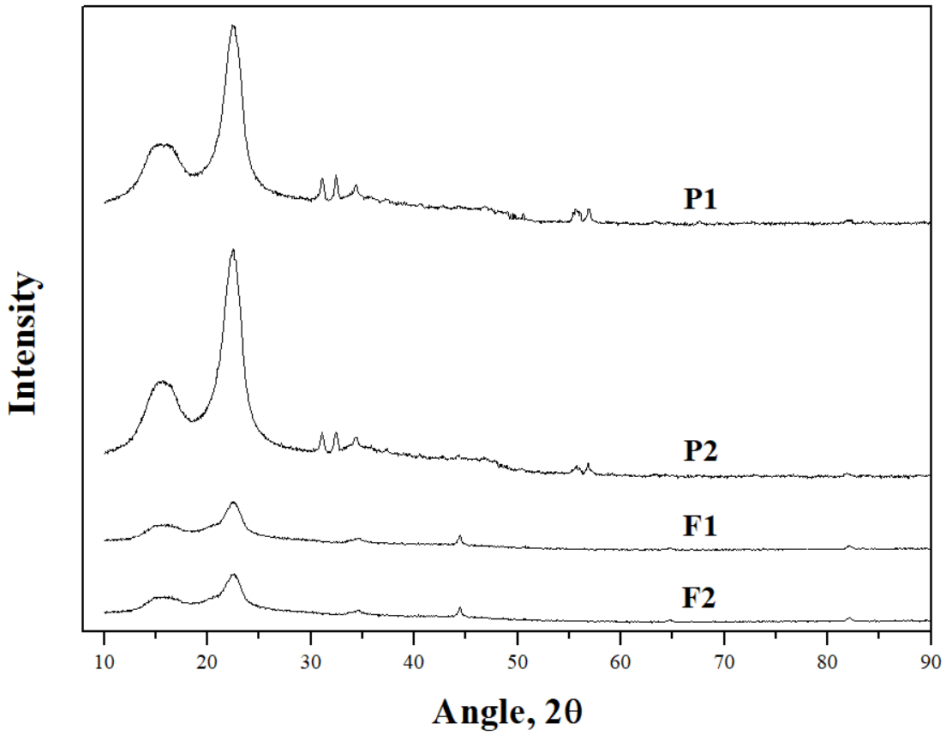

Figure 4. XRD diffractograms of selected pulp and MCC samples (labelled in the figure).

Table 6. Crystallinity index and crystallite size of selected pulps and MCC products

Pulp	Crystallinity index (%)	Crystallite size (nm)
P1	50.2	3.81
P2	50.7	3.34
F1	49.2	3.34
F2	48.6	3.48

4.7. *SEM*

The surface morphology of the MCC powder samples was analysed by SEM and the resulting micrographs are shown in **Figure 5**. The surface morphology of the pulp samples (P1 and P2) are given in the Chapter 2. The particle size distribution of commercial MCC grades is determined during the spray drying step and it should be noted that both MCC Avicel® PH102 samples relevant to this study were both produced within the tight specification range for particle size.

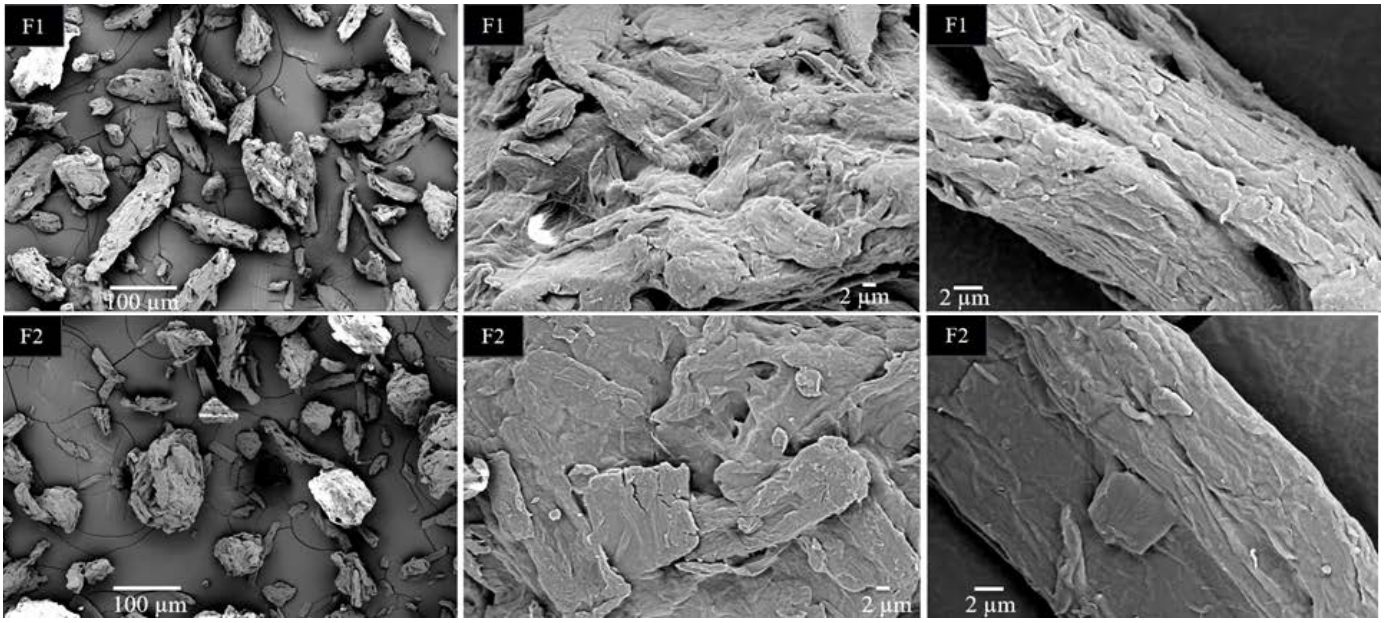

Figure 5. SEM images of selected MCC samples F1 and F2

From **Figure 5,** the F1 powder sample shows the typical rod-like shape common to MCC, whereas the SEM micrograph for F1 at the same 100 µm range shows the particles as having a more even length / diameter ratio. Sample F1 was produced from pulp sourced from a softwood (spruce), while sample F2 was produced from pulp sourced from a hardwood (eucalyptus) which has a significantly shorter fibre length than the spruce softwood (demonstrated in the SEM images in Section 4 of Chapter 2). The shorter fibre associated with pulp P2 may result in the smaller particle sizes agglomerating during the spray drying MCC production stage, giving the more rounded like particles for F2, in contrast to the more rod like particles of sample F1.

4.8. *TEM analysis of MCC samples*

The two MCC samples, F1 and F2 were analysed by Transmission Electron Microscope (TEM) and the resulting micrographs are given in **Figure 6**.

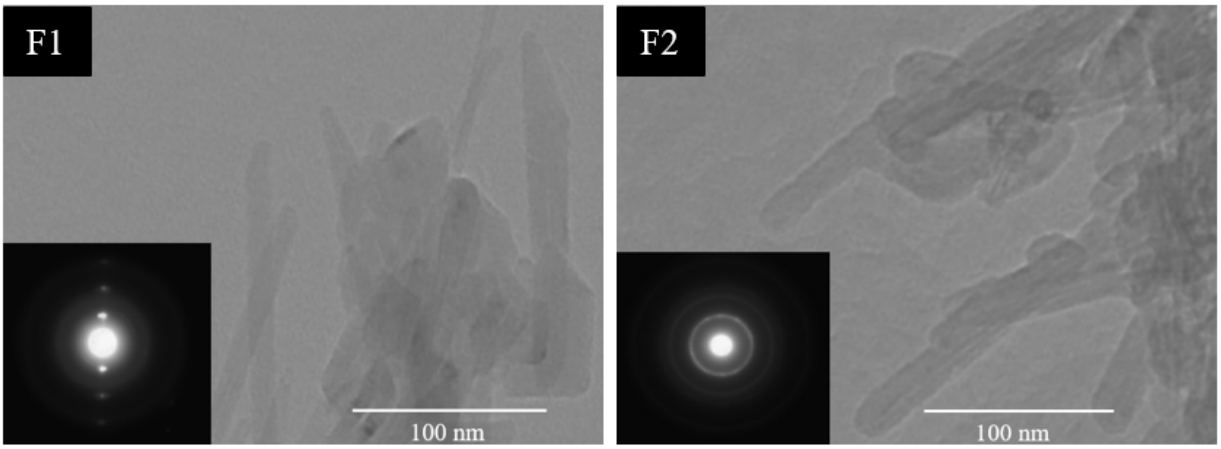

Figure 6. TEM microcgraphs and electron diffraction pattern (*insert*) for MCC samples F1 and F2

Electron microscopic imaging of microcrystalline cellulose is challenging and usually more suited to nanocellulose 'whiskers'. Following hydrolysis of the pulp, the microcrystals liberated tend to agglomerate to small particles and further agglomerate to larger particles during the spray drying stage (as shown in the SEM images above). Therefore, even with sonication and other preparation techniques it is difficult to obtain individualised cellulose microfibrils. It has been suggested in the literature that more aggressive hydrolysis may lead to an increase in individualised microfibrils, however this is not advantageous as it will also result in reducing the microfibril length and damage to the crystalline structure (**Chanzy, 1990; Elazzouzi-Hafraoui et al., 2008; Sugiyama et al., 1994**). The images shown in **Figure 6** show fibril diameter in the order of 15 to 25 nm for both F1 and F2 samples, with no significant differences in images between the two MCC samples studied.

Electron diffraction may be used to understand crystallinity and crystalline structural parameters, however the reflection intensities of electron diffraction for microcrystalline cellulose prove to be very difficult to evaluate (**Zugenmaier, 2008**). Analysis of multiple diffraction patterns for both F1 and F2 samples did not show significant differences nor information regarding crystallinity. In contrast, XRD analysis clearly shows the 002 plane and crystallinity indices may be determined as outlined above.

4.9. *TGA analysis of pulps*

Thermogravimetric analysis (TGA) was carried out on the two MCC powder products, F1 and F2, and their respective celluloses pulps P1 and P2. **Figure 7** shows the TGA results at the three selected heating rates: 5 °C min^{-1}, 10 °C min^{-1}, 20 °C min^{-1}. A minor weight loss region is observed from around 35 °C to 130 °C for both the pulp and MCC powder samples, which can be attributed to water loss, and the amount of weight lost for all samples during this step is comparable. A major thermal degradation stage takes place in the 320 °C to 375 °C temperature range for the two pulp samples and slightly lower for the MCC powder samples: 285 °C to 360 °C. The major degradation step corresponds to the decomposition of cellulose and hemicellulose (**Poletto et al., 2011**). The depolymerisation of both the crystalline α-cellulose and the various hemicelluloses occurs *via* random cleavage of the glycosidic linkages and subsequent rapid oxidative decomposition, with the hemicellulose content degrading first in the 150 °C to 350 °C range while the α-cellulose decomposition occurs from 275 °C (**Kim et al., 2006**). A third significant degradation step occurs from around 350°C to 500°C and this is attributed to ash formation. Lignin present on the pulp is also likely to contribute to the char formation (**Sonia and Pryia Dasan, 2012**).

The chemical structure of hemicellulose is amorphous with random branching and is easily hydrolyzed; it is this structural property that may result in higher thermal activity than the α-cellulose (**Poletto et al., 2011**). The α-cellulose structure is highly organized consisting of long chained polymers of glucose units arranged in a crystalline manner, with free hydroxyl groups likely to be involved in intramolecular and intermolecular hydrogen bonding (consistent with the FT-IR peak observed at 3309 cm^{-1}). High crystallinity coupled with hydrogen bonding is likely to be the reason for the increased thermal stability of cellulose relative to hemicellulose (**Ouajai and Shanks, 2005)**. **Figure 7** shows that for all four samples, the onset temperature of the major degradation step is increased with increasing heating rate. As the temperature intervals of the hemicellulose and cellulose decomposition steps partially overlap (**Poletto et al., 2011**), noticeable separation of the decomposition steps will only be possible when the hemicellulose content is relatively high (alkali solubility analysis shows hemicelluloses content of pulps P1 and P2 to be in the region of 5% to 6%).

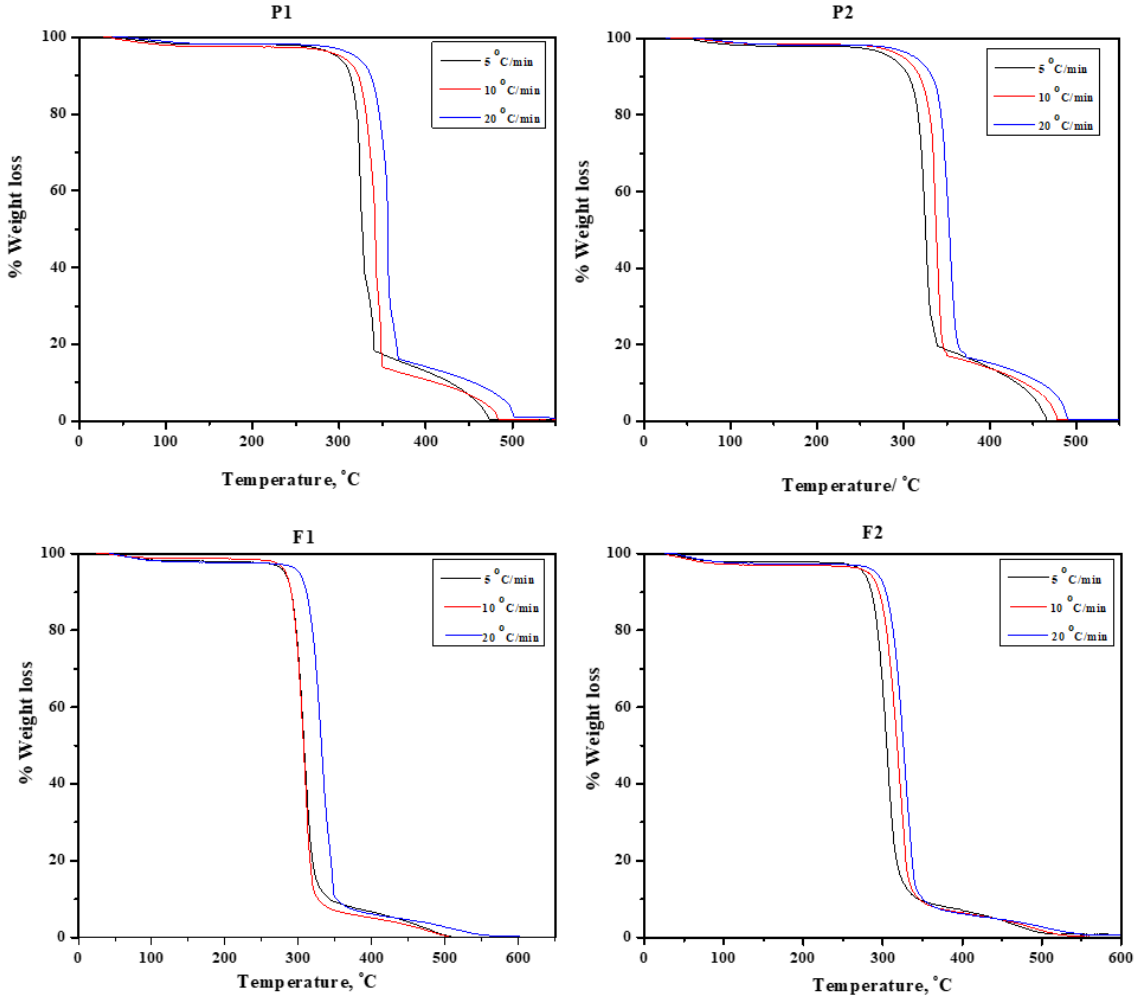

Figure 7. TGA thermograms of selected pulp samples (labelled in the figures).

The temperature range and weight loss percentage for the minor and major decomposition steps for each of the three heating rates are given in **Table 7**. The results show that the temperature interval and weight loss percentage associated with the major cellulose degradation step for both P1 and P2 pulps are comparable. The respective results for the F1 and F2 MCC powder product major degradation step show a slight reduction in the onset temperature, with the onset temperatures averaging at ~300°C for the MCC in comparison to ~330°C for the pulps.

Table 7. Weight loss data from TG analysis of selected pulps

Pulp	Heating Rate (°C/min)	Weight Loss Temperature Range (°C)		Weight Loss (%)	
		Minor	Major	Minor	Major
P1	5	38 – 120	319 – 340	1.7	64.1
P1	10	38 – 126	331 – 350	2.3	65.3
P1	20	55 – 130	342 – 373	1.7	69.3
P2	5	50 – 125	313 – 338	1.9	64.9
P2	10	57 – 130	326 – 350	1.4	67.4
P2	20	67 – 136	338 – 374	1.5	69.9
F1	5	37 – 113	285 – 342	1.4	82.5
F1	10	40 – 129	301 – 352	1.3	81.1
F1	20	44 – 132	313 – 358	1.2	76.9
F2	5	35 – 108	288 – 349	1.9	81.2
F2	10	38 – 130	300 – 355	2.0	78.6
F2	20	40 – 131	308 – 362	2.1	78.0

The lower onset temperatures for the MCC F1 and F2 samples may be attributed to lower crystallinity (**Ouajai and Shanks, 2005**) as also observed by XRD and XPS analyses. Furthermore, given that the MCC samples are in the form of a fine powder with far greater surface area than the pulp samples, it would be likely that the powder form of cellulose would show an earlier thermal degradation onset when compared with pulp cellulose.

A significant difference was observed in the percentage weight loss of the major degradation steps, with the pulp samples showing greater thermal stability, possibly due to higher crystallinity, and maybe also due to lignin content in the pump prior to the hydrolysis (**Sonia and Pryia Dasan, 2012**)**.** Importantly, there was no significant difference in the thermal degradation profile when comparing the MCC products F1 and F2 against each other.

4.10. *Kinetic analysis of pulp and MCC samples*

Kinetic parameters for the thermal decomposition of the speciality cellulose dissolving pulps under investigation were determined by application of the Coats and Redfern integral model (**Coats and Redfern, 1964**) equation. The pulp degradation was assumed to follow first order reaction kinetics (n = 1) and a plot of ln $\left[\frac{-\ln(1-\alpha)}{T^2}\right]$ against 1/T in all cases showed pseudo-straight lines across the range of the major decomposition step as can be seen in **Figure 7**.

Application of the Freeman and Carroll's (**Freeman and Carroll, 1958**) differential kinetic model can be seen in **Figure 8** below, where for "n=1" plotting log $\left[\frac{\frac{dw}{dt}}{\alpha-w}\right]$ against 1/T gives pseudo-straight lines and numerical values of Ea and A were calculated from the slope and intercept, respectively.

Plots of $\frac{\log\log\alpha}{\alpha-w}$ against θ for the "n=1" case of Horowitz and Metzger's kinetic model (**Horowitz and Metzger, 1963**) gives straight lines as can be seen in **Figure 9** below.

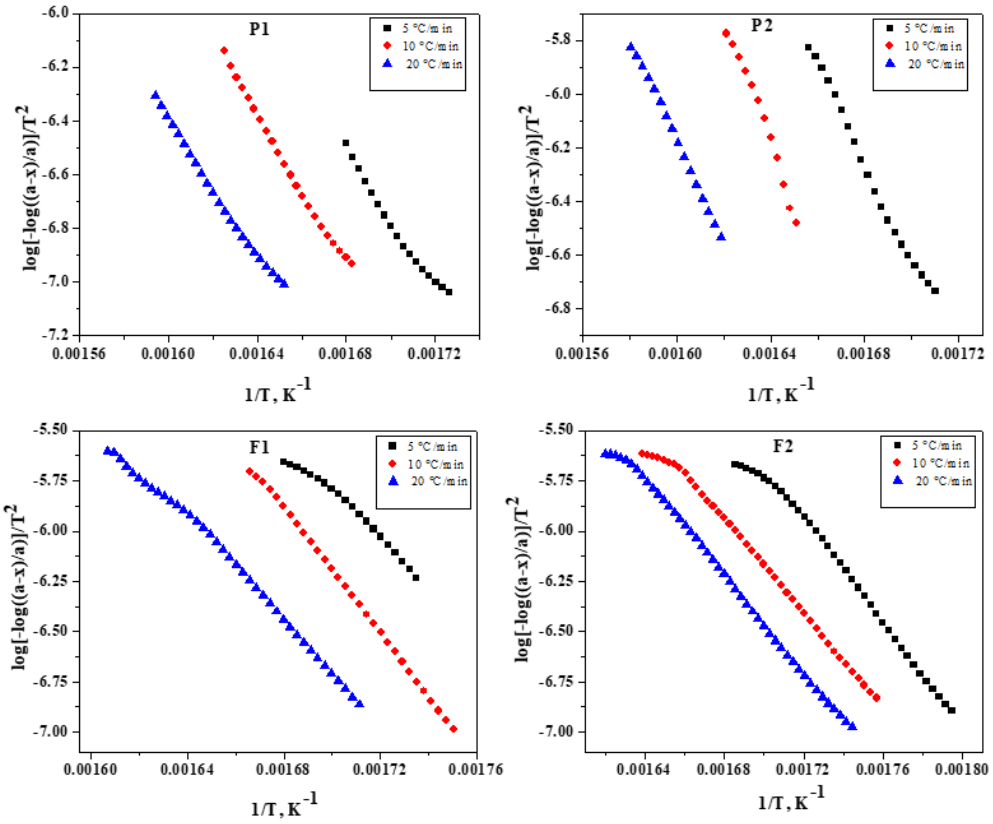

Figure 7. Coats and Redfern kinetic plots for the selected pulps (labelled in the figure).

The results for each of the three kinetic models are given below in **Table 8**. Activation energy values were comparable for all four samples for each of the three kinetic models, (with the Coats and Redfern and Horowitz and Metzger model results matching closely). The activation energy for P2 pulp being higher than the P1 pulp and a reason for this may be due to the relative fibre size. As demonstrated by the SEM analysis in Chapter 2, the average fibre diameter for the P2 hardwood pulp was significantly lower than for the P1 pulp. The tight packing of the cellulose chains of the P2 pulp (which also had the highest crystallinity level) may contribute to the higher activation energy required for thermal decomposition.

The frequency factor for the P2 pulp was also significantly higher than P1 pulp and this was observed for all three kinetic models. This is again likely to be due to the relative differences in the pulp morphologies. As can be seen from the SEM analysis in Chapter 2, the P2 pulp has more fibres per given weight and will therefore tend to have more collisions during the decomposition stage.

Both MCC products did not have significant differences in their kinetic parameters. Importantly, the higher activation energy and frequency factor associated with P2 did not replicated in its respective powder MCC product F2. The MCC products had slightly reduced activation energy when compared against the pulps, again likely due to the slight reduction in crystallinity (supported by the XRD and XPS analyses).

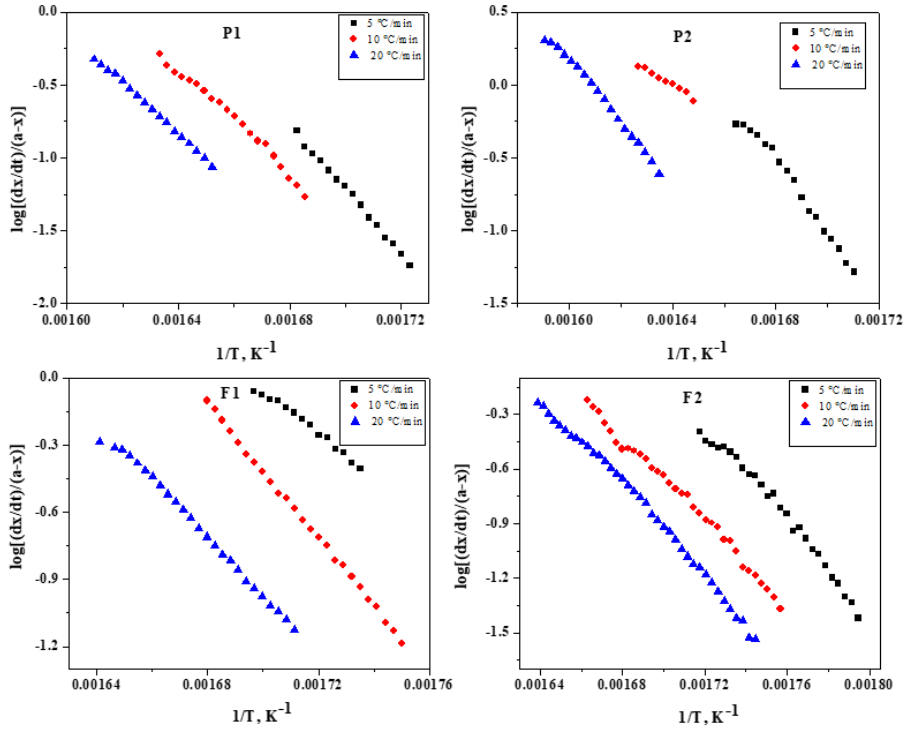

Figure 8. Freeman and Carroll kinetic plots for the selected pulps (labelled in the figure)

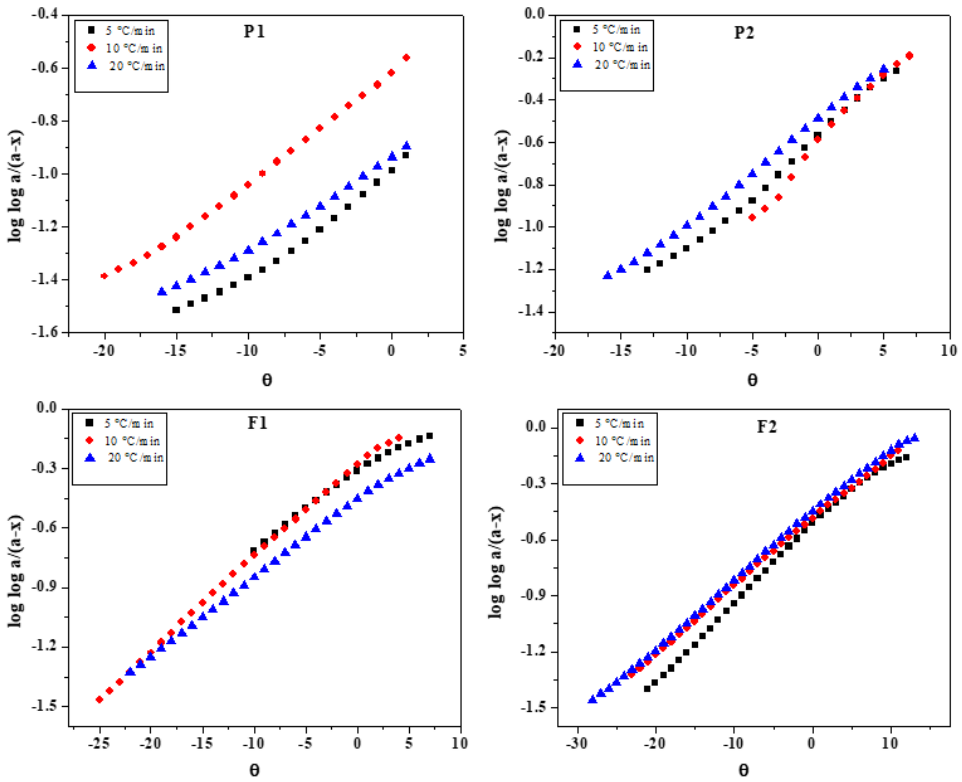

Figure 9. Horowitz and Metzger kinetic plots for the selected pulps (labelled in the figure).

Table 8. Kinetic parameters for the non-isothermal degradation of selected pulps and MCC powders.

		Coats & Redfern	Freeman & Carroll	Horowitz & Metzger	Coats & Redfern	Freeman & Carroll	Horowitz & Metzger	Coats & Redfern	Freeman & Carroll	Horowitz & Metzger
Pulp	**Heating rate ($°C\ min^{-1}$)**	**Specific rate constant (s^{-1})**			**Activation energy ($kJ\ mol^{-1}$)**			**Frequency factor (s^{-1})**		
P1	5	2.40×10^{-22}	1.67×10^{-38}	1.92×10^{-24}	231	423	247	7.49×10^{18}	2.14×10^{36}	3.47×10^{19}
P1	10	5.36×10^{-26}	1.03×10^{-31}	9.99×10^{-29}	269	341	287	7.14×10^{21}	7.16×10^{28}	2.28×10^{22}
P1	20	9.81×10^{-24}	9.97×10^{-32}	6.73×10^{-25}	237	337	241	4.00×10^{18}	1.00×10^{28}	1.13×10^{18}
P2	5	5.81×10^{-32}	2.16×10^{-41}	2.12×10^{-34}	346	459	361	2.50×10^{29}	4.97×10^{39}	3.24×10^{29}
P2	10	8.52×10^{-54}	4.55×10^{-39}	2.50×10^{-36}	471	427	375	3.44×10^{29}	3.27×10^{36}	1.39×10^{30}
P2	20	3.50×10^{-33}	6.54×10^{-38}	2.78×10^{-36}	364	407	365	4.01×10^{29}	1.61×10^{34}	2.35×10^{28}
F1	5	1.98×10^{-19}	3.59×10^{-16}	1.57×10^{-22}	205	178	227	1.52×10^{17}	5.32×10^{15}	1.30×10^{18}
F1	10	9.03×10^{-28}	4.12×10^{-26}	2.09×10^{-30}	298	289	319	1.39×10^{25}	1.67×10^{25}	1.47×10^{26}
F1	20	4.94×10^{-23}	7.08×10^{-23}	2.10×10^{-26}	236	245	271	1.06×10^{19}	5.97×10^{20}	6.58×10^{21}
F2	5	9.22×10^{-22}	1.54×10^{-22}	1.76×10^{-24}	232	251	254	4.26×10^{19}	1.53×10^{22}	7.96×10^{20}
F2	10	1.47×10^{-20}	1.32×10^{-20}	2.10×10^{-23}	212	221	239	2.33×10^{17}	7.82×10^{18}	1.67×10^{19}
F2	20	5.01×10^{-22}	4.35×10^{-22}	3.99×10^{-24}	226	236	247	2.29×10^{18}	1.06×10^{20}	8.05×10^{19}

4.11. *Thermodynamic analysis of pulps*

The thermal degradation of the two pulp samples and their respective MCC powder products enable determination of thermodynamic parameters via the activated complex theory; results for enthalpy (ΔH), entropy (ΔS) and Gibb's free energy (ΔG) are given in **Table 9** for the respective kinetic models applied. The positive value of ΔH indicates the endothermic nature of cellulosic pulp degradation. There was no significant difference in enthalpy between the two MCC powder samples, F1 and F2, and were generally comparable with the pulp samples. Pulp P2 showed a larger value for ΔH (observed by all three models) relative to the other pulps and MCC samples.

The ΔS values for all four samples are positive indicating that thermal decomposition leads to an increase in disorder. The positive value of Gibb's free energy, ΔG confirms the non-spontaneous nature of the decomposition of cellulose.

Table 9. Thermodynamic parameter for the non-isothermal degradation of selected pulps and MCC powders.

		Coats & Redfern	Freeman & Carroll	Horowitz & Metzger	Coats & Redfern	Freeman & Carroll	Horowitz & Metzger	Coats & Redfern	Freeman & Carroll	Horowitz & Metzger
Pulp	**Heating rate ($°C\ min^{-1}$)**	**ΔH ($kJ\ mol^{-1}$)**			**ΔS ($J\ mol^{-1}\ k^{-1}$)**			**ΔG ($kJ\ mol^{-1}$)**		
P1	5	229	420	244	108	442	121	196	289	208
P1	10	266	339	285	165	299	175	217	250	233
P1	20	235	334	238	103	283	92	250	250	211
P2	5	343	456	358	310	507	312	305	305	265
P2	10	469	425	373	312	446	324	292	292	276
P2	20	362	405	362	314	402	290	285	285	276
F1	5	202	175	225	76	48	93	161	161	197
F1	10	295	286	316	228	230	248	218	218	242
F1	20	233	242	269	111	145	164	199	199	220
F2	5	230	249	252	123	172	147	197	197	209
F2	10	210	218	237	79	108	115	186	186	202
F2	20	224	234	245	98	130	128	195	195	207

5. Conclusions

A single commercial grade of microcrystalline cellulose (MCC) can be produced using pulps from different wood type and/or different delignification processes and subsequently released to customers following compliance with tight quality control and assurance systems. However, it is known that there are significant differences in pulps used to produce MCC, particularly in crystallinity and morphology (see Chapter 2 of this thesis), and the research objective of the present study was to understand if differences were observed in the final powder products produced solely from different pulps.

Pulp P1 and P2 were generated from softwood and hardwood sources respectively and a large difference in degree of polymerisation between the pulps was measured and attributed to difference in wood type. The resultant powder products F1 and F2 showed close alignment in degree of polymerisation indicating that the hydrolysis reaction in the MCC production step was tightly controlled to ensure that both powder products were produced within the specification constraints as expected. However, the crystallinity of both powder products was surprisingly lower than that of their respective starting pulps, suggesting that the industrial hydrolysis step resulted in damage to both amorphous *and* crystalline content of the pulps. This observation is significant for MCC manufacturers who could possibly benefit from adjusting reaction parameters to reduce damage to crystalline regions and increase yield.

There is little published research available concerning thermal degradation kinetics of MCC products made from different starting pulps. The results of this study showed that differences in activation energy and frequency factor for the decomposition of pulps from different wood type were significantly diminished when the kinetic parameters of the two respective powder products were compared. It is therefore suggested that processing of different pulps during the industrial production of MCC leads to significant reduction in differences in the final products, and observation highly important to commercial producers.

Acknowledgements

The authors wish to acknowledge AMBER Centre, Trinity College Dublin for providing financial support to carry out the research, and DuPont Nutrition and Health for pulp supply and onsite laboratory access. The authors would also like to acknowledge the Department of Anatomy & Neuroscience Imaging Centre, BioSciences Institute, University College Cork, for assistance in preparing and imaging specimens for this research.

References

Agarwal, U.P., Reiner, R.S., Ralph, S.A. (2010). Cellulose I crystallinity determination using FT-Raman spectroscopy: univariate and multivariate methods. Cellulose 17(4), 721-733.

Agarwal, U.P., Ralph, S.A. (1997). FT-Raman spectroscopy of wood: Identifying contributions of lignin and carbohydrate polymers in the spectrum of Black Spruce (Picea mariana). Appl. Spec. 51, 1648-1655.

Almaya, A., Aburub, A. (2008). Effect of particle size on compaction of materials with different deformation mechanisms with and without lubricants. AAPS PharmSciTech 9, 414–418.

Chanzy, H. Kennedy, J.F., Philips, G.O., William, P.A. (1990). Aspects of cellulose structure. In Cellulose Sources and Exploitation. Ellis Horwood Ltd.: New York, NY, USA, pp. 3–12.

Chen, Y., Geng, B., Ru, J. (2017). Cellulose 24: 4831. https://doi.org/10.1007/s10570-017-1478-4

Coats, A.W. and Redfern, J.P. (1964). Kinetic Parameters from Thermogravimetric Data. Nature, 201, 68-69

Dorris, G.M., Gray, D.G. (1978). The surface analysis of paper and wood fibres by ESCA. II. Surface composition of mechanical pulps. Cell. Chem. Technol. 12, 721-734.

Dumarey, M., Wikstrom, H., Fransson, M., Sparen, A., Tajarobi, P., Josefson, M., Trygg, J. (2011). Combining experimental design and orthogonal projections to latent structures to study the influence of microcrystalline cellulose properties on roll compaction. Int. J. Pharm. 416, 110–119.

Elazzouzi-Hafraoui, S.; Nishiyama, Y.; Putaux, J.L.; Heux, L.; Dubreuil, F.; Rochas, C. (2008). The shape and size distribution of crystalline nanoparticles prepared by acid hydrolysis of native cellulose. Biomacromolecules *9*, 57–65.

Freeman, E. S. and Carroll, B. J. (1958). Phys. Chem., 62, 394

Gierlinger, N., Keplinger, T., Harrington, M., Schwanninger, M. (2013). Raman imaging of lignocellulosic feedstock, Cellulose - Biomass Conversion. Prof. John Kadla, InTech, DOI: 10.5772/50878.

Gustafsson, J., Ciovica, L., Peltonen J. (2002). The ultrastructure of spruce kraft pulps studied by atomic force microscopy (AFM) and X-ray photoelectron spectroscopy (XPS). Polymer 44, 661-670.

Hon, D. N.-S., Shiraishi, N. (2000). Wood and Cellulosic Chemistry, Second Edition, Revised, and Expanded (2000-11-08). 1786. ISBN: 9780824741358

Horowitz, H. H. and Metzger G. (1963). Anal. Chem., 35, 1464.

Humienik, M.O., Mozejko, J. (2000). Thermodynamic functions of activated complexes created in thermal decomposition processes of sulphates. Thermochim. Acta 344, 73-79.

Ibarra, D., Köpcke, V., Larsson, P.T., Jääskeläinen, A.S., Ek, M. (2010). Combination of alkaline and enzymatic treatments as a process for upgrading sisal paper-grade pulp to dissolving-grade pulp. Bioresour. Technol. 101, 7416-7423.

Jahan, M.S., Al-Maruf, A, Quaiyyum, M.A. (2007). Bangladesh Journal of Scientific and Industrial Research. 1952, 01/2007; 42(4):425-434

Johansson, L.S., Campbell, J.M., Koljonen, K., Stenius, P. (1999). Evaluation of surface lignin on cellulose fibers with XPS. Appl. Surf. Sci. 144-145, 92-95.

Kačuráková, M., Capek, P., Sasinková, V., Wellner, N., Ebringerová, A. (2000). FT-IR study of plant cell wall model compounds: pectic polysaccharides and hemicelluloses. Carbohyd. Polym. 43, 195-203.

Kim, H.-S., Kim, S., Kim, H.-J., Yang, H.-S. (2006). Thermal properties of bio-flour-filled polyolefin composites with different compatibilizing agent type and content. Thermochim. Acta 451, 181-188.

Koo, O.M.Y., Heng, P.W.S. (2001). The influence of microcrystalline cellulose grade on shape and shape distributions of pellets produced by extrusion–spheronization. Chem. Pharm. Bull. 49, 1383–1387.

Krassig, H. (1985). Cellulose and its derivatives: Chemistry, biochemistry and applications, J.F. Kennedy, G.O. Phillips, D.J. Wedlock, P.A. Williams (eds), Ellis Horwood Limited Publishers, Chichester, UK.

Landín, M., Martínez-Pacheco, R., Gómez-Amoza, J.L., Souto, C., Concheiro, A., Rowe, R.C. (1992). Effect of batch variation and source of pulp on the properties of microcrystalline cellulose. Int. J. Pharm. 91, 133-141.

Landin, M., Vazquez, M.J., Souto, C., Concheiro, A., Gomezamoza, J.L., Martinezpacheco, R. (1992). Comparison of 2 varieties of microcrystalline cellulose as filler-binders. 1. Prednisone tablets. Drug Dev. Ind. Pharm. 18, 355–368.

Lee, C., Dazen, K., Kafle, K., Moore, A., Johnson, D.K., Park, S., Kim, S.H. (2016). Correlations of apparent cellulose crystallinity determined by XRD, NMR, IR, Raman, and SFG methods. Adv. Pol. Sci. 271, 115-132.

Maréchal, Y., Chanzy, H. (2000). The hydrogen bond network in Iβ cellulose as observed by infrared spectrometry. J. Mol. Struct. 523, 183-196.

Mohkami, M., Talaeipour. M. (2011). Investigation of the chemical structure of carboxylated and carboxymethylated fibers from waste paper *via* XRD and FTIR analysis. Bioresources 6, 1988-2003.

Ohlsson, K. E. (1952). The Alkali Solubility of Pulps. Svensk Papperstid. 55(10): 347.

Ouajai, S., Shanks, R. A. (2005). Morphology and structure of bioscouring hemp fibre. J. Macromol. Biosci. 5, 124-134.

Park, S., Baker, J. O., Himmel, M.E., Parilla, P.A., and Johnson, D. K. (2010). CEllulsoe crystallinity index: Measurement techniques and their impact on interpreting cellulase performance, Biotechnol. Biofuels 3(10), 1-10.

Poletto, M., Pistor, V., Zeni, M., Zattera, A.J. (2011). Crystalline properties and decomposition kinetics of cellulose fibers in wood pulp obtained by two pulping process. Polym. Degrad. Stab. 96, 679-685.

Poletto, M., Zattera, A.J., Forte, M.M.C., Santa, R.M.C. (2011). Thermal decomposition of wood: Influence of wood components and cellulose crystallite size. Bioresource Technol. 109, 148-153.

Schenzel, K., Fischer, S., Brendler, E. (2005). New method for determining the degree of cellulose I crystallinity by means of FT-Raman spectroscopy. Cellulose 12(3), 223-231.

Segal L., Creely, J.J., Martin Jr., A.E., and Conrad, C.M. (1959). An empirical method for estimating the degree of crystallinity of native cellulose using X-ray diffractometer, Textile Research Journal 29, 786-794.

Soh, J.L.P., Wang, F., Boersen, N., Pinal, R., Peck, G.E., Carvajal, M.T., Cheney, J., Valthorsson, H., Pazdan, J. (2008). Utility of multivariate analysis in modeling the effects of raw material properties and operating parameters on granule and ribbon properties prepared in roller compaction. Drug Dev. Ind. Pharm. 34,1022–1035.

Sonia, A., Priya Dasan, K. (2013). Chemical, morphology and thermal evaluation of cellulose microfibers obtained from Hibiscus sabdariffa. Carbohyd. Polym. 92, 668-674.

Straszko, J., Humienik, M.O., Mozejko, J. (1997). Kinetics of thermal decomposition of $ZnSO_4 \cdot 7H_2O$. Thermochim. Acta, 292, 145-150.

Sugiyama, J.; Chanzy, H.; Revol, J.F. (1994). On the polarity of cellulose in the cell wall of Valonia. Planta, 193, 260–265

Sun, Y., Lin, L., Deng, H., Li, J., He, B., Sun, R., and Ouyang, P. (2008). Structureal changes of bamboo cellulose in formic acid, BioResources 3(2), 297-315.

Tappi, (2000). Alkali solubility of pulp, Tappi T235 OM- 60, Tappi Press, Atlanta.

Thoorens, G., Krier, F., Leclercq, B., Carlin, B., Evrard, B. (2014). Microcrystalline cellulose, a direct compression binder in a quality by design environment—A review, International Journal of Pharmaceutics 473 64–72.

Tolonen, K. L., Zuckerstatter, G., Penttyla, P.A., Milacher, W., Habicht, W., Serimaa, R., Kruse, A., and Sixta, H. (2011). Structural changes in microcrystalline cellulose in subcritical water treatment, Biomacromolecules 12(7), 2544-2551.

Vanhatalo, K.M., and Dahl, O.P. (2014) Effect of mild acid hydrolysis parameters on properties of microcrystalline celloluse, BioResources 9(3), 4729-4740.

Wilson, K., Ringstrom, E., and Hedlund, I. (1952). The Alkali Solubility of Pulp, Svensk Papperstid. 55(2): 31

Zhang, J., Zhang, J., Lin, L., Chen, T., Zhang, J., Liu, S., Li, Z., Ouyang, P. (2009). Dissolution of microcrystalline cellulose in phosphoric acid- molecular changes and kinetics. Molecules 14, 5027-5041.

Zugenmaier, P. (2008). Crystalline Cellulose and Cellulose Derivatives: Characterization and Structures, Springer-Verlag, Berlin-Heidelberg, pp. 101–174.

Chapter 4

Study of Acid Hydrolysis of Pulp to Microcrystalline Cellulose

Study of Acid Hydrolysis of Pulp to Microcrystalline Cellulose

Conor O'Regan*[a,b], Justin D Holmes[a,c,d], and Michael A Morris*[c,d]

[a] Materials Chemistry, Department of Chemistry, University College Cork, Cork, Ireland,

[b] DuPont Nutrition and Health, Cork, Ireland

[c] AMBER, Trinity College Dublin, Dublin 2, Ireland,

[d] Tyndall National Institute, Lee Maltings, Prospect Row, Cork, Ireland,

*Corresponding author: Email: conor.o-regan@dupont.com (Conor O'Regan), morrism2@tcd.ie (Michael A Morris) Ph: +353 18963089

ABSTRACT

A pulp sample used in the industrial MCC process was selected for an acid hydrolysis study. Degree of polymerisation reduction curves were generated for various temperature and acid concentration conditions and differences in reaction rate and equilibrium degree of polymerisation point were observed; with increasing temperature having a greater effect on both the rate and equilibrium point when compared with increasing acid concentration impact. Scanning electron microscopy and particle size distribution analyses surprisingly showed that large quantities of material remained physically intact during the early hydrolysis stages even though the degree of polymerisation reduction was at its fastest rate, an observation not given in the current literature and significant in terms of control of the reaction industrially. Furthermore, it was observed that samples continued to reduce in both particle size and degree of crystallinity throughout the degree of polymerisation equilibrium range, giving an important opportunity for identification of an optimum reaction end-point based on these parameters; such an end-point signal is not currently utilised in the industrial production of MCC and offers highly significant potential benefits to the commercial process.

Keywords: MCC; Pulp; Cellulose; Hydrolysis; Degree of Polymerisation

1. Introduction

During the conversion of pulp to MCC, industrial producers are required to reduce the degree of polymerisation to below 350 glucose units (**Thoorens et al., 2014**) however, there is no clearly defined end-point to the reaction, with producers only retrospectively adjusting reaction conditions and quench times based on downstream processing parameters and product final quality. For example, quenching the reaction too early leads to a viscous slurry that is difficult to transport and spray dry, while quenching too late results in poor filtration and increased yield losses. The goal of this study was to characterise the acid hydrolysis reaction of a pulp used in the industrial MCC process and understand the effect of temperature and acid concentration on degree of polymerisation, particle size and crystallinity; parameters of high importance to MCC producers. Furthermore, given that there is no clearly defined end-point to the hydrolysis reaction, this study endeavours to understand how changes in both particle size and crystallinity may be helpful in providing a real-time indication for such an optimum quench point.

The hydrolysis of cellulose to its glucose monomer requires high temperature and pressure (374°C / 22 MPa) and/or use of a catalyst to achieve effective reaction rates (**Kupiainan et al., 2014**). The production of *microcrystalline* cellulose (MCC), however, requires only partial depolymerisation of the cellulose which can be achieved with mineral acids at temperatures below 150°C.

The 'fringed fibrillar model' (**Hearle, 1963; Frey-Wyssling and Muhlethaler, 1965**) of the structure of cellulose describes cellulosic material of consisting of crystalline regions arranged in microfibrils interconnected by disordered amorphous areas. Hydrolysis depolymerization occurs when the β -1,4-glycosidic bonds of the cellulose are cleaved, however, access of the reactants to these sites is greatly inhibited due to the crystalline nature of α-cellulose where the structure is tightly packed. In contrast, the interconnecting amorphous kinks described in the fringed fibrillar model are less tightly packed and provide easier access for the reaction to occur. The rate of hydrolysis of the amorphous regions is therefore known to be much higher than that of the crystalline region (**Zhao et al., 2006**), and results in the release of the microfibril crystallites (**Gurnagul et al. 1992**) which ultimately form the MCC powder product following downstream filtration and drying steps.

The hydrolysis reaction proceeds rapidly initially with an exponential reduction in DP. As the reaction continues the rate of reduction in DP slows and reaches what is known as the level-off degree of polymerisation (LODP), with the LODP typically in the range of 180 to 210 for hardwood pulps and 210 to 250 for softwood pulps (**Doelker, 1993**). The reacted cellulose

samples were analysed by SEM, laser diffraction, Raman spectroscopy and XRD to understand changes in morphology, particle size distribution and crystallinity as the reaction proceeds over time for a given temperature and acid concentration. Mark-Houwink-Sakurada (MHS) parameters were applied to intrinsic viscosity results and average molecular weights calculated (**Łojewski et al., 2010**). In addition, the analyses described above were carried out to compare samples at LODP for reaction samples generated at different temperature and acid concentrations.

2. Materials and Methods

2.1. *Materials*

A sample of commercially available pulp used in the industrial manufacturing process of microcrystalline cellulose (MCC) was selected for this study. The pulp, labelled 'P3' in this paper, was generated originally from southern softwood (mostly Loblolly Pine), and delignified v*ia* the Kraft process followed by oxidative elemental chlorine free (ECF) bleaching (**Aro and Fatehi, 2017**). All materials were supplied courtesy of DuPont Nutrition and Health, Cork, Ireland.

2.2. *Hydrolysis of Pulp*

Acid hydrolysis was performed using 5 g (oven-dried) samples diced to approximately 2 x 2 mm chips. The samples were added to solutions of HCl which were pre-heated to the selected reaction temperature. For this study, HCl acid concentrations of 1M and 2M were used, at temperatures of 85°C and 95°C. Reactions were carried out in a 'Syrris Orb' 1 litre jacketed glass reactor under atmospheric pressure with cold water condensation applied. Temperature control of the reactor contents was maintained by thermal oil circulated via 'Julabo' temperature control unit using direct temperature measurement of the acid solution. Mild agitation of the reactor contents was applied consistently for all reactions.

On completion of the hydrolysis reaction at the selected reaction time, the reactor contents were immediately filtered and carefully washed with deionised water until a neutral pH was observed. The samples were air-dried before further analysis. All reactions were completed in duplicate.

2.3. *Degree of Polymerisation*

The degree of polymerisation (DP) for each sample was determined by ASTM D1795 standard method as required by the harmonized pharmacopoeia regulations for pharmaceutical grade MCC. This uses cupriethylenediamene (CUEN) solution to measure intrinsic viscosity and subsequent relation to average DP. The monograph stipulates viscosity measurement by

capillary type viscometer with the measured flow time multiplied by the apparatus constant to give a kinematic viscosity result. The intrinsic viscosity, $[\eta]_c$, is then determined by interpolation of the tabular relationship given in ASTM D1795. The DP is subsequently calculated by the following equation:

$$DP = \frac{95[\eta]_c}{m[(100-b)x10^{-2}} \quad \textbf{(1)}$$

Where *DP* is the degree of polymerisation, $[\eta]_c$ is the intrinsic viscosity, *m* is the sample mass, and *b* is the loss on drying (%).

2.4. *Raman Spectroscopy*

Raman spectra were obtained using a HORIBA Jobin Yvon labRAM HR. The bench-top micro-Raman unit has an 800 mm focal length spectrometer giving it a resolution of < 1 cm^{-1}. Samples were excited with a Nd:YAG laser emitting at 532-nm. An objective lens 100x was utilized and the signal was collected on a high resolution air-cooled CCD. The spectrometer was calibrated using a polished, non-oxidised silicon standard. The spectra were collected in the range 340 to 3200 cm^{-1} and the laser power was set at 100%. Spectra collection time was 30 s and 20 accumulations were taken for each sample. The samples analysed were pre-scanned to reduce auto-fluorescence and the spectra were subject to a second-order polynomial background subtraction, excluding the position of the specific peaks, to reduce the fluorescence background.

2.5. *Scanning Electron Microscopy (SEM)*

SEM images were obtained by a high resolution (< 1 nm) Field Emission Zeiss Ultra Plus-SEM with a Gemini® column operating at an accelerating voltage of 5 kV.

2.6. *X-Ray Diffraction (XRD)*

XRD spectra were recorded by a PANanalytical X'Pert PRO instrument with Ni-filtered Cu-Kα radiation (λ = 0.1542 nm) generated at 40 kV and 40 mA. The scanning was made through 2θ = 10° to 90°, and intensity data was recorded with a digital recorder. The crystallinity index (*CrI*) was calculated *via* **equation (2)**:

$$CrI = \frac{I_{002}-Iam}{Iam} \quad \textbf{(2)}$$

where, I_{002} the maximum intensity of the peak corresponding to the plane in the sample with the Miller indices 002 at a 2θ angle of around 22.6°, and I_{am} is the intensity that corresponds to the non-crystalline peak at about 2θ = 18°.

2.7. *Particle Size Distribution*

Particle size distributions of the post hydrolysis samples were determined using Malvern Mastersizer 3000 with HYDRO insert attached to Malvern Hydro MV (Medium VolumeAutomated Dispersion Unit) wet cell.

3. Theory

3.1. *Mark-Houwink-Sakurada Molecular Weight*

Having determined the average DP via viscosity measurements per pharmacopoeial requirements and ASTM D1795 method as outlined above, the Mark-Houwink-Sakurada (MHS) equation (**Łojewski et al., 2010)** can be applied to determine average molecular weight:

$$[\eta] = K.M_n^{\alpha} \quad \textbf{(3)}$$

Where, *[η]* is the intrinsic viscosity, M_n is the number average molecular weight, *K* and *α* are constant coefficients. *K* and *α* are known as the Mark-Houwink-Sakurada or MHS coefficients and various values have been proposed over many years: **Łojewski et al., 2010; Immergut et al., 1953; Evans, 1987.** It is proposed by **Kes and Christensen (2013)** that the following MHS equation is applicable to cellulose in aqueous cupriethylenediame (CUEN) solution which is applicable to the present study:

$$[\eta] = 1.33\ x\ 10^{-4}\ M_n^{0.905} \quad \textbf{(4)}$$

4. Results and Discussion

4.1. *Hydrolysis Reaction / Degree of Polymerisation curve*

The pulp samples were hydrolysed under varying temperature and acid concentration conditions, with the reaction quenched a different time intervals. For the present study, the reactions were carried out at 95°C using 1M HCl and 2M HCl, and at 85°C again using both 1M and 2M HCl solutions. Each reaction scenario was quenched at the following time intervals: 30 min, 60 min, 120, and 240 min. Samples were taken and intrinsic viscosity measured to estimate DP. **Figure 1** shows the DP reduction curves obtained for these reactions.

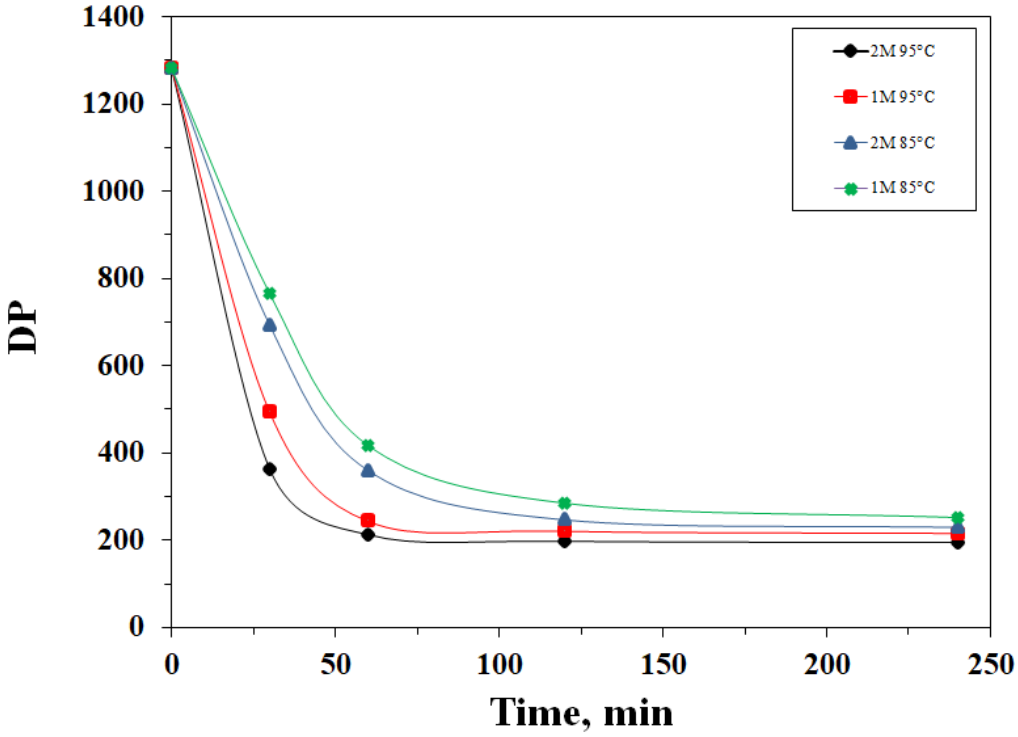

Figure 1. DP reduction curves for the hydrolysis reaction of a selected pulp at given temperature and acid concentrations

The DP of the unreacted pulp was used as the 'time zero' value. There was a sharp reduction in DP from the starting point observed in all reaction scenarios as expected, and LODP was reached between 2 and 4 hours for all cases. The DP reduction curves for both 95°C reactions proceeded faster than both 85°C reactions, and lower LODPs were reached for the higher temperature scenarios. For a given reaction temperature, the change from 1M to 2M HCl resulted in an increase in reaction rate and also lower LODP. **Figure 2** shows that the DP reduction curves are grouped more closely in terms of temperature effect rather than acid concentration effect; for instance, the LODP of the 1M sample of 95°C as higher than the 2M sample at 85°C. Similar observations were found by **Hakansson and Ahlgren (2005)**, and in addition they confirmed that an acid concentration of 3M was required for their selected pulp to reach LODP for a reaction temperature of 80°C, therefore comparable to the present study. The DP reduction in all cases proceeded beyond the 350-unit pharmacopoeia cut-off point. Therefore, the resultant samples at LODP can be defined as being microcrystalline cellulose.

4.2. *SEM*

The change in surface morphology of the pulp as the reaction proceeds was analysed by SEM and the results are given below in **Figure 2**.

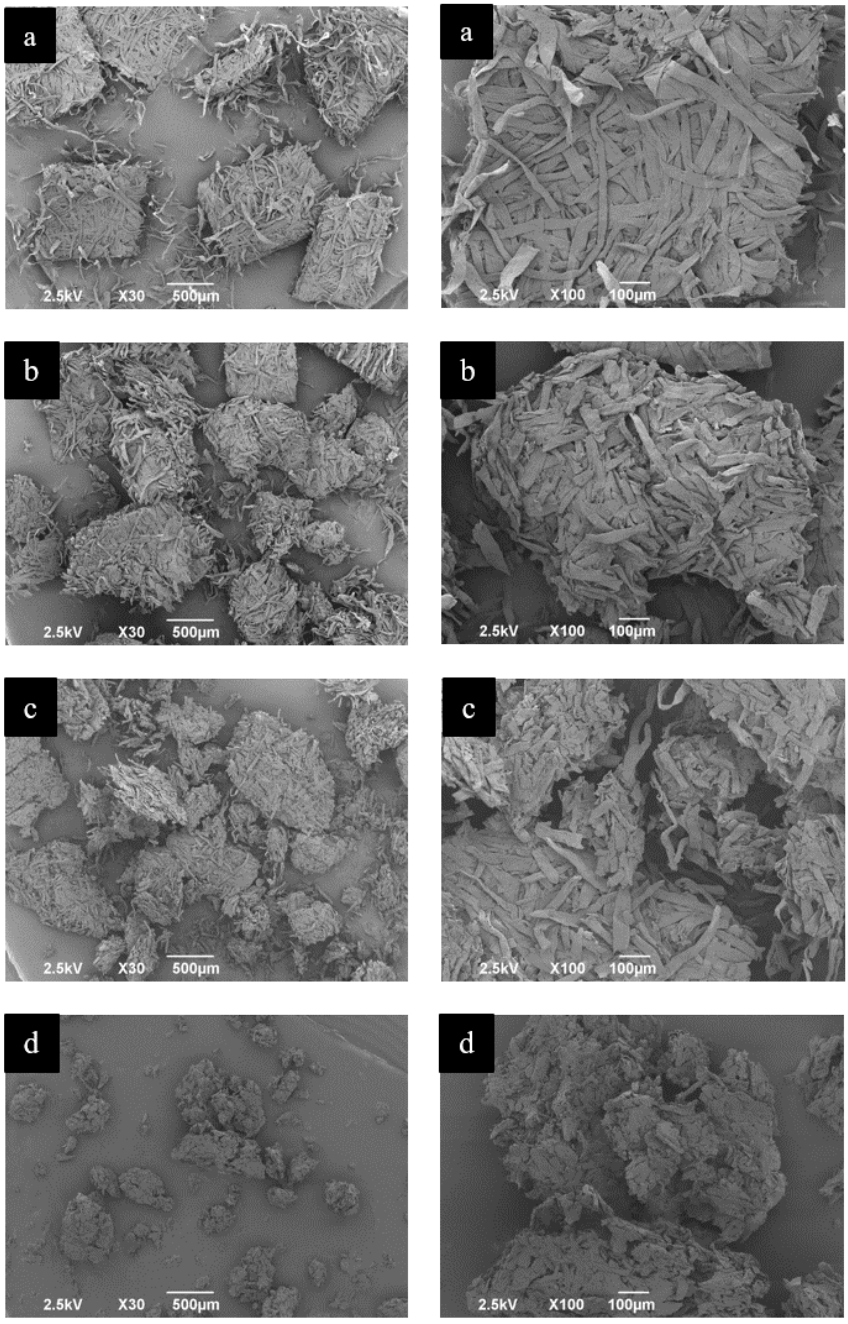

Figure 2. SEM micrographs of a pulp sample undergoing acid hydrolysis at 1M HCl and 95°C. Top down: a) 30 min, b) 60 min, c) 120 min, d) 240 min.

The images provided in **Figure 2** show pulp samples hydrolysed at 95°C and 1M HCl acid concentration at various time intervals and in to the LODP zone. The images on the top row labelled ‘a’ show that after 30 minutes the pulp chips were still largely intact, with some

minor surface release of microfibrils. After 60 minutes reaction time, the images (b) show that degradation of the chips has become more apparent, and it is also shown that the chips are subject to swelling at this stage as the reactants penetrate in to the fibrils. The 120 minute samples (c) show increased degradation and significant breakdown was observed at the 240 minute stage (images d).

It is of interest to note that the largest rate of reduction in DP takes place in the first 30 to 60 minutes as shown in **Figure 1** above. However, the SEM images for this period (a and b in **Figure 2**) do not appear to show significant morphological changes, which only become more apparent later in the reaction time. **Davidson (1943)** showed that only a very small amount of the glycosidic linkages of cellulose are required to be hydrolysed for a rapid reduction in DP to occur, therefore, although the SEM images for the early stages of the reaction appear less degraded than one would expect, it must be pointed out that these images are of generally unreacted sections of pulp, whereas the DP measured at this stage is representative of the overall *average* degree of polymerisation of the pulp sample.

Furthermore, it was observed during handling and filtration of the reaction contents for the 30 minute and 60 minute samples, that the material was soft and malleable with chip like sections easily breaking down physically to finer powder like material, especially during the deionised water washing stage. Trial hydrolysis reactions were carried out with more aggressive agitation settings and it was found that the chip like content of early reaction samples were reduced, confirming that the material had indeed undergone hydrolysation at that stage per the DP results.

4.3. *Particle size distribution*

Samples of hydrolysed pulp for the 95°C in 1M HCl reaction scenario were analysed by Malvern wet cell laser diffraction to investigate changes in particle size distribution over the reaction timeframe; the results are given in **Figure 3**. Both the 30 minute and 60 minute samples showed a bi-modal type distribution, likely representing the broken down more hydrolysed material and also the less reacted material (the chip-like material revealed in the early stage SEM images in **Figure 2**).

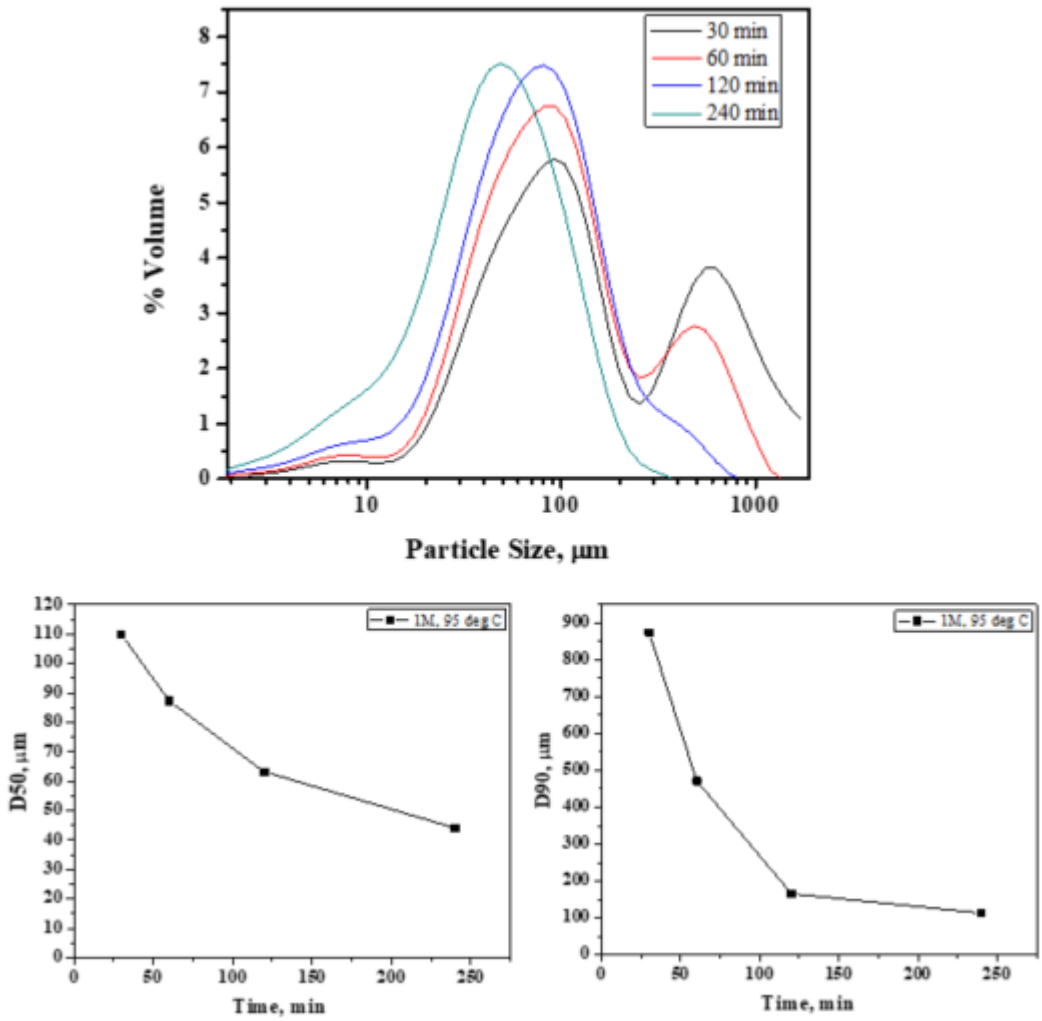

Figure 3. Particle size distribution of cellulose pulp samples for the 95°C, 1M HCl hydrolysis scenario at selected quench times (top); D50 and D90 changes for the same reaction (bottom left and right respectively)

As the reaction proceeds from 30 minutes to 60 minutes the right-hand peak reduces in height and the overall curve shifts slightly to the left towards lower particle sizes. At the 120 minute stage, the right-hand peak is reduced further and appears now only as a shoulder to the dominant distribution curve, with again an overall shift left. Finally, the 240 minute sample only shows a single distribution mode with an increase on the left hand side of the curve indicating an increase in smaller particle sizes.

The lower section of **Figure 3** gives the change in D50 (the diameter at which 50% of a sample's mass is comprised of smaller particles) and D90 (the diameter at which 90% of a sample's mass is comprised of smaller particles) values for the selected reaction. The D50 reduces to ~50 µm at the 240 minute sample, and the distribution curve is similar to that of

commercial Avicel® grade PH101. The rapid fall in D90 is representative of the reduction in 'less reacted chip-like material' to the finer reacted product, consistent with the rapid reduction in DP observed in **Figure 1**. It is of interest, however, to point out that both the D50 and the D90 continue to drop throughout the reaction even from the 120 to 240 minute samples, in contrast to the levelling-off of the degree of polymerisation during this time period in **Figure 1**. **Hakansson and Ahlgren (2005)** have suggested the although LODP may be considered as a *de-facto* endpoint of the hydrolysis reaction, this is not fully the case, as weight loss measurements show that the reaction still proceeds slowly throughout the LODP period and may even proceed indefinitely on maintaining the reaction conditions (the authors report that the hydrolysis reaction was observed to be continuing at very slow rates even after 400 hours from start of reaction). Nickerson (**Nickerson and Harble, 1947**) suggested that following hydrolysis of amorphous zones, the reaction continues slowly at the surface of the remaining crystallites. Later, **Sharples (1957)** proposed the continuation of the reaction was focused on the attack of the crystallite ends. These observations are consistent with effects at a plant scale level whereby MCC produced from reactions that proceeded well in to the LODP period tend to be finer and of higher bulk density in comparison to MCC produced at early stages of LODP (**O'Regan, 2018**).

To investigate the effect of temperature and acid concentration on particle size distribution, the curves given on **Figure 4** were generated. These curves represent the particle size distribution of the four reaction scenarios each at the 240 minute point, where LODP been well established for all samples. **Table 1** below summarises the D50 values for these four reactions. It was observed that the D50 reduced with both increasing temperature and increasing acid concentration. In addition, it can be seen that the increase in temperature from 85°C to 95°C had a greater effect in D50 change than the increase in acid from 1M to 2M concentration (complimenting the DP reduction curve temperature vs acid relationship given in **Figure 1**).

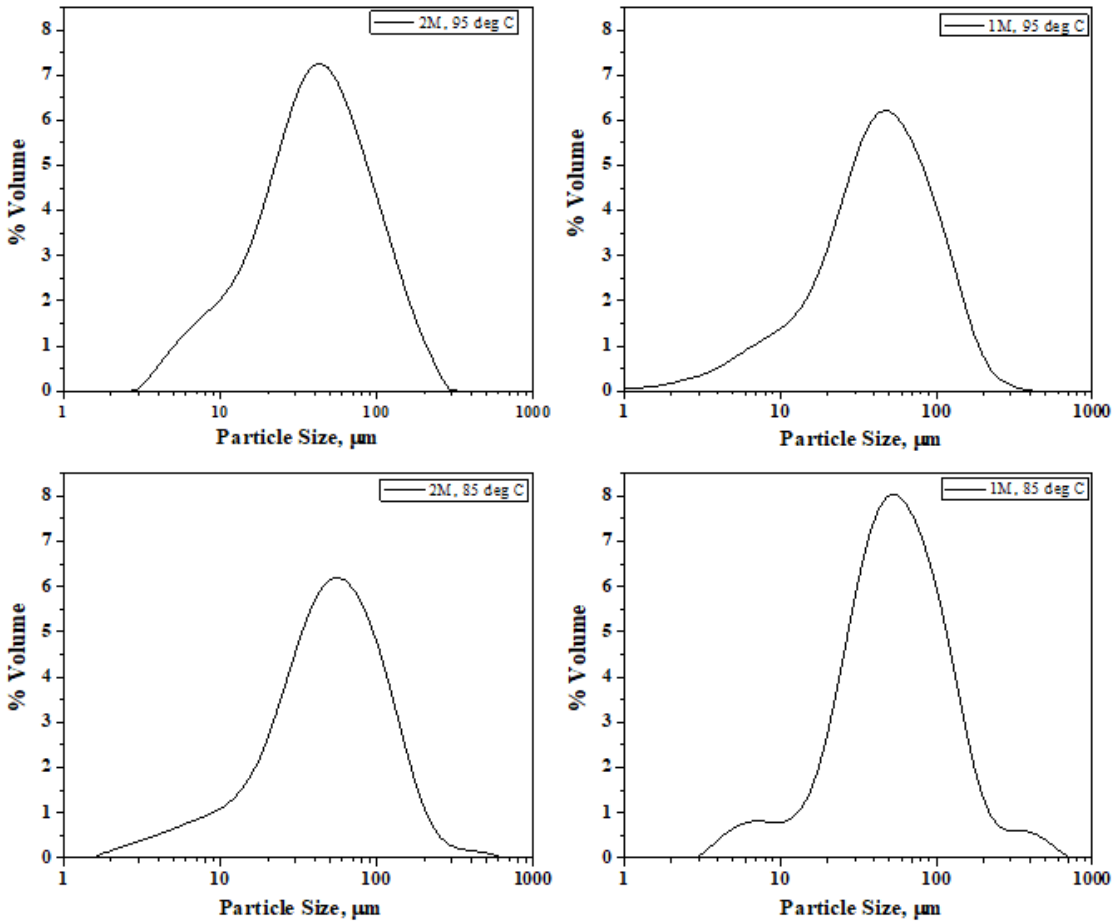

Figure 4. Particle size distribution curves for different cellulose hydrolysis conditions (labelled inset) quenched at LODP (240 minutes).

Table 1. D50 values cellulose hydrolysis at 240 minutes (LODP) for given reaction conditions

Temperature (°C)	HCl concentration [M]	D50 (µm)
85	1	53.9
85	2	49.8
95	1	44.1
95	2	40.3

4.4. *Mark-Houwink-Sakurada Molecular Weight*

The molecular weight of the samples reacted at 95°C in 1M HCl at the given quench times were estimated by application of the Mark-Houwink-Sakurada (MHS) equation (**Łojewski et al., 2010)**, using MHS coefficients proposed by **Kes and Christensen (2013)** for cellulose with intrinsic viscosity measured in CUEN solution (and given in Section 3 above), applicable to the present study. **Table 2** summarises the results:

Table 2. Estimated molecular weight of cellulose hydrolysis samples for 95°C and 1M HCl at given quench times.

Time (min)	**Molecular Weight (g mol^{-1})**
30	65,006
60	64,292
120	62,226
240	50,927

The results show the expected reduction in molecular mass over time as the hydrolysis reaction proceeds. The molecular mass values estimated are in agreement with **Vanhatalo et al., (2016)** who reported a molecular weight of 57,700 g mol^{-1} for Avicel grade PH101 cellulose determined experimentally by Gel Permeation Chromatography (GPC). This value, when applied to the DP reduction curve in the present study would lie in the early in the LODP range typical for MCC production. The results in **Table 2** are also in agreement with the findings of **Jasiukaityte-Grojzdek et al., (2012)** and **Cao et al., (2012)** who demonstrated that more intensive hydrolysis of cellulose gave shorter molecule chains, and in the order of the results given above.

4.5. *Raman analysis of hydrolysed samples*

The Raman spectra of the pulp starting material and hydrolysis samples for the 95°C and 1M HCl reaction are given in **Figure 5.** All spectra are similar and exhibit the characteristic peaks attributed to cellulose (**Gierlinger et al., 2013**) and outlined in detail in Chapters 2 and 3 of this thesis.

The peak at 380 cm^{-1} is known to be characteristic of crystalline cellulose (**Lee at al., 2016; Agarwal et al., 2010; Schenzel et al., 2005**) and in general hemicelluloses do not exhibit a peak at 380 cm^{-1}. The spectra in Figure 5 did not show a consistent difference in intensity of

this peak over the reaction timeframe. Agarwal et al. studied the effect of changes in crystallinity on the shape cellulose Raman bands and resulted that amorphous cellulose shows significant decline in band heights accompanied by band broadening (**Agarwal and Ralph, 1997**). Differences in peaks at 436 cm^{-1} and 493 cm^{-1} are also characteristic of differences in amorphous content, and the samples at 240 minutes showed some reduction in intensity at these wavelengths, however, the relationship and trend is not clear when compared to the other samples.

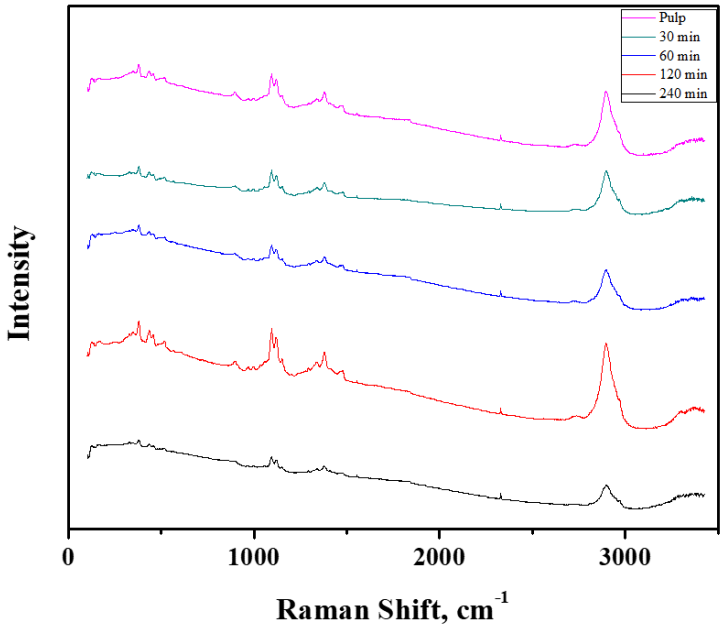

Figure 5. Raman spectra of pulp and 95°C in 1M HCl at given quench times

4.6. *XRD analysis*

The effect of the hydrolysis reaction on the crystallinity of cellulose is of particular interest. The study given in Chapter 3 of this thesis found that there was an unexpected marginal reduction in crystallinity of MCC powder products (post hydrolysis) when compared against the starting pulp raw material. The present study offers the opportunity to examine the transition from pulp to MCC in more detail, **Figure 6** below shows the X-ray diffraction scans for the 95°C in 1M HCl reaction scenario at the given quench times.

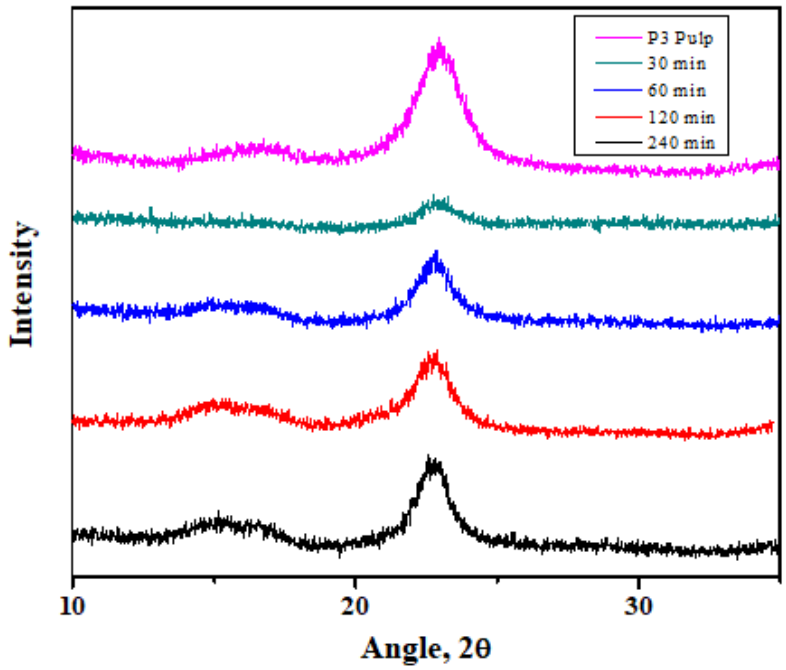

Figure 6. X-ray diffraction patterns for pulp and hydrolysis samples for the 95°C in 1M HCl reaction scenario at given quench times.

The characteristic cellulose I_{002} peak at around 22.6° 2θ as assigned by **Segal et. al (1959)** is observed in all samples in addition to the amorphous peak at around 18° 2θ. The relative intensity of the I_{002} and amorphous peaks was used to determine the degree of crystallinity index results are trended in **Figure 7.**

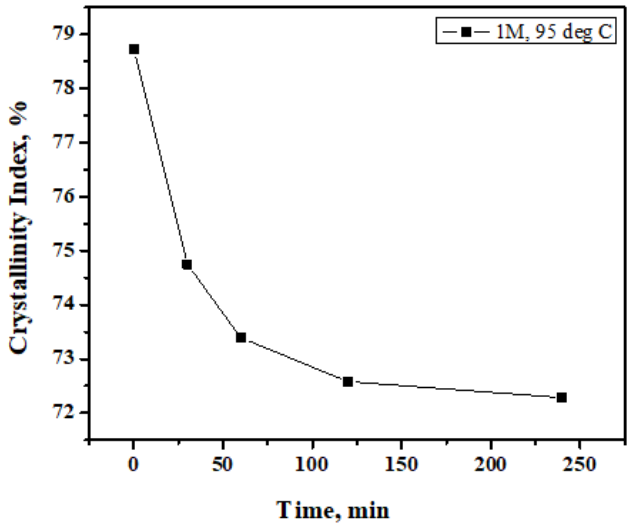

Figure 7. Crystallinity index change over time for the 95°C and 1M HCl reaction.

The crystallinity index was again found to reduce from the starting pulp level and through the reaction timeframe. The largest reduction in crystallinity was observed in the first 30 to 60 minutes, which suggests that the hydrolysis at this stage is acting on both the amorphous and crystalline regions. Similar results have been found by **Vanhatalo and Dahl (2014)** and also **Tolonen et al., (2011)**. An explanation for this is proposed by **Vanhatalo and Dahl (2014)** whereby two counter-mechanisms may be at operation: firstly, the hydrolysis of the amorphous content releasing individual crystallites and therefore increasing crystallinity, and secondly, damage to crystalline regions (by swelling and hydrolysis) leading to a reduction in crystallinity. This conclusion is also proposed by **Sun et al., (2008)**.

To understand the effect of varying hydrolysis reaction conditions **Figure 8** gives the XRD patterns for the four selected scenarios, all at the 240 minute LODP quench time.

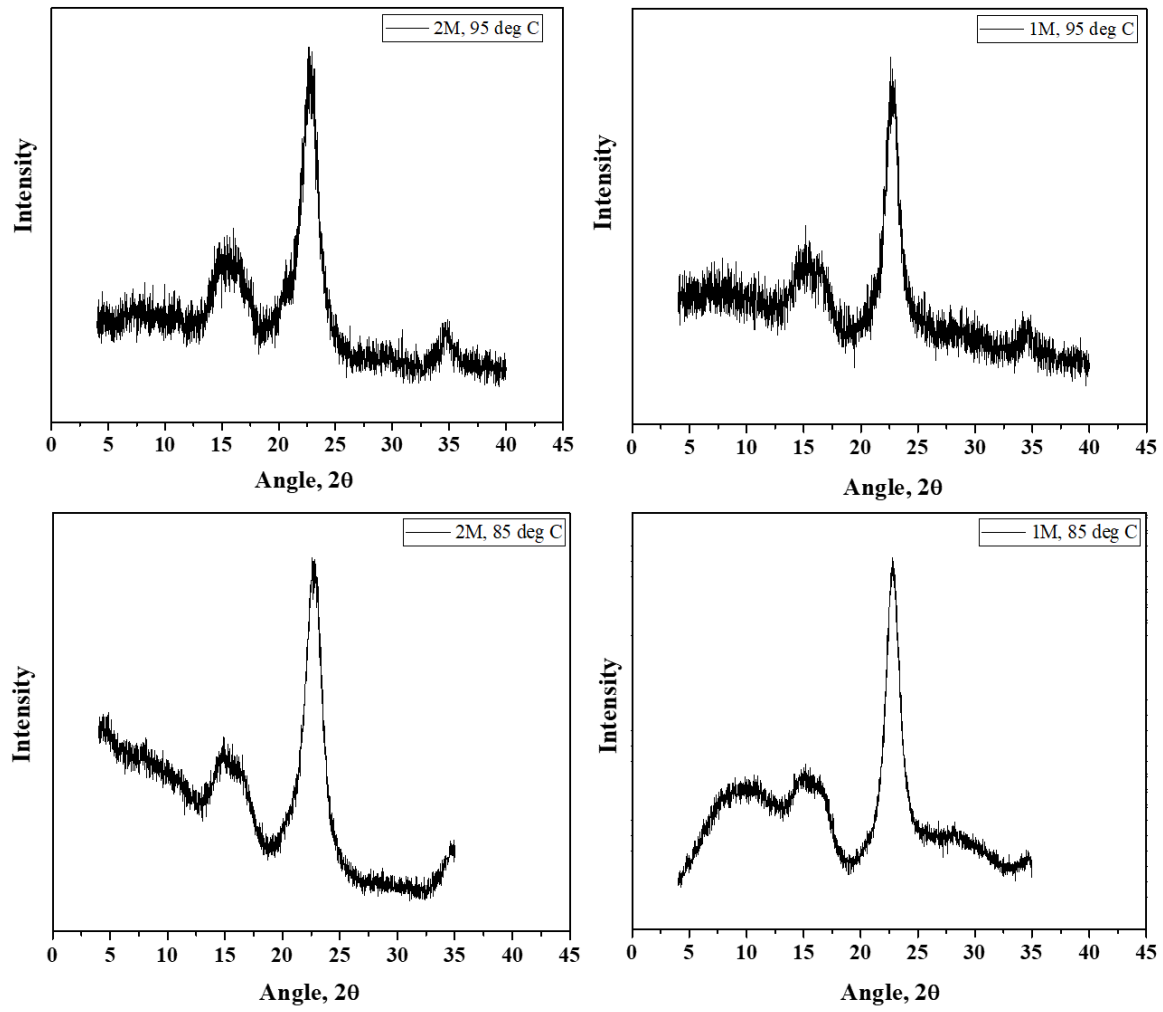

Figure 8. XRD patterns for the 240 minute LODP samples of the four hydrolysis reactions (labelled inset).

The respective crystallinity indices generated from the above XRD pattern are given in **Table 3**. The results confirm that in increase in hydrolysis intensity leads to a reduction in crystallinity for the given hydrolysis conditions applicable to the present study.

Table 3. Crystallinity Index of hydrolysis samples at 240 minutes (LODP) for given temperature and acid concentrations.

Temperature (°C)	HCl concentration [M]	Crystallinity Index (%)
85	1	77.8%
85	2	76.4%
95	1	72.3%
95	2	71.8%

5. Conclusions

Identification of an indicator for optimum end-point determination of hydrolysis of pulp during the industrial production of MCC is of high interest and potential value to commercial producers, and there is little, if any, published literature concerning same.

The results of the present study show that the degree of polymerisation of the starting pulp rapidly reduces over the first 30 to 60 minutes of acid hydrolysis for given conditions but then plateaus and continues largely unchanged when measured over a number of hours, in alignment with current literature. Scanning Electron Microscope (SEM) images of the reactant samples, however, unexpectedly showed that large quantities of pulp remained physically intact during the period of rapid reduction in degree of polymerisation, an observation that was subsequently corroborated by particle size analysis.

Furthermore, it was also observed that the average particle size surprisingly continued to reduce during the period where degree of polymerisation had levelled off, even as far as four hours. Particle size measurements are, therefore, of use over the entire hydrolysis timeframe and simple conversion of the particle size distribution curves to D50 and D90 values (the diameter at which 50% and 90% respectively of a sample's mass is comprised of smaller particles) allows for quantitative tracking of the hydrolysis reaction and opportunity for end-point selection in real time. In addition, utilization of particle size values for tracking the reaction can be of significant benefit in determining optimum downstream processing

conditions, for instance particle size is a factor in both slurry viscosity and filtration effectiveness which are of high concern to manufacturers.

It was also observed that the crystallinity of the pulp reduced throughout the hydrolysis reaction time, with more intense hydrolysis (higher temperature and higher acid concentration) resulting in greater reduction in crystallinity. The relatively sharp reduction in crystallinity was unexpected (there is little current literature concerning this, and a lack of quantitative crystallinity measurements over hydrolysis time) and suggests that both amorphous and α-cellulose content is being hydrolysed, an observation which is of particular concern to commercial MCC producers who wish to maximise α-cellulose yield of the product. The results of this study show that crystallinity (and, hence, α-cellulose yield) is impacted by both hydrolysis time and intensity, with such impact being quantified herein, accordingly offering an opportunity to MCC producers to optimise reaction conditions to reduce yield losses.

Acknowledgements

The authors wish to acknowledge AMBER Centre, Trinity College Dublin for providing financial support to carry out the research, and DuPont Nutrition and Health for pulp supply and onsite laboratory access.

References

Agarwal, U.P., Reiner, R.S., Ralph, S.A. (2010). Cellulose I crystallinity determination using FT-Raman spectroscopy: univariate and multivariate methods. Cellulose 17(4), 721-733.

Agarwal, U.P., Ralph, S.A. (1997). FT-Raman spectroscopy of wood: Identifying contributions of lignin and carbohydrate polymers in the spectrum of Black Spruce (Picea mariana). Appl. Spec. 51, 1648-1655.

Aro, T., Fatehi, P. (2017). Production and application of lignosulfonates and sulfonated lignin. ChemSusChem 10, 1861–1877.

Cao,S., Pu, Y., Studer, M., Wyman, C., and Ragauskas, A. J. (2012). Chemical transformations of Populus trichocarpa during dilute acid pretreatment, RSC Adv. 2(29), 10925-10936. DOI: 10.1039/C2RA22045H

Davidson, G. F. (1943). The rate of change in the properties of cotton cellulose under the prolonged action of acids. Journal of the Textile Institute Transactions, 34(10), T87–T96. http://dx.doi.org/10.1080/19447024308659271

Doelker, E. (1993). Comparative compaction properties of various microcrystalline cellulose types and generic products. Drug Dev. Ind. Pharm. 19, 2399–2471.

Evans, R., Wallis, A.F.A. (1987). Fourth Int. Symp. Wood Chem., Paris, p. 201

Frey-Wyssling A., and Muhlethaler K. (1965). Ultrastructural Plant Cytology with an Introduction to Molecular Biology. Elsevier, Amsterdam, The Netherlands.

Gierlinger, N., Keplinger, T., Harrington, M., Schwanninger, M. (2013). Raman imaging of lignocellulosic feedstock, Cellulose - Biomass Conversion. Prof. John Kadla (Ed.) InTech, DOI: 10.5772/50878.

Gurnagul N. (1992). The effect of cellulose degradation on the strength of wood pulp fibres. Nordic Pulp Pap. Res. J. 7(3): 152.

Hakansson, H., Ahlgren, P. (2005). Acid hydrolysis of some industrial pulps: effect of hydrolysis
conditions and raw material, Cellulose 12: 177–183, 2005.

Hearle J.W.S. (1963). The fine structure of fibres and crystalline polymers. J. Appl. Polym. Sci. 7: 1175–1192.

Immergut, E.H., Schurz, J., Mark, H. (1953). Monatsh. Chem. 84 219

Jasiukaityte-Grojzdek, E., Kunaver, M., and Poljansek, I. (2012). Influence of cellulose polymerization degree and crystallinity on kinetics of cellulose degradation, BioResources 7(3), 3008-3027.

Kes, M., Christensen, B.E. (2013). A re-investigation of the Mark-Houwink-Sakurada paramters for cellulose in Cuen: A study based on size-exclusion chromatography combined with
multi-angle light scattering and viscometry, Journal of Chromatography A, 1281 (2013) 32–37

Kupiainan, L., Ahola J., Tanskanen J. (2014). Kinetics of Formic Acid-catalysed Cellulose Hydrolysis. Bioresources 9(2), 2645-2658.

Lee, C., Dazen, K., Kafle, K., Moore, A., Johnson, D.K., Park, S., Kim, S.H. (2016). Correlations of apparent cellulose crystallinity determined by XRD, NMR, IR, Raman, and SFG methods. 2016, Adv. Pol. Sci. 271, 115-132.

Łojewski, T., Zieba, K., Łojewska, J. (2010). Size exclusion chromatography and viscometry in paper degradation studies. New Mark-Houwink coefficients for cellulose in cupri-ethylenediamine. Journal of Chromatography A, 1217 (2010) 6462–6468

Nickerson R.F. and Harble J.A. (1947). Cellulose intercrystalline structure. Study by hydrolytic methods. Ind. Eng. Chem. 39(11): 1507–1512.

O'Regan, C. (2018). Personal observations of the MCC industrial process at DuPont, Cork, Ireland.

Schenzel, K., Fischer, S., Brendler, E. (2005). New method for determining the degree of cellulose I crystallinity by means of FT-Raman spectroscopy. 2005, Cellulose 12(3), 223-231.

Segal L., Creely, J.J., Martin Jr., A.E., and Conrad, C.M. An empirical method for estimating the degree of crystallinity of native cellulose using X-ray diffractometer, Textile Research Journal 29, 786-794.

Sharples A. (1957). The hydrolysis of cellulose and its relation to structure. Trans. Faraday Soc. 53: 1003–1013.

Sun, Y., Lin, L., Deng, H., Li, J., He, B., Sun, R., and Ouyang, P. (2008). Structureal changes of bamboo cellulose in formic acid, BioResources 3(2), 297-315.

Thoorens, G., Krier, F., Leclercq, B., Carlin, B., Evrard, B. (2014). Microcrystalline cellulose, a direct compression binder in a quality by design environment—A review, International Journal of Pharmaceutics 473 (2014) 64–72.

Tolonen, K. L., Zuckerstatter, G., Penttyla, P.A., Milacher, W., Habicht, W., Serimaa, R., Kruse, A., and Sixta, H. (2011). Structural changes in microcrystalline cellulose in subcritical water treatment, Biomacromolecules 12(7), 2544-2551.

Vanhatalo, K.M., and Dahl, O.P. (2014). Effect of mild acid hydrolysis parameters on properties of microcrystalline celloluse, BioResources 9(3), 4729-4740.

Vanhatalo, K. (2016). Comparison of conventional and lignin-rich microcrystalline celloluse, BioResources 11(2), 4037-4054.

Zhao, H., Kwak, J. H., Wang, Y., Franz, J. A., White, J. M., & Holladay, J. E. (2006). Effects of crystallinity on dilute acid hydrolysis of cellulose by cellulose ball-milling study. Energy & Fuels, 20, 807–811.

Chapter 5

Acid Hydrolysis Kinetics of Cellulose Pulps: Effect of Raw Material Source

Acid hydrolysis kinetics of cellulose pulps: effect of raw material source

Conor O'Regan*[a,b], Justin D Holmes[a,c,d], and Michael A Morris*[c,d]

[a] Materials Chemistry, Department of Chemistry, University College Cork, Cork, Ireland,

[b] DuPont Nutrition and Health, Cork, Ireland

[c] AMBER, Trinity College Dublin, Dublin 2, Ireland,

[d] Tyndall National Institute, Lee Maltings, Prospect Row, Cork, Ireland,

*Corresponding author: Email: conor.o-regan@dupont.com (Conor O'Regan), morrism2@tcd.ie (Michael A Morris) Ph: +353 18963089

ABSTRACT

Hydrolysis experiments were carried out on two pulp samples produced from different wood sources and delignification processes. Degree of polymerisation reduction curves were generated and Ekenstam plots used to determine the hydrolysis reaction rates. The hardwood acid-sulphite pulp was found to have a higher reaction rate compared to the softwood Kraft pulp. Kinetic parameters revealed that the hardwood pulp had a higher activation energy but also a significantly higher frequency factor, attributed to previously identified differences in crystallinity and morphology respectively. A modified version of the industry standard equation for determining hydrolysis intensity was proposed, which for the first time quantitatively accommodated differences in pulp crystallinity and morphology by inclusion of corrected activation energy and frequency factor terms, offering significant improvement in industrial reaction control.

Keywords: MCC; Pulp; Cellulose; Hydrolysis; Kinetics

1. Introduction

Production of microcrystalline cellulose (MCC) for the pharmaceutical and food industries is carried out by the partial depolymerisation of speciality pulps (**Brittain et al., 1993**). In recent years, primarily for commercial and security of raw material supply reasons, MCC manufacturers have introduced diversification of pulp type usage. The objective of the present study was to subject two pulps of different wood type origin and delignification process to a series of acid hydrolysis experiments and identify differences in the reaction kinetic and thermodynamic parameters. Furthermore, it was endeavoured to link quantified differences in hydrolysis reaction rate with both crystallinity and morphology of pulps, a link not given in the current literature and of high significance to MCC producers with respect to control of the primary MCC producing reaction.

Acid hydrolysis of cellulose is based on the scission of the β-1,4-glycosidic bond (**Fan et al., 1987**). However, access of the reactants to these sites is greatly inhibited due to the crystalline nature of α-cellulose where the structure is tightly packed. The 'fringed fibrillar model' (**Hearle, 1963; Frey-Wyssling and Muhlethaler, 1965**) of the structure of cellulose describes cellulosic material of consisting of crystalline regions arranged in microfibrils interconnected by disordered amorphous areas. The interconnecting amorphous kinks described in the model are less tightly packed and provide easier access for the reaction to occur. As a result, the rate of hydrolysis of the amorphous regions is be much higher than that of the crystalline region (**Zhao et al., 2006**). Hydrolysis at the amorphous site results in the release of the microfibril crystallites (**Gurnagul et al. 1992**) which ultimately form the MCC powder product following downstream filtration and drying steps.

Control of the hydrolysis step in the commercial production of MCC is challenging. Differences in crystallinity and morphology between pulp types has been demonstrated (**Chapter 2** of this thesis) and, therefore, kinetic parameters are also likely to vary between these pulp types. Understanding the magnitude of differences in reaction kinetics is of a high importance for refinement of the reaction end-point selection.

DuPont Corporation currently utilises a 'hydrolysis intensity' equation to quantify the intensity of the hydrolysis reaction for given temperature and acid concentration conditions and therefore predict an optimum time to quench the reaction. The activation energy value used in the hydrolysis intensity equation is not changed for pulp type, and, furthermore, the equation does not allow for differences in frequency factor. Modifications to the industry standard hydrolysis intensity equation are proposed based on the results of the present hydrolysis study.

2. Materials and Methods

2.1. *Materials*

Two pulp types used in the industrial manufacturing process of microcrystalline cellulose (MCC) were selected for this study. Pulp 'P2' was generated from hardwood (Eucalyptus) which was delignified via the acid-sulphite process. Pulp 'P3' was generated originally from southern softwood (mostly Loblolly Pine), and delignified via the Kraft process. Oxidative elemental chlorine free (ECF) bleaching was carried out on both materials during the pulping process (**Aro and Fatehi, 2017; Hua et al., 2018**).

Both pulps were extensively characterised in **Chapter 2** of this thesis. Differences were observed in α-cellulose content, with pulp P2 having a higher level compared to P3 which in turn had a higher content of amorphous material. XPS analysis suggested the that surface chemistry of P3 also contained more amorphous and less crystalline content than P2. The crystallinity of both pulps was determined by X-ray diffraction and also indicated higher levels of crystallinity for P2. Large morphological differences between the pulps were observed via SEM analysis, with P2 having significantly smaller average fibre diameter with a narrower distribution range when compared with P3. Pulp P2 also appeared to have more inter-fibre connections and was tightly packed compared with P3.

TGA analysis revealed that pulp P3 had a lower onset temperature suggesting lower crystallinity and also higher thermal stability during the major degradation step suggesting possible lignin content not observed in pulp P2. Application of the standard kinetic models to the TGA data indicated that P2 had significantly higher activation energy and frequency factor in comparison to P3 which were attributed to the tighter and more crystalline packing for P2.

All materials were supplied courtesy of DuPont Nutrition and Health, Cork, Ireland.

2.2. *Hydrolysis of Pulp*

Acid hydrolysis was performed using 5 g (oven-dried) samples diced to approximately 2 mm x 2mm chips. The samples were added to solutions of HCl which were pre-heated to the selected reaction temperature. For this study, reactions were carried out at 85°C, 90°C and 95°C. HCl acid concentration was kept constant at 2M for all reactions. Reactions were carried out in a 'Syrris Orb' 1 litre jacketed glass reactor under atmospheric pressure with cold water condensation applied. Temperature control of the reactor contents was maintained by thermal oil circulated via 'Julabo' temperature control unit using direct temperature measurement of the acid solution. Mild agitation of the reactor contents was applied consistently for all reactions.

On completion of the hydrolysis reaction at the selected reaction time, the reactor contents were immediately filtered and carefully washed with deionised water until a neutral pH was observed. The samples were air-dried before further analysis. All reactions were completed in duplicate.

2.3. *Degree of Polymerisation*

The degree of polymerisation (DP) for each sample was determined by ASTM D1795 standard method per the required harmonized pharmacopoeia regulations for pharmaceutical grade MCC, using cupriethylenediamene (CUEN) solution to measure intrinsic viscosity and subsequent relation to average DP. The monograph stipulates viscosity measurement by capillary type viscometer with the measured flow time multiplied by the apparatus constant to give a kinematic viscosity result. The intrinsic viscosity, $[\eta]_c$, is then determined by interpolation of the tabular relationship given in ASTM D1795. The DP is subsequently calculated by the following equation:

$$DP = \frac{95[\eta]_c}{m[(100-b)x10^{-2}} \quad \textbf{(1)}$$

Where *DP* is the degree of polymerisation, $[\eta]_c$ is the intrinsic viscosity, *m* is the sample mass, and *b* is the loss on drying (%).

3. Theory

3.1. *Acid Hydrolysis Reaction Mechanism*

The hydrolysis of cellulose with acid has been extensively studied and is known to proceed by rapid protonation of the glycosidic oxygen followed by slower splitting of the glycosidic bond and the subsequent addition of a water molecule (**Fan et al., 1987, Tee et al., 2013; Nevell, 1976; Parikh, 1967; Szejtli, 1975**). Hydrolysis may also proceed by protonation of the cyclic oxygen (rather than the glycosidic oxygen), which shifts the position on the carbonium cation formation for the scission of the glycosidic bond and water addition site. Both proposed mechanisms are given in **Figure 1**.

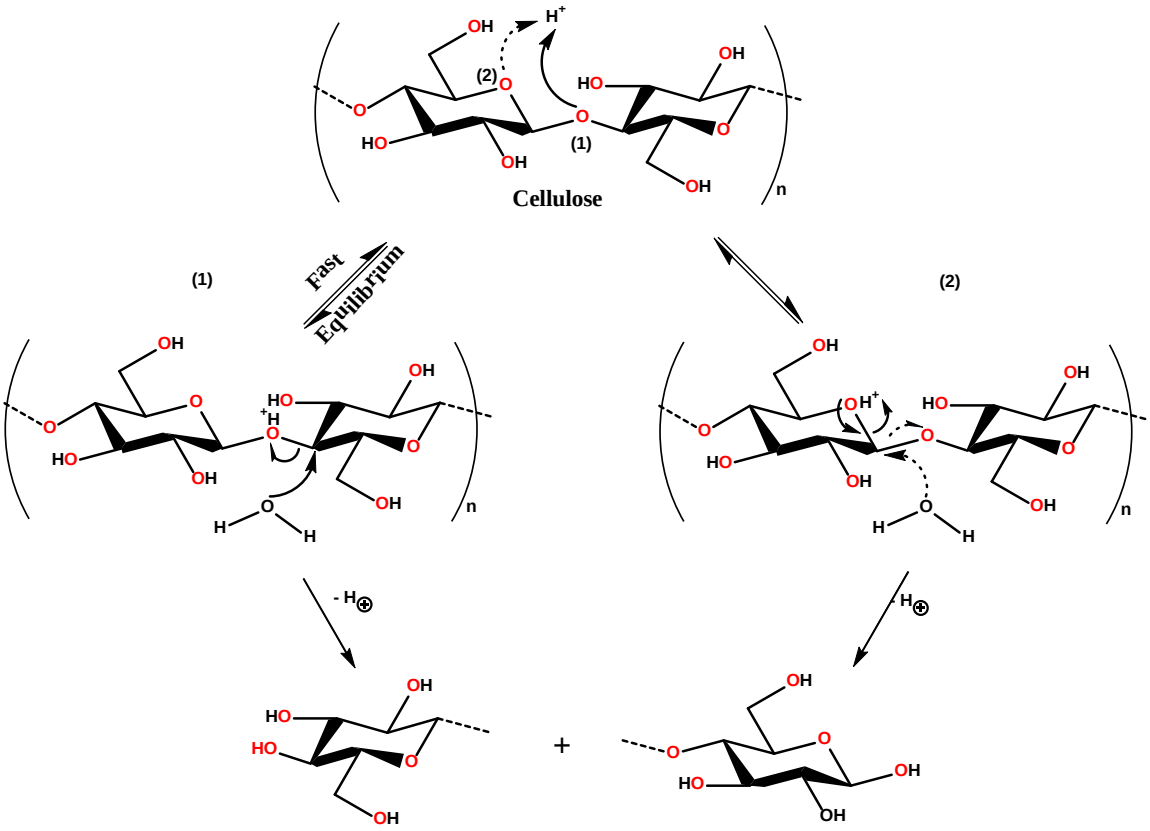

Figure 1. Reaction mechanisms for acid hydrolysis of cellulose

Additionally, it has been shown (**Szejtli, 1975**) that partial protonation of both oxygens (glycosidic and cyclic) can take place simultaneously. Identification of the course of the hydrolysis as being either type-1 or type-2 shown in **Figure 8** above may be possible based on the following suggested method (**Whalley, 1959a; Whalley, 1959b**). If the entropy of the reaction, ΔS^*, is negative, then the mechanism is most likely to be type-2, that is the mechanism proceeds via protonation of the cyclic oxygen. The probability of type-2 increases the more negative ΔS^* becomes. If ΔS^* is positive, then both type-1 and type-2 mechanisms are likely, with the probability of type-1 mechanism increasing as ΔS^* increases.

3.2. *Hydrolysis Kinetics*

Measurement of the change in degree of polymerisation (DP) of the cellulose samples can be used as a basis for determining kinetic parameters for the selected acid hydrolysis reaction. The relationship between DP and reaction rate, k, is given by the Ekenstam equation for pseudo zero-order reactions (**Palme et al., 2016**):

$$\frac{1}{DP_t} - \frac{1}{DP_0} = kt \qquad (2)$$

where DP_t is the degree of polymerization at time *t*, DP_0 is the starting degree of polymerization, *k* is the hydrolysis rate, *t* is the hydrolysis time. The DP values were measured as described above. **Calvani et al. (2008)** showed that the Ekenstam equation could be modified to describe first order reactions, and it is found that when DP_0 is high, both pseudo zero-order and first order rate equations are equivalent. The rate *k* may therefore be determined by plotting

$\frac{1}{DP_t} - \frac{1}{DP_0}$ vs *t*, with *k* being the measured slope.

Utilising the Arrhenius Equation, *k* can be correlated with the activation energy, Ea, and temperature as follows:

$$k = Ae^{\left(\frac{-E_a}{RT}\right)} \qquad (3)$$

where *A* is the frequency factor, E_a is the activation energy, *R* is the ideal gas constant, and *T* is the hydrolysis temperature. Plots of *ln(k)* vs (*1/T*) will give a slope of ($-E_a/R$) and the activation energy therefore determined.

Following determination of the kinetic parameters via the above relationships, the thermodynamic parameters can therefore be calculated as follows: **Straszko et al., 1997; Humienik, and Mozejko, 2000**):

$$\Delta H = Ea - RT \qquad (4)$$

$$Ae^{\frac{-Ea}{RT}} = \frac{KBT}{h} e^{\frac{-\Delta G}{RT}} \qquad (5)$$

$$\Delta G = \Delta H - T\Delta S \qquad (6)$$

where, ΔG, ΔH and ΔS are free energy, enthalpy and entropy, receptivity. K_B and *h* are the Boltzmann and Plank constant, respectively.

Inclusion for acid concentration in the Arrhenius equation (Eqn 3 above) may be represented by a modified form of the equation and is shown in Eqn (7) (**Zou et al., 1996**):

$$k = A(a[H^+])e^{\left(\frac{-E_a}{RT}\right)} \qquad (7)$$

where *a* is the coefficient of hydrogen ion effect, and $[H^+]$ is the hydrogen ion concentration. If the hydrolysis reaction of a given pulp type is carried out at different temperatures (but at the same acid concentration) and the hydrolysis rate k determined from Eqn (2) using measured DP values at various times as the reaction proceeds, then Arrhenius plots can be generated to determine the reaction activation energy E_a.

4. Results and Discussion

4.1. *Hydrolysis Reaction / Degree of Polymerisation curve*

To determine the starting degree of polymerisation, both pulps were tested per the ASTM 1795D method as given above and the results obtained were as follows:

Table 1. DP results for unhydrolyzed starting pulp material

Pulp	Degree of Polymerisation
P2	770
P3	1284

The results in **Table 1** indicate that the hardwood acid-sulphite pulp P2 has a significantly lower DP than the softwood Kraft pulp P3.

Both pulp type samples were hydrolysed in 2M HCl solutions for all reactions. Three reaction temperatures were used for each pulp: 85°C, 90°C, and 95°C. Each reaction scenario was quenched at the following time intervals: 30 min, 60 min, and 120 minutes. Samples were taken and intrinsic viscosity measured to estimate DP. **Figure 2** shows the DP reduction curves obtained for pulp P2, and the corresponding results for P3 are given in **Figure 3**.

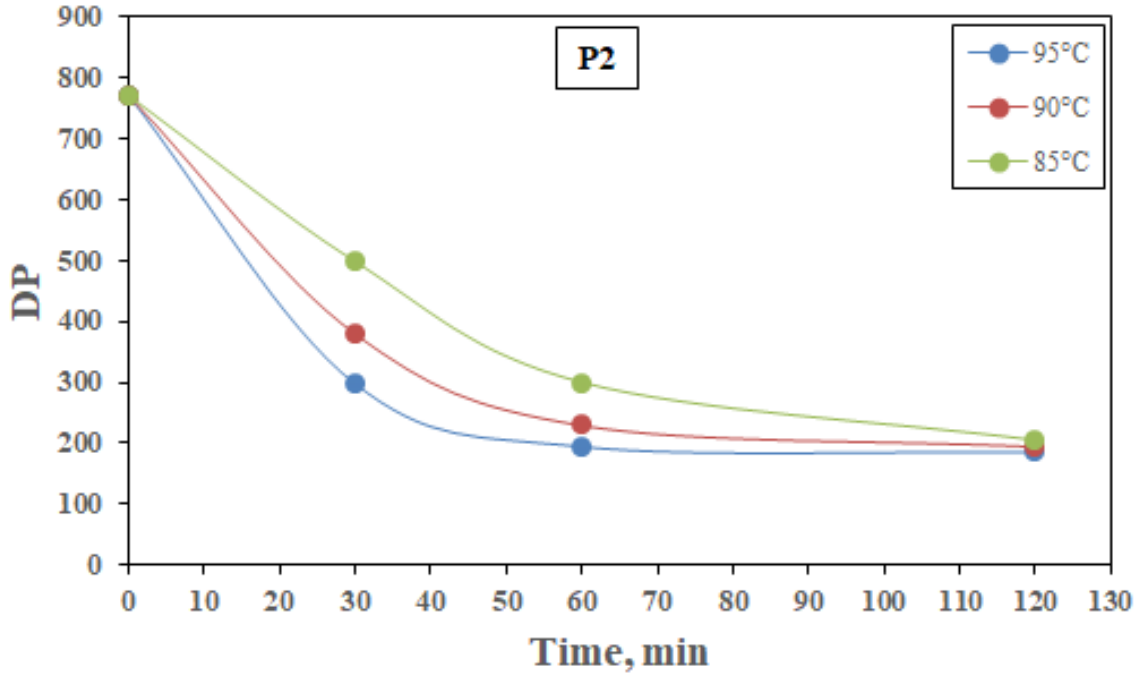

Figure 2. DP reduction curves for the hydrolysis reaction of pulp P2 in 2M HCl

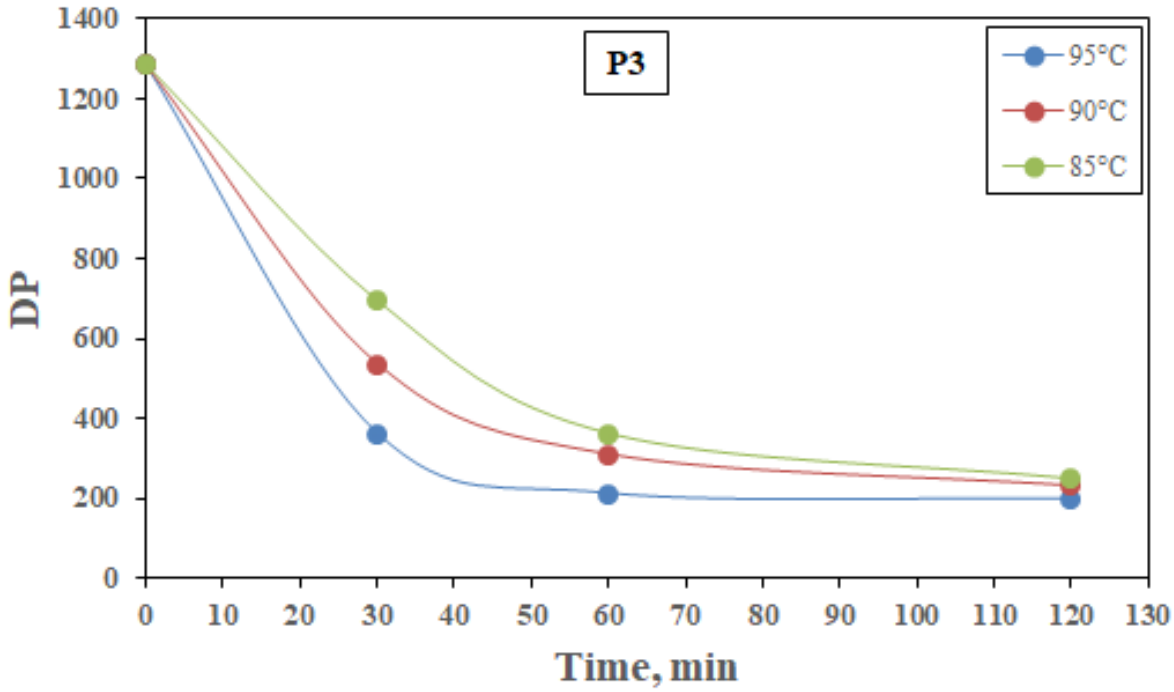

Figure 3. DP reduction curves for the hydrolysis reaction of pulp P3 in 2M HCl

The DP of the unreacted pulp was used as the ‘time zero’ value and it can be seen for both pulp reduction curve sets that the rate of reduction in DP increases with increasing temperature as expected. Lower levelling of points (LODP) were reached with increasing

temperature in both cases, with 85°C reactions only reaching LODP around 120 minutes; the sample DPs measured at this point were below the 350-unit pharmacopoeia cut-off point, therefore the material may be described as *microcrystalline* cellulose (**Thoorens et al., 2014**). It was observed that reactions carried out with temperatures below 85°C struggled to reach LODP after several hours. Although pulp P2 starting DP is significantly lower than P3's equivalent starting point, both pulps reached LODP in relatively similar times. The LODPs for pulp P2 were marginally lower for each reaction when compared against their respective P3 reactions.

4.2. *Acid Hydrolysis Kinetic Parameters*

The activation energy and pre-exponential frequency factor values for both P2 and P3 pulp hydrolysis reaction in 2M HCl were determined as described in Section 3 above. Plots of $\frac{1}{DP_t} - \frac{1}{DP_0}$ vs t for both pulps are given in **Figure 4**. The resultant slopes are the reaction rates and are given in **Table 2**:

Table 2. Hydrolysis reaction rates for P2 and P3 pulp in 2M HCl at given temperatures

Pulp	**Reaction Temperature, °C**	**Hydrolysis Rate k, min^{-1}**
P2	85	2.00 x 10^{-5}
P2	90	3.50 x 10^{-5}
P2	95	5.54 x 10^{-5}
P3	85	1.42 x 10^{-5}
P3	90	2.38 x 10^{-5}
P3	95	3.62 x 10^{-5}

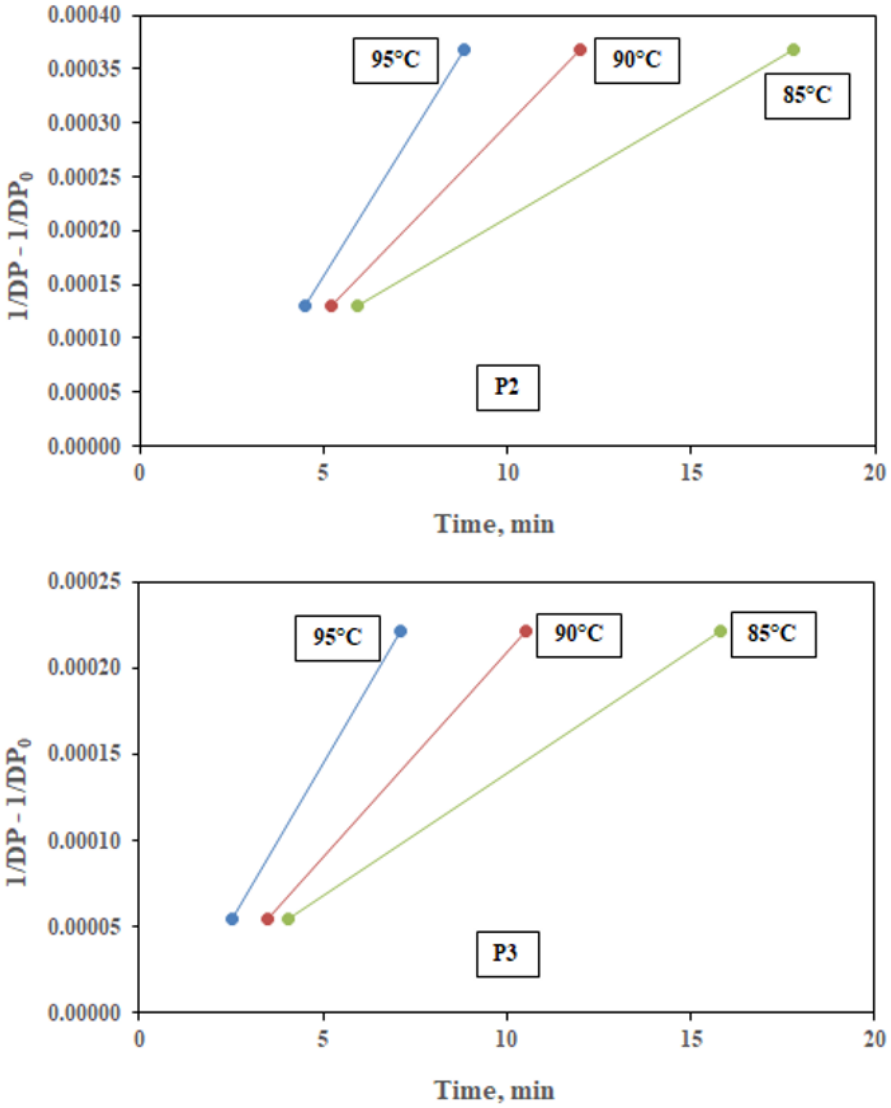

Figure 4. Ekenstam equation plots for pulp P2 (top) and pulp P3 (bottom).

The reaction rate results in **Table 2** are consistent in order of magnitude with cellulose hydrolysis (**Mu et al., 2015; Tizazu and Moholkar, 2018**). Pulp P2 reaction rates are greater than each of the P3 pulp reaction rates for the equivalent reaction temperatures. To understand the difference in reaction rates, Arrhenius plots were generated for the hydrolysis reaction rates at the three given reaction temperatures for both pulps. **Figure 5** shows plots of *ln(k) vs 1/T* for P2 and P3 (top and bottom respectively) with the measure slope being ($-E_a/R$).

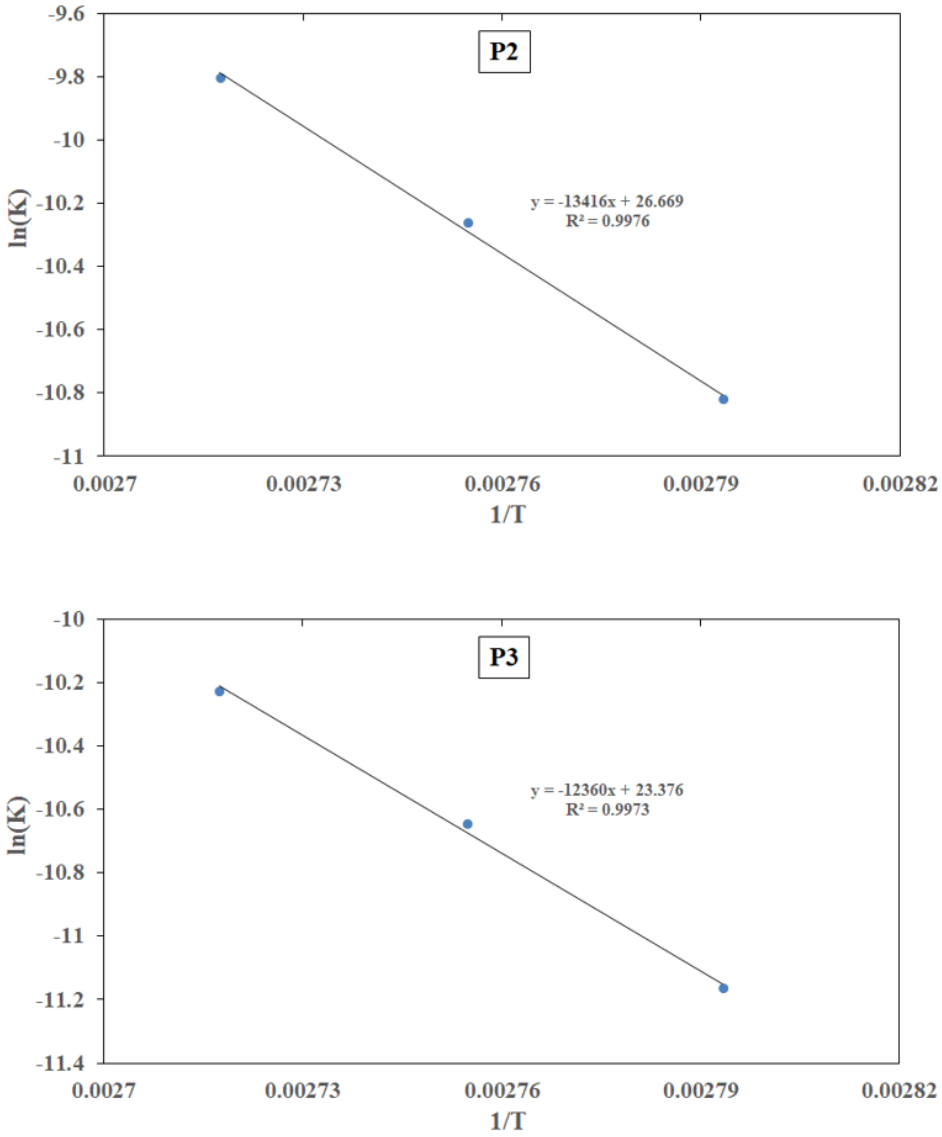

Figure 5. Arrhenius plots for pulps P2 (top) and P3 (bottom)

Both Arrhenius plots show very good fitting of data ($R^2 > 0.99$) and the resultant activation energies and frequency factors are given in Table 3:

Table 3. Activation energy for acid hydrolysis reaction of pulps P2 and P3 in 2M HCl

Pulp	**E_a, kJ mol^{-1}**	**A, min^{-1}**
P2	111.5	3.82×10^{11}
P3	102.8	1.42×10^{10}

The activation energies determined for the pulps are within the general range expected for the acid hydrolysis of cellulosic material: 102 to 147 kJ mol^{-1}, **Higgins et al., (1958)**. An activation energy value of 132 kJ mol^{-1} was experimentally determined by **Mu et al., (2015)** for similar cellulose hydrolysis reactions. It is of interest to point out that pulp P2 has over 10% higher activation energy compared to pulp P3. However, pulp P2 also had a higher reaction rate (**Table 2**). As P2 requires an increased energy level over P3 for the hydrolysis reaction to proceed, the higher rate of reaction (governed by the Arrhenius equation) must be due to the difference in frequency factor (given that the acid concentration, temperature conditions, and agitation level etc. were consistent for both sets of experiments).

Characterisation of both pulps in **Chapter 2** of this thesis indicated that pulp P2 had a higher level of crystallinity than that of P3. The hydrolysis of cellulose based on the fringed fibrillar model (referred to above in the Introduction section above) suggests that the DP reduction is hastened by hydrolysis of the amorphous areas (**Gurnagul et al. 1992**), with tighter crystalline areas inhibiting access of the reactant to the β-1,4-glycosidic bonds (**Zhao et al., 2006**). Furthermore, P2 is a hardwood with lower degree of polymerisation and with smaller and tighter fibres. Therefore, the increased crystallinity and tighter packing of P2 versus P3 may contribute to the higher activation energy required for the hydrolysis reaction. Conversely, SEM analysis of both pulps showed pulp P2 of having significantly more fibres per area and given that the fibres are shorter and more crystalline, opportunities for more successful collisions during hydrolysis of the chain ends may contribute to the large frequency factor (and kinetic rate) difference. The concept of crystallinity in relation to polymers is complex. Regions of structural order and disorder are both present and the macromolecules are longer than the unit cell parameters; each chain, therefore, passes through multiple cell units (**De Rosa and Auriemma, 2014**).

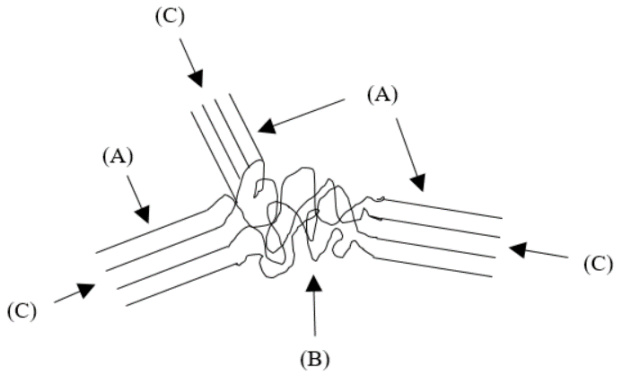

Figure 6. Fringed model of polymer crystallinity. Surface reaction at (A) is unfavourable when compared to amorphous reaction at (B) and readily available ‘end-attack’ hydrolysis at (C).

It was originally proposed by **Sharples (1957)** that hydrolysis of cellulose chain-ends, termed the 'end-attack' model was influential to kinetic rate. **Figure 6** shows a representation of a polymer with both crystalline and amorphous regions. The 'end attack' model is based on the relative availability of chain ends for hydrolysis, shown at position (C), whereas hydrolysis at the crystalline surface (A) is less favourable. **Sixta (2018)** explains the end-attack model by noting that the surface reaction at the crystalline region (A) is unfavourable in comparison with (C) as the solubilisation of cellulose fragments requires two simultaneous breaks by a distance less than the solubility limit. Hydrolysis at the amorphous areas (B) is also more favourable than (A), but depending on morphology constraints, access to the amorphous areas may not be easy, especially with a densely packed crystalline pulp of type P2. Furthermore, given that pulp P2 is a short fibre hardwood, it is likely that there are more chain ends readily available for end-attack, resulting in more successful collisions in comparison to the less crystalline, large fibre softwood pulp P3. This model correlates with the hydrolysis rate differences between the two pulp types observed in the present study. The kinetic analysis herein, therefore, suggests that morphology / pulp wood-type is an important factor in hydrolysis rate and may be linked to large frequency factor differences explained by polymer chain end-attack model.

4.3. *Cellulose hydrolysis thermodynamics*

Thermodynamic parameters for the present acid hydrolysis study were determined from application of the equations outline in Section 3 above. The results are given in **Table 4.** The enthalpy change for both pulps are comparable with pulp P2 requiring just slightly greater energy input. The positive Gibbs Free Energy for both pulps are closely aligned.

Table 4. Thermodynamic parameters for P1 and P2 cellulose pulp hydrolysis in 2M HCl.

Pulp	**ΔH, J mol^{-1}**	**ΔG, J mol^{-1}**	**ΔS, J mol^{-1} K^{-1}**
P2	1.09 x 10^5	1.29 x 10^5	-65.54
P3	1.00 x 10^5	1.28 x 10^5	-92.93

The negative entropy values are of particular interest, as it is suggested that the likely mechanism for the hydrolysis reaction can be identified from the entropy values – see Section 3 above **(Whalley, 1959a; Whalley, 1959b)**. The negative values for ΔS calculated in the

present study suggest that the hydrolysis reactions for the present study likely proceeded via protonation of the cyclic oxygen rather than the glycosidic oxygen: 'Path 2' in **Figure 1** above.

4.4. *DuPont 'Hydrolysis Intensity' equation*

DuPont Corporation (formerly FMC Health and Nutrition) produce MCC at numerous sites worldwide, with the largest global MCC manufacturing plant based in Cork, Ireland. To quantify how far the hydrolysis reaction has proceeded in their plant scale batch reactors, FMC's technical department developed a hydrolysis intensity equation where one 'Reaction Unit' (RU) is a discreet measurement of hydrolysis intensity by time for given acid and temperature conditions. By selecting and adjusting how many RU's that are applied to a reaction, the site's production engineers can, therefore, calculate the reaction time required to elapse that quantity of RU's and control the process accordingly. Additionally, the impact of changes in temperature or acid concentration will be absorbed by the RU calculation and the hydrolysis time required adjusted as required. The RU calculation was developed as follows:

Acid Concentration: FMC experimental data indicated that the rate of hydrolysis reaction was proportional acid concentration by a power factor so 1.2, therefore:

$$k \propto [HCl]^{1.2} \tag{8}$$

The base acid concentration for standard production setting in the plant scale was selected as being 0.65% HCl. Changes in acid concentration are therefore given by:

$$\frac{k_1}{k_2} = \frac{[HCl]_1^{1.2}}{[HCl]_2^{1.2}} \tag{9}$$

Where k_1 is the reaction rate at $[HCl]_1$ acid concentration (assigned 0.65% by FMC) and k_2 is the reaction rate at $[HCl]_2$ acid concentration.

Changes in temperature can be captured via the Arrhenius equation as follows:

$$\frac{k_1}{k_2} = exp\left[\frac{E_a}{R}\left(\frac{1}{T_2} - \frac{1}{T_1}\right)\right] \tag{10}$$

Where k_1 is the hydrolysis rate at temperature T_1, and k_2 is the reaction rate at temperature T_2, E_a is the activation energy and R is the universal gas constant. FMC assigned an activation energy of 30,000 calories per mole (125.5 kJ mol^{-1}) for the acid hydrolysis of cellulose and importantly kept this value irrespective of pulp type. Assigning an arbitrary rate constant vale of 1 for k_1 for a base temperature T_1 of 100°C for all reactions, Equation (10) can be therefore used to calculate a new rate k_2 for new a temperature T_2.

Combining (9) and (10) gives the following:

$$k_2' = \frac{k_2}{exp\left[\frac{Ea}{R}\left(\frac{1}{T_2}-\frac{1}{T_1}\right)\right]} \quad (11)$$

Where k_2' is the overall new reaction rate at temperature T_2, now including k_2 in the numerator to capture acid new concentration per equation (9). The Reaction Unit (RU) is, therefore, expressed as:

$$RU = k_2'.\Delta t \quad (12)$$

Where Δt is the reaction time, usually expressed in minutes onsite for practical reasons. Having set constant activation energy and base temperature and acid values as given above, the RU's elapsed per time can be measured for any reaction temperature and acid concentration. Furthermore, for a given reaction, the production engineer can target a hydrolysis intensity by choosing an RU value and can use equation (12) to back calculate the target time required for the reaction. This is usually carried out via the automated control system onsite.

For historical reasons, the activation energy of 30,000 calories per mole was assigned to the RU calculation as a constant value. In more recent times, primarily due to commercial and raw material supply diversification reasons, different pulp combinations have been introduced to the production of MCC. The results in **Table 3** above indicate that activation energy values may change for different pulp types, 112 kJ mol^{-1} vs 103 kJ mol^{-1} for pulp P2 vs P3 respectively. If the approximate difference in activation energy of 10% between pulp types (as observed in the present study) is applied to the RU equation, then the reaction target time calculated for a typical 800 RU reaction would differ by ~20 minutes. That is, 1 RU value for pulp P2 does not give the same hydrolysis intensity for pulp P3. 20 minutes difference in reaction time is highly significant and may result undesirable changes in crystallinity and particle size distribution as outlined in **Chapter 4**. It is, therefore, recommended that DuPont consider identifying activation energies per specific pulp type and apply to the RU equation as required.

Furthermore, the present study identified significant differences in the frequency factor calculated for the hydrolysis reaction of both pulps; in fact, the impact of frequency factor has been identified as the main driver in difference in reaction rates between the pulp types analysed. It is worth noting that the DuPont RU equation does not take account of differences in frequency factor. If it is assumed that the frequency is equal for all pulp types, it results in the cancelling out of the term in the Arrhenius equation per equation (10) above. It is proposed, therefore, that the term be included in the RU equation as follows:

$$k_2' = \frac{k_2}{exp\left[\frac{Ea}{R}\left(\frac{1}{T_2}-\frac{1}{T_1}\right)\right]} \cdot \frac{A_1}{A_2} \quad (13)$$

Where A_1 is a selected 'base' frequency factor and A_2 is the frequency factor assigned to the pulp being hydrolysed.

5. Conclusions

Given that MCC producers interchange pulps from different origins in their process, a greater understanding of impact of different pulp types on the main hydrolysis reaction is required. The present study revealed that hydrolysis experiments of two pulps (from different wood-type and delignification process) used in the industrial production of MCC had significant differences in measured reaction rate, with the hardwood acid-sulphite pulp (P2) hydrolysing significantly quicker than the softwood Kraft pulp (P3).

Over and under reacting pulp during the industrial MCC process has significant consequences for both downstream operations and final product quality, therefore it is important for manufacturers to understand the reasons for difference in hydrolysis rate and in addition to accurately quantify the difference. The present study showed pulp P2 had a higher activation energy than pulp P3 (correlating with higher crystallinity observed in Chapter 2), so it was unexpected that its reaction rate was higher. However, it was also found that pulp P2's frequency factor was significantly higher than P3's and was the primary driving force for its greater rate of hydrolysis. Frequency factor may be correlated with pulp morphology; pulp P2 was shown to be more densely packed with shorter more crystalline fibres which may result in a greater number of successful collisions at chain ends. This observation is highly significant as it links rate of hydrolysis with morphological characteristics of pulp, which is not given in the current literature. Furthermore, pulp morphology is generally not assessed by MCC producers during pulp selection.

The hydrolysis of pulp to MCC is controlled industrially by combining acid concentration and reaction temperature parameters in a modified Arrhenius type equation and comparing actual processing parameters set for a given reaction against 'base' constant values that were historically set during the first application of the equation. It has been well observed in industry that use of this equation to apply the same hydrolysis intensity to different pulps results in different outcomes, whereby some pulps will be under or over reacted when compared against each other. The present study found that pulps differ significantly in hydrolysis activation energy and frequency factor parameters, and given that the industry standard equation has a

single fixed activation energy value and no frequency factor allowance, it can be concluded that the variance in hydrolysis intensity observed is likely to be driven by these parameters.

A modified version of the industry standard hydrolysis intensity equation was therefore proposed, accounting for differences in pulp activation energy values, and also introducing frequency factor terms. A more accurate hydrolysis intensity equation is of very high benefit to MCC producers and offers the potential for significant processing and product quality improvements. Initial trials at DuPont Cork have resulted in very positive improvements to the MCC production process.

Acknowledgements

The authors wish to acknowledge AMBER Centre, Trinity College Dublin for providing financial support to carry out the research, and DuPont Nutrition and Health for pulp supply and onsite laboratory access.

References

Aro, T., Fatehi, P. (2017). Production and application of lignosulfonates and sulfonated lignin. ChemSusChem 10, 1861–1877.

Brittain, H.C., Lewen, G., Newman, W., Fiorelli, K., Bogdanowich, S. (1993). Changes in material properties accompanying the national formulary (NF) identity test for microcrystalline cellulose. Pharm. Res. 10, 61-67.

Calvini, P., Gorassini, A., Merlani, A. (2008). On the kinetics of cellulose degradation: looking beyond the pseudo zero order rate equation. Cellulose, 15(2):193–203.

De Rossa, C., Auriemma F. (2014). Crystals and Crystallinity in Polymers, Diffraction Analysis of Ordered and Disordered Crystals, John Wiley & Sons, Inc., Hoboken, New Jersey, ISBN 978-0-470-17576-7.

Fan, L., Gharpuray, M.M., Lee, H. (1987). Cellulose Hydrolysis, ISBN-13: 978-3-642-72577-7, DOl: 10.1007/978-3-642-72575-3 Springer-Verlag.

Frey-Wyssling A., and Muhlethaler K. (1965). Ultrastructural Plant Cytology with an Introduction to Molecular Biology. Elsevier, Amsterdam, The Netherlands.

Gurnagul N. (1992). The effect of cellulose degradation on the strength of wood pulp fibres. Nordic Pulp Pap. Res. J. 7(3): 152.

Hearle J.W.S. (1963). The fine structure of fibres and crystalline polymers. J. Appl. Polym. Sci. 7: 1175–1192.

Higgins, H., Goldsmith, V., McKenzie, A. (1958). The reactivity of cellulose. IV. The activation energy for heterogeneous acid hydrolysis. J. Polym. Sci. 32 (124), 247–252.

Humienik, M.O., Mozejko, J. (2000). Thermodynamic functions of activated complexes created in thermal decomposition processes of sulphates. Thermochim. Acta 344, 73-79.

Hua, J., Zhanga, Q., Lee, D.J. (2018). Kraft lignin biorefinery: A perspective, Bioresource Technology 247 1181–1183.

Mu B., Xu H., Yang, Y. (2015). Accelerated hydrolysis of substituted cellulose for potential biofuel production: Kinetic study and modelling, Bioresource Technology 196 (2015) 332–338

Nevell, T.P., Upton, W.R. (1976). Carbohydrate Res 49:163

Palme, A., Theliandera, H., Brelidb, H. (2016). Acid hydrolysis of cellulosic fibres: Comparison of bleached kraft pulp, dissolving pulps and cotton textile cellulose. Carbohydrate Polymers 136 1281–1287

Parikh, R.S. (1967). Textile Res. J, ibid. 37:538

Sixta, H. (2018). Chem-E1150, Biomass pretreatment and fractionation, Lecture 6, Hot water treatment 1, Aalto Universtiy, School of Chemical Engineering, website:

https://mycourses.aalto.fi/pluginfile.php/611796/mod_resource/content/1/Lecture%206.pdf Accessed on 23rd of May 2018.

Sharples, A. (1957). The hydrolysis of cellulose and its relation to structure, Trans. Faraday Soc. 53, 1003.

Straszko, J., Humienik, M.O., Mozejko, J. (1997). Kinetics of thermal decomposition of $ZnSO_4 \cdot 7H_2O$. Thermochim. Acta, 292, 145-150.

Szejt1i, J. (1975). Siiurehydrolyse glycosidischer Bindungen. VEB, Leipzig

Tee T.T., Sin, L.T., Gobinath, R., Bee, S.T., Hui. D., Rahmat, A.R. (2013). Investigation of nano-size montmorillonite on enhancing polyvinyl alcohol-starch blends prepared via solution cast approach. Compos Part B 47:238e47.

Thoorens, G., Krier, F., Leclercq, B., Carlin, B., Evrard, B. (2014). Microcrystalline cellulose, a direct compression binder in a quality by design environment—A review, International Journal of Pharmaceutics 473 64–72.

Tizazu, B.Z., Moholkar, V.S. (2018). Kinetic and thermodynamic analysis of dilute acid hydrolysis of sugarcane Bagasse, Bioresource Technology 250 (2018) 197–203

Whalley, E. (1959a). Can J Chern 37:788.

Whalley, E. (1959b). Trans Faraday Soc 55:798.

Zhao, H., Kwak, J. H., Wang, Y., Franz, J. A., White, J. M., & Holladay, J. E. (2006). Effects of crystallinity on dilute acid hydrolysis of cellulose by cellulose ball-milling study. Energy & Fuels, 20, 807–811.

Zou, X., Uesaka, T., Gurnagul, N. (1996). Prediction of paper permanence by accelerated aging I. Kinetic analysis of the aging process. Cell 3 (1), 243‑267.

Chapter 6

FT-IR Spectroscopy to Identify Silica Content of Silicified Microcrystalline Cellulose

FT-IR Spectroscopy to identify silica content of silicified microcrystalline cellulose

Conor O'Regan*[a,b], Vivek Verma[e], Justin D Holmes[a,c,d], and Michael A Morris*[c,d]

[a] Materials Chemistry, Department of Chemistry, University College Cork, Cork, Ireland,

[b] DuPont Nutrition and Health, Cork, Ireland,

[c] AMBER, Trinity College Dublin, Dublin 2, Ireland,

[d] Tyndall National Institute, Lee Maltings, Prospect Row, Cork, Ireland,

[e] University of Limerick, Limerick, Ireland

*Corresponding author: Email: conor.o-regan@dupont.com (Conor O'Regan), morrism2@tcd.ie (Michael A Morris) Ph: +353 18963089

ABSTRACT

Silicified microcrystalline cellulose (SMCC) has advantages over conventional MCC in the application of pharmaceutical tableting processes, such as improved tablet strength, retention of compressibility after wet granulation, and superior flow characteristics. Production of SMCC is achieved by addition of approximately 2% by weight of fumed silica to the MCC dispersion prior to the drying phase. Control of the silica addition in a continuous process is challenging, and in-process quality control measurement of silica content by sulphated ash method is time consuming; there is no rapid method given in the current literature. Consequently, deviations from the silica content of the SMCC dried product may not be known until hours after the material has been produced, and only then can corrective action be taken to adjust the production process. Fourier Transform - Infra Red spectroscopy studies of both SMCC and standard MCC material indicate that the silica peak at 808 cm^{-1} is not present in the MCC spectrum. Calibration curves were generated based on the area of this peak for samples of two grades of SMCC and compared against the sulphated ash results. No statistical difference was observed between the two methods. A new rapid method for determination of silica in SMCC products was, as a result, proposed, offering highly significant processing advantages industrially.

Keywords: SMCC; silica; FT-IR; spectroscopy; cellulose

1. Introduction

Microcrystalline cellulose (MCC) is widely used as a compression aid in the direct compression tableting formulations, and also as a diluent in the wet granulation process. The addition of fumed silica is known to increase the effective surface area of the MCC material, and tablets produced with silicified microcrystalline cellulose (SMCC) by wet granulation are shown to have much higher tensile strength than tablets produced with standard grade MCC (**Sherwood & Becker, 1998**). In addition, SMCC products have been shown to have superior flow properties (**Buckton and Yonemochi, 1999**) and improved tablet strength (**Edge et al., 2000**).

The USP-NF (United States Pharmacopeia - National Formulary) monograph for SMCC products dictate that silica content is verified by a 'Residue on Ignition' procedure, commonly known as the sulphated ash test. This procedure is based on the ignition of an SMCC sample in the presence of sulphuric acid and measurement of the portion not volatized. The test requires high temperatures (~ 600°C) and is time consuming with results typically known in the order of three hours from start of test. As the SMCC production process is a continuous process, and deviations in the specification for silica content in the SMCC material produced are not readily known for some time, large quantities of SMCC product may be produced out of specification. A quicker, indicative test for silica content is therefore highly desirable to SMCC producers.

There is currently a lack of published literature showing spectroscopic techniques for silica content identification in SMCC products. **Buckton and Yonemochi (1999)** give a Near-IR method for distinguishing SMCC products from simple physical mixtures of fumed silica with MCC powder products. However, they do not calibrate the N-IR method against the sulphated ash method for accurate quantification of the silica percentage.

Analysis of FT-IR spectra in the present study indicated that fumed silica has a broad peak at 808 cm^{-1} while standard MCC product does not exhibit a peak at that wavenumber. Hence this peak was selected to develop a rapid method for the indicative determination of silica in the SMCC products. The goal of this study was to generate accurate calibrations for the FT-IR method and compare against the standard sulphated ash method for silica content quantification of selected SMCC grades.

2. Materials and Methods

2.1. *Materials*

Samples of silicified MCC grades SMCC50 (lot S61704C) and SMCC90 (lot S71704C) were selected for this study. All materials were supplied courtesy of DuPont Nutrition and Health, Cork, Ireland.

2.2. *FT-IR analysis of SMCC and MCC*

The FT-IR spectrum for standard MCC material is well known, with the characteristic C-O-C cellulose ring mode identifiable as an intense peak at the 1033 cm^{-1} band area (**Maréchal, and Chanzy, 2000**). The FT-IR spectrum for silica also has an intense and broad band from round 1095 to 1089 cm^{-1} which is assigned to the Si-O-Si asymmetric stretching (**Al-Oweini and El-Rassy, 2009**), and partially overlaps with the cellulose C-O-C peak, see **Figure 1**. However, the silica peak at around 808 cm^{-1} (which is assigned to Si-O-Si stretching) is identifiable when compared against the MCC spectrum (dashed red area in **Figure 1**). This peak was therefore selected for calibration to determine the silica content in SMCC products.

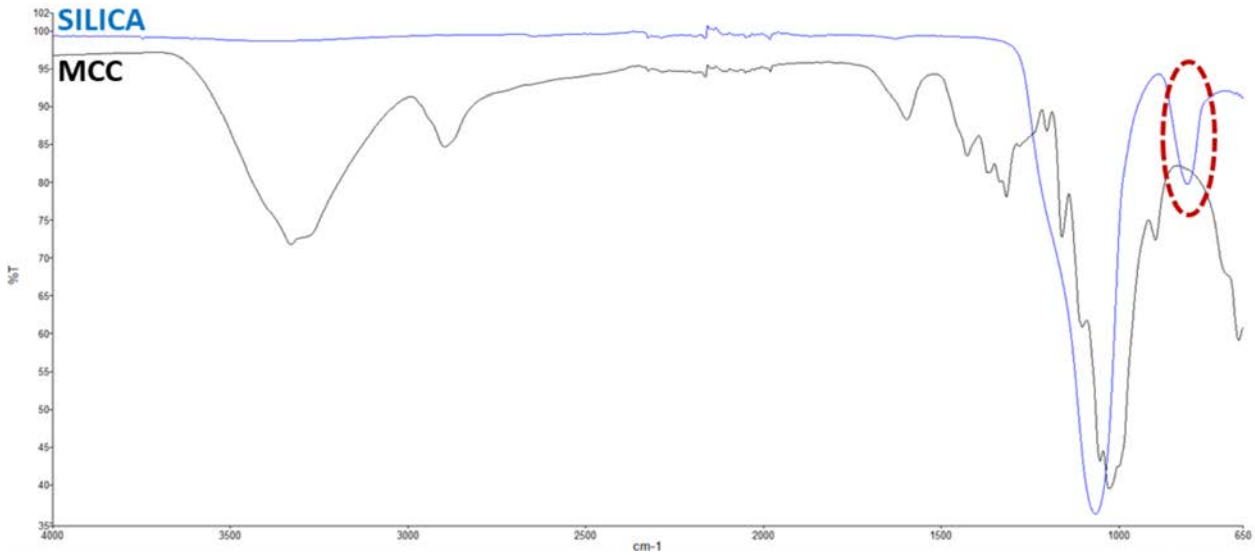

Figure 1. FT-IR spectrum of Silica (Blue) and standard MCC (Black). Distinct peak of Silica (808 cm^{-1}) in area of no MCC peak (dashed red circle).

3. Results and Discussion

3.1. *SMCC50 Calibration*

The area under the Si-O-Si peak centred around 808 cm^{-1} from Base-1 (830.01 cm^{-1}) to Base-2 (785.45 cm^{-1}) was correlated with the amount of silica present in the sample confirmed using the sulphated ash test. Five different SMCC50 samples containing a known amount of silica were selected to make a calibration plot. **Figure 2** below gives an example spectrum showing the peak selected for the calibration plot, and the area under it.

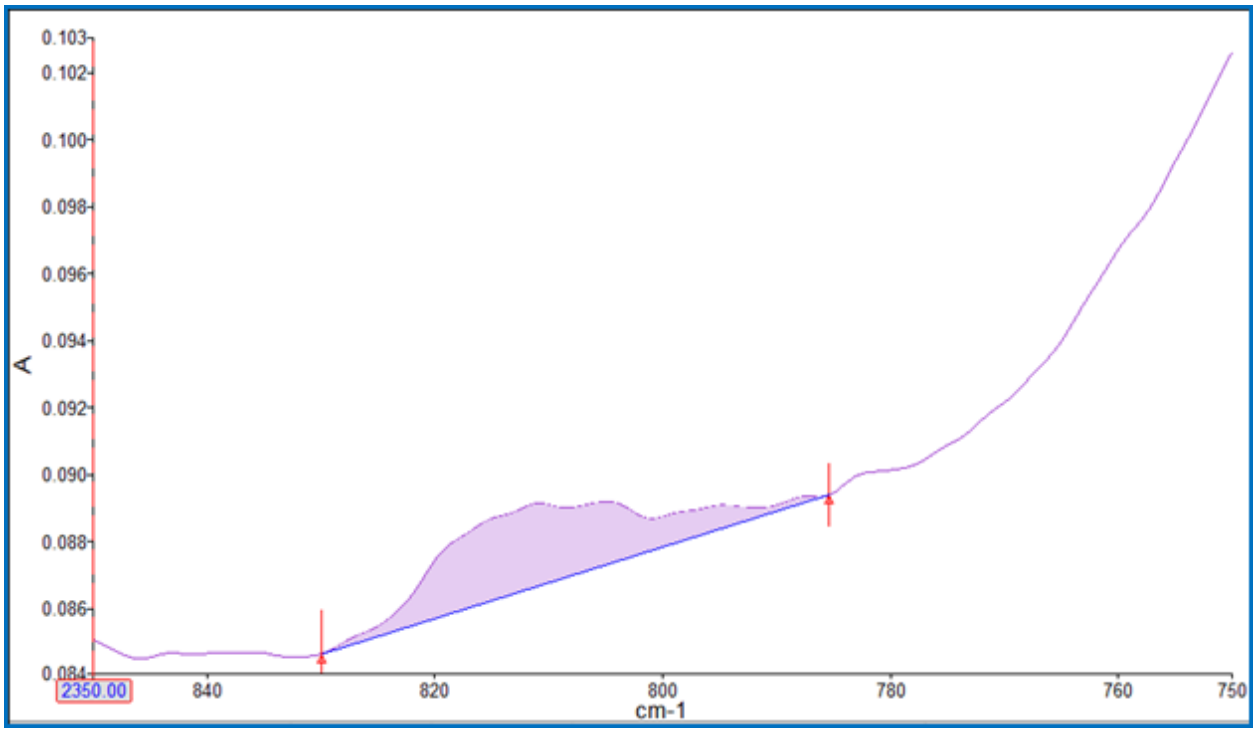

Figure 1: Area of the FT-IR spectrum selected for calibration curve for SMCC50 (Lot S61704C)

Table 1 presents the samples used for the calibration plot for the SMCC50 (S61704C) batch. The silica content of each sample was determined using the sulphated ash test method. Duplicate testing was carried out for all samples. The silica content of each sample was within the 1.8% to 2.2% specification range for SMCC grade products.

Table 1. Calibration samples for SMCC50 with known amount of silica from ash test

Sample	Ash Test Silica, (%)
S61704C-136	1.93
S61704C-151	1.87
S61704C-166	1.87
S61704C-451	1.99
S61704C-505	1.81

The calibration plot for SMCC50 (using samples from lot S61704C) is given in Figure 3. Correlation value for the plot is 0.99 with a standard error of 0.003 and a standard prediction error of 0.005

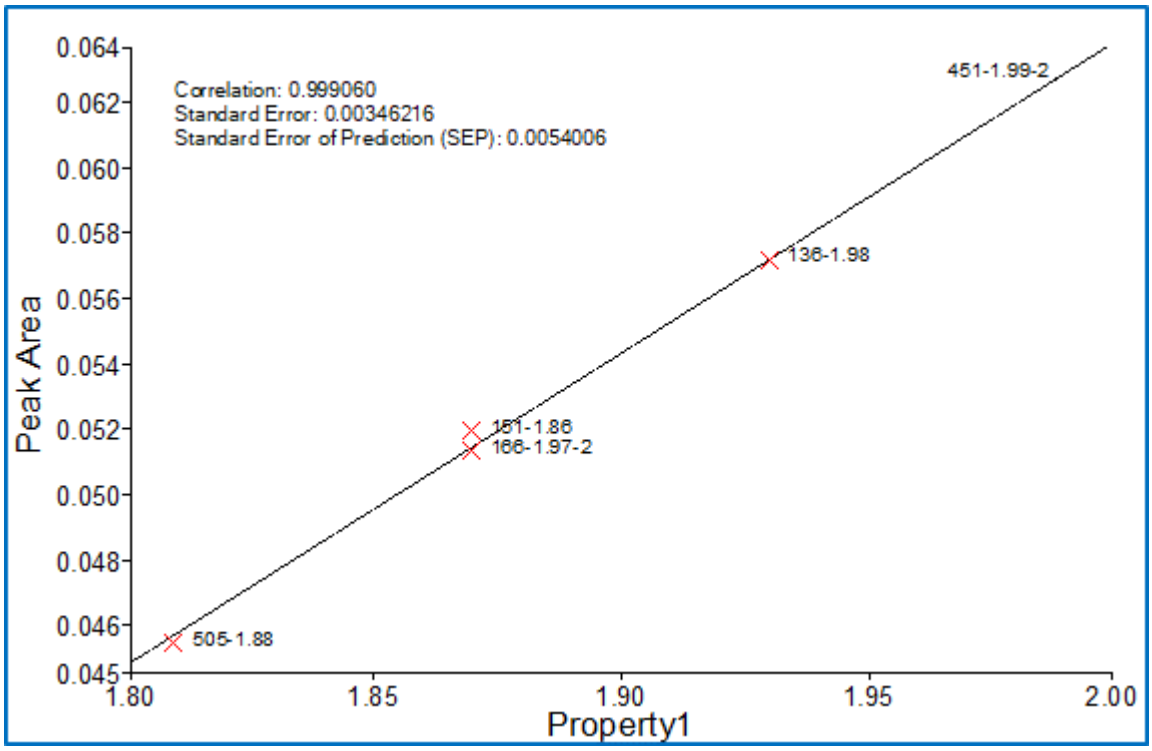

Figure 3. Calibration plot for SMCC50 (lot S61704C)

This method was validated using other SMCC50 samples (from the same lot) for which the amount of silica was already known previously using the sulphated ash test method; the results are presented below in **Table 2**. A high correlation between the sulphated ash method and the FT-IR calibration method was achieved. Sample number S61704C-61 showed a large difference (0.11% silica) between the two methods, however, on re-testing the sample by sulphated ash method the difference was reduced. Statistical analysis of the results showed that

the mean of ash tent results is not significantly different from the mean of FT-IR method (p = 0.524 for a paired t-test).

Table 2: Validation results for SMCC50 samples using the FT-IR method

Sample	Ash Test Silica, %	FT-IR Silica, %	Repeat Ash Test silica, %
S61704C-46	2.10	2.10	-
S61704C-61	1.79	1.90	1.84
S61704C-76	2.01	2.02	-
S61704C-106	2.00	1.99	-
S61704C-121	1.98	1.94	-
S61704C-487	1.84	1.88	-

3.2. *SMCC90 Calibration*

For the SMCC90 samples (lot S71704C), the area under the peak from Base-1 (829.47 cm^{-1}) to Base-2 (781.15 cm^{-1}) was correlated with the amount of silica present in the sample confirmed using the sulphated ash test. Four different SMCC samples containing known amount of silica were selected to make a calibration plot. **Figure 4** shows an example spectrum of the peak and area under it that was selected for the calibration plot.

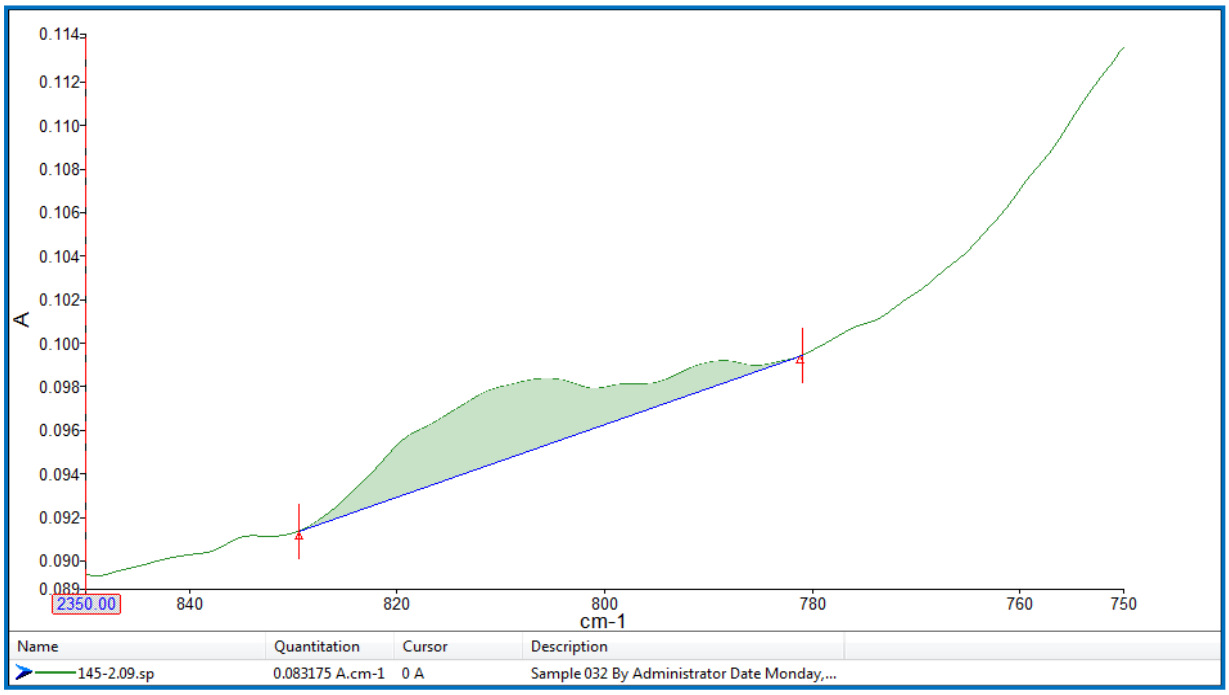

Figure 4: Area of the FT-IR spectrum selected for calibration curve for SMCC90 (S71704C)

Table 3 gives the samples used for the calibration plot for S71704C batch and the corresponding silica content in each sample as determined by the ash test method.

Table 3. Calibration samples for SMCC90 with known amount of silica from ash test

Sample	Ash Test Silica, (%)
S71704C-55	1.94
S71704C-91	2.12
S71704C-145	2.09
S71704C-451	1.85

The resultant calibration plot is given below in **Figure 5**. The correlation value for the plot is 0.99 with a standard error of 0.009 and a standard prediction error of 0.023.

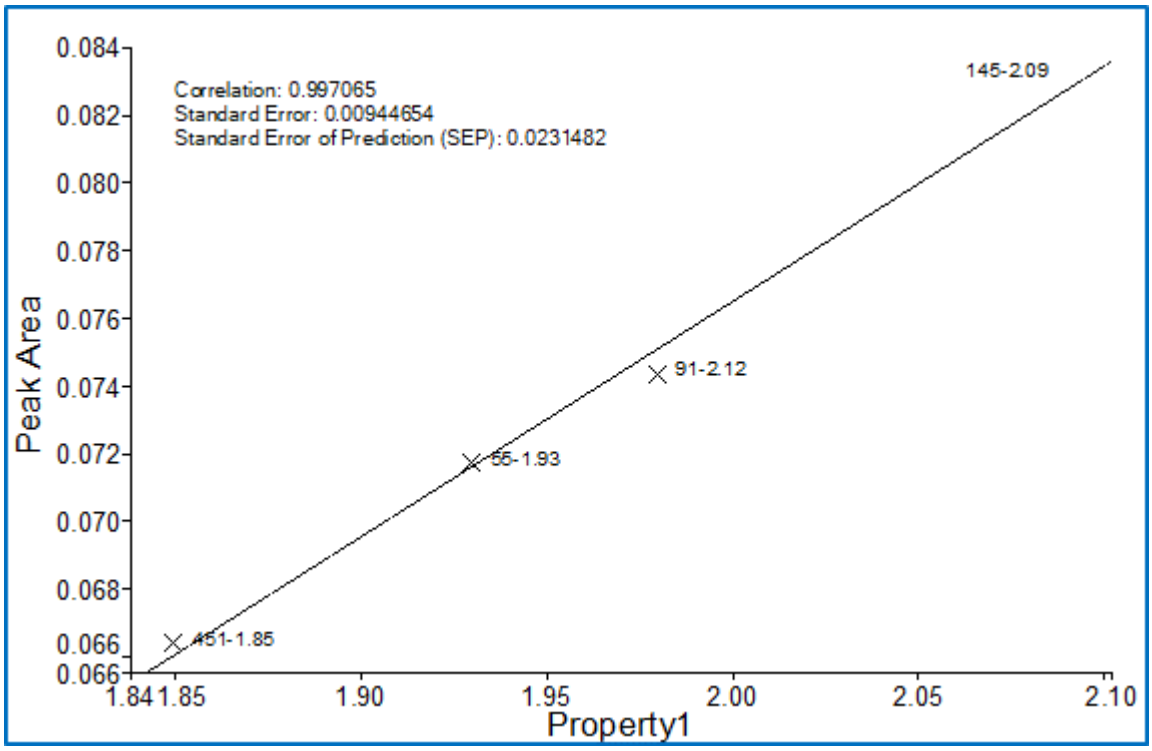

Figure 5: Calibration plot for SMCC90 (S71704C)

Again, the calibration was validated by testing of other SMCC90 samples from the same lot that had previously had their silica content determined by the sulphated ash method. The results are given in **Table 4**.

Table 4: Validation results for SMCC90 samples using the FT-IR method

Sample	Ash Test Silica, %	FT-IR Silica, %	Repeat Ash Test silica, %
S71704C-31	1.83	1.83	-
S71704C-307	1.61	1.63	1.64
S71704C-325	1.83	1.77	-
S71704C-343	1.92	1.80	1.82
S71704C-433	1.86	1.87	-
S71704C-469	1.97	1.92	-

The correlation between the results for both methods is high. Samples S71704C-307 and S71704C-343 were re-tested by the sulphated ash method and a closer correlation was achieved. Statistical analysis of the results by paired t-test showed no significant difference between the means ($p= 0.115$).

4. Conclusions

The quantification of silica content in SMCC product grades by the sulphated ash method is time consuming and labour intensive. Identification of a more rapid spectroscopic method has a number of advantages for the commercial production process and no such method is currently given in the literature. The Si-O-Si stretching peak at around 808 cm^{-1} was identified for calibration of silica content as standard MCC grades do not have a peak in this area. Calibration plots for lots of two grades of SMCC were generated with high accuracy of fit in both cases. Validation of the calibration was carried out with other samples of the selected SMCC grades and excellent correlation was achieved.

Production rates of SMCC are typically in the order of 500 to 1000 kg $hour^{-1}$ of finished product, and as a result up to 3 metric tonnes of product may be produced before onsite laboratory results of silica content via the sulphated ash method are known. Given the very tight specification on silica content of the final product, it is highly possible that the material may be produced out of specification, incurring large re-processing or write-off costs for the manufacturer. Furthermore, should the material be out of specification, the effect of adjustments to the silica dosing rate will not be known for a further three hours, by which time another 3 metric tonnes of product may have been produced. It is therefore of immense benefit to SMCC producers to employ an accurate rapid and simple spectroscopic method such as the FT-IR method developed in the present study, that has been demonstrated to compliment the

sulphated ash method with excellent correlation. Initial trials of the proposed FT-IR method at DuPont Cork have been very successful and formal adoption of the procedure is ongoing.

Acknowledgements

The authors wish to acknowledge AMBER Centre, Trinity College Dublin for providing financial support to carry out the research, and DuPont Nutrition and Health for material supply and onsite laboratory access.

References

Al-Oweini, R., El-Rassy, H. (2009). Synthesis and characterization by FTIR spectroscopy of silica aerogels prepared using several Si(OR)4 and R00Si(OR0)3 precursors / Journal of Molecular Structure 919 140–145

Buckton, G., Yonemochi, E. (1999). Near IR spectroscopy to quantify the silica content and difference between silicified microcrystalline cellulose and physical mixtures of microcrystalline cellulose and silica, European Journal of Pharmaceutical Sciences 10 77–80.

Edge, S., Fraser Steele, D., Chen, A., Tobyn, M.J., Staniforth, J.N. (2000). The mechanical properties of compacts of microcrystalline cellulose and silicified microcrystalline cellulose, International Journal of Pharmaceutics 200 67–72

Maréchal, Y., Chanzy, H. (2000). The hydrogen bond network in Iβ cellulose as observed by infrared spectrometry. J. Mol. Struct. 523, 183-196.

Sherwood, B.E., Becker, J. (1998). A new class of high functionality excipients: silicified microcrystalline cellulose. Pharm. Technol. 22, 183–194.

Chapter 7

Summary and Future Work

7. Summary

The primary research objectives and results detailed in this thesis concern the challenges of commercial production of microcrystalline cellulose (MCC) via acid hydrolysis of speciality cellulose pulps. In recent years MCC manufacturers have diversified pulp sourcing and usage, and as a consequence, have experienced significant challenges to maintain accurate control of the process in the absence of detailed knowledge of the key characteristics and parameters of their primary raw material. The impact of over or under reacting during the hydrolysis step cannot be overstated and is the most significant root cause of production losses (such as reduced production rate, uptime, and product quality) in the commercial MCC process.

The detailed characterisation (outlined in Chapter 2) of pulps from different origins (wood-type and delignification process) showed significant differences, particularly in terms of α, β and γ cellulose content, crystallinity and morphology. These differences were clearly manifested in the thermal degradation kinetic results which linked crystallinity with activation energy and rate. Furthermore, pulp morphology was linked with kinetics via frequency factor differences; a link not given in the current literature. The equivalency of pulps assumed by MCC manufacturers was therefore clearly challenged and this research provides quantification to the observed differences previously not available to producers.

Given that significant differences were found between the pulps, it was of interest to understand if MCC grades produced from different pulps also contained variances as a result. If MCC grades were found to have had significant differences due to pulp selection, it would be of serious importance to MCC producers who do not differentiate products based on starting pulp type. Furthermore, any differences in MCC would be of high importance to MCC customers in the pharmaceutical industry and therefore of significant commercial importance to MCC producers. It was, therefore, noteworthy that the results of the research outlined in Chapter 3 showed that the differences in pulp crystallinity and morphology observed in Chapter

2 did not lead to variances between the respective MCC product grades. However, it was unexpectedly found that the MCC products were lower in crystallinity when compared to the starting pulp raw material, suggesting that the hydrolysis step impacted both amorphous and α-crystalline regions of the cellulose. It is generally understood by MCC producers that industrial hydrolysis conditions result in selective depolymerisation of amorphous regions only. Therefore, a reduction in crystallinity is highly significant as it represents a potential yield loss to MCC producers, who may now wish to investigate adjustment of reaction parameters accordingly.

With the hydrolysis step being the key reaction during the conversion of pulp to MCC, the research in Chapter 4 characterises the hydrolysis of a given pulp under different temperature and acid conditions. It was surprisingly found that the pulp stayed largely physically intact in the early stages of the reaction although the rate of depolymerisation was then at its highest; an observation not given in the current literature. Particle size distribution analysis showed clear changes in D50 and D90 values as the reaction proceeded and importantly the particle size reduction continued throughout the full reaction time even though the degree of polymerisation reduction had levelled off. Particle size measurements, therefore, present an opportunity for real time feedback of hydrolysis progression and an opportunity to select a reaction end point indicator that is currently not utilised industrially. Given the impact of over and under reacting, discussed above, such an indicator is likely to be of significant benefit to MCC producers. In addition, the reduction in crystallinity from pulp to MCC observed in Chapter 3 was also found to occur during these hydrolysis experiments, again alerting to the possibility of important adverse yield impacts industrially.

Following on from the characterisation of the cellulose hydrolysis reaction, the research outlined in Chapter 5 confirmed that pulps of different origin can have significantly different hydrolysis kinetics, which validates the challenges experienced by MCC producers in

following changes of pulp in the industrial process. It was unexpectedly found that the hardwood pulp that was higher in crystallinity and activation energy, had a higher rate of hydrolysis. Kinetic analysis revealed that the frequency factor of the hardwood pulp was significantly higher than that of the softwood pulp and that this was the primary factor driving the difference in reaction rate. The research, therefore, demonstrated the importance of pulp wood-type and morphology over delignification process and crystallinity. Such a link is not readily available in the literature and offers MCC producers highly useful quantitative kinetic analysis of pulps. In addition, the industry standard hydrolysis equation was modified based on the outcome of the research, and initial trials at DuPont have proved very successful in reducing process variability due to pulp changes.

Finally, production of silicified microcrystalline cellulose (SMCC) is highly challenging, particularly due to the absence in the literature of a rapid method for the determination of silica content in the SMCC material. Given the lengthy test time of the sulphated ash method, SMCC producers risk having large quantities of out-of-specification material, which is of significant potential cost to the business. The FT-IR method developed during the present research provides an accurate complimentary method, reducing testing time from three hours to a couple of minutes, greatly enhancing the processing capability of the product range. The method is currently being introduced at DuPont Cork and initial trials have proven to be very successful.

7.1 Research Objectives

(i) The various cellulose pulps used in the industrial production of microcrystalline cellulose (MCC) are essentially deemed ‘equivalent’ within that business sector, and it has been shown that commercial MCC product grades can be manufactured within specification limits while interchanging the starting pulp type.

MCC production is however highly challenging and variability in the pulp raw material is considered likely to be the primary driver of the processing difficulties. The research in **Chapter 2** endeavours to characterise selected pulps of different wood origin and delignification process and identify relevant differences between them in terms of content, surface chemistry, morphology, structure, and crystallinity etc. In addition, characterisation of the pulps via thermogravimetric analysis allows for investigation of how these differences affect the thermal degradation process. Subsequent application of three kinetic models (of different mathematical basis) allow for determination of kinetic and thermodynamic parameters of the thermal decomposition, which can then be correlated with the pulp characterisation analysis.

The relevance of this research lies in the successful determination of key differences between pulp types of various origins which are currently not well understood. This is of high importance to MCC manufacturers as they attempt to continuously improve and optimise their production processes in an ever-increasing competitive market. An understanding of differences in pulp type offer potential opportunities for improved processing and subsequent reduction of variance.

(ii) Having identified significant differences in the cellulose pulps, the goal of **Chapter 3** was to investigate and understand if these differences contribute to variability in the MCC products that have been directly produced from these pulps. Two samples of Avicel PH102 which were each produced exclusively from different pulp sources were selected and the detailed characterisation techniques and kinetic models applied in **Chapter 2** were also applied to these MCC powder products.

A key tenet within the MCC production business is that the interchangeability of qualified pulps of various origins does not introduce adverse variability to the commercial products. As all products released to the primary users of MCC

(generally pharmaceutical tableting operations) are passed by rigorous Quality Control and Assurance functions, MCC manufactures are confident of the equivalency in application of the Avicel grades produced from different pulp types. However, apart from confirmation of production to specification limits, it is not well understood if pulp variances can be identified in the finished powder products. Differences in parameters such as crystallinity levels and morphology may not impact the release specification of the MCC grades, however they may contribute to variance in performance during the application of the products in the pharmaceutical sector. It is therefore highly important that MCC producers understand the nature of any differences introduced to their products as a result of the use of raw materials from different origins.

(iii) The key processing step in the production of MCC is the hydrolysis reaction of the cellulose pulp. The pulp raw material already contains cellulose provided by nature, and the objective of MCC production is the partial depolymerisation of this cellulose to a *microcrystalline* level, the production of which has been found to have excellent compaction properties applicable to the tableting process. The goal of **Chapter 4** was to provide a detailed characterisation of the hydrolysis process for a selected pulp type. By varying the key hydrolysis conditions such as temperature and acid concentration, changes in the reduction of the degree of polymerisation can be identified. Analysis of samples taken at various stages throughout the reaction time can provide important information on how key parameters such as particle size distribution, morphology and crystallinity are affected as the reaction proceeds. Furthermore, the impact of changes in temperature and acid concentration on these parameters at a consistent quench time are also understood.

The investigation detailed in **Chapter 4** is of high relevance in furthering the technical understanding of the main reaction step in the MCC production process. Control of the hydrolysis step is challenging as there is currently no real-time analysis to identify the optimum time to quench the reaction. Under-reacting the product results in viscous slurries which are difficult to process downstream from the reaction step, whereas over-reacting leads to adverse filtration performance and a dense powder product that may exceed tight bulk density specification limits. A greater understanding of the changes in critical parameters during the conversion of pulp to MCC is therefore crucial to the optimisation of the hydrolysis step at an industrial level.

(iv) Following the detailed characterisation of the hydrolysis profile of a selected pulp, the objective of **Chapter 5** was to understand differences in the hydrolysis profile of pulps form different origins. Two pulps were selected that had already been characterised in **Chapter 2** and were found to have had the largest differences on the parameters investigated (degree of polymerisation, crystallinity, thermal degradation kinetics etc). By carrying out hydrolysis experiments on the selected pulps at different temperatures, differences in the reactions rates of the pulps could be determined via established kinetic models. The differences identified were therefore related to the pulp characteristics previously assessed.

Application of the Arrhenius equation to the reaction rate results for the given reaction temperatures allowed for determination of the acid hydrolysis kinetic parameters for both pulp types and identification of relevant differences.

Subsequent calculation of thermodynamic parameters was also carried out and information as to the likely reaction mechanism pathway identified.

The relevance of this research is directly applicable to the manufacturing process. The DuPont 'Reaction Unit' equation, which measures hydrolysis intensity per time for given temperature and acid concentration conditions is the 'tool' used by DuPont's technical production team to control the reaction. As a consequence of the research outlined in **Chapter 5**, important limitations of the 'Reaction Unit' equation were identified and modifications proposed. Improvement in the control of the hydrolysis intensity is critical to the MCC production process.

(v) Silicified microcrystalline cellulose (SMCC) is a variant of MCC used in certain tableting applications due to its increased compaction properties over standard MCC. The rate of addition of fumed silica to the MCC liquid phase dispersion is required to be tightly controlled during continuous processing to meet the tight specification of silica content on the final product. The regulatory method dictated by the pharmaceutical monograph for silica content quantification is via 'Residue on Ignition' testing, commonly known as the sulphated ash method. This test is time consuming and labour intensive, with results only known in the order of 3 hours following start of the test. During this time, the continuous production operation may have produced over 1.5 metric tonnes of product with unknown silica content, risking failure of release during Quality Control. Identification and development of a rapid spectroscopic technique (not currently apparent in the published literature) is therefore of significant benefit to SMCC producers.

Chapter 6 outlines the development of a rapid FT-IR spectroscopic calibration for the accurate quantification of silica content in selected SMCC grades, complimentary and statistically equivalent to the required sulphated ash test.

7.2 Research Results & Further Work

The results of the research outlined in Chapters 2 to 6 of this thesis, and opportunities for further investigation are summarised at a high level as follows:

(i) The characterisation of pulps from different sources (**Chapter 2**) revealed significant differences in cellulose content: pulps that were delignified via the acid-sulphite process had higher α-cellulose content were more crystalline than pulps generated from the Kraft pulping process. Morphological differences were identified and related to wood type; the hardwood eucalyptus pulp had significantly smaller fibre size and more inter-connecting surface area compared to the softwood pulps. Kinetic and thermodynamic parameters for the thermal degradation of the pulps revealed that the hardwood acid-sulphite pulps required more energy to breakdown and had a significantly higher frequency factor. The potential impact of these difference was explored in the subsequent technical chapters.

The sample of pulps tested did not comprise of the full range of pulps available to MCC producers. Additionally, it is likely that variances within lots of the same pulp type are also present. Therefore, further characterisation of pulps, particularly focused on α-cellulose content, crystallinity, and morphology is recommended.

(ii) **Chapter 3** gives the analysis of two sets of samples of MCC grades (each produced exclusively by a pulp characterised in **Chapter 2**) and the significant differences in pulp type were largely not observed in their resultant MCC powder products. This

finding is highly important for MCC manufactures, as it confirms that the variance in raw material appears to be negated by control of the MCC process, and the MCC grades released can be deemed ‘equivalent’ for the parameters investigated.

As the conversion of pulp to MCC is based on the hydrolysis of the amorphous areas (per the fringed fibrillar model) it was surprising to find that the crystallinity of the MCC products was slightly reduced compared to the starting pulps. It was concluded that hydrolysis of the crystalline areas must also be taking place during the reaction. Investigation of this phenomenon is carried out in the following technical chapter.

Further detailed characterisation of MCC powder products from varying pulp sources, and indeed pulp blends, would advance the current state of the art knowledge.

(iii) The hydrolysis experiments of a hardwood pulp previously characterised in **Chapter 2** formed the basis of **Chapter 4**. DP reduction curves showed a rapid reaction rate in the initial stages, which in all cases slowed to a levelling off in the degree of polymerisation reduction (LODP). It was found that higher temperatures and acid concentrations resulted in sharper decline in DP, and a lower level of LODP reached. For the conditions examined, the change in temperature had a greater influence than the change in acid concentration.

Surface morphology imaging revealed that material tended to remain physically intact in the early stages of the reaction (although the DP reduction was greatest during this time); an observation highly significant for MCC producers, who make similar observations at a plant scale level.

Particle size analysis revealed that the material continues to reduce in average particle size even after DP has levelled off. This is again significant, as it confirms observations at the plant level, whereby product produced from longer reaction times is finer and denser. Furthermore, the reduction in crystallinity between pulp and MCC product observed in **Chapter 3** was again confirmed with more detail in **Chapter 4.** Interestingly, the reduction in crystallinity proceeded in to the LODP range per the continued reduction in particle size observed, suggesting that the reaction of the crystalline regions is indeed occurring.

Characterisation of the hydrolysis reaction at a wider range of temperatures and acid concentrations would further enhance the understanding of the hydrolysis reaction and provide additional confirmation of the results given in the present study.

(iv) **Chapter 5** outlined the hydrolysis experiments of two pulps that showed the largest relative differences identified in **Chapter 2**. DP reduction curves indicated that the pulps reached LODP in comparable times, however the hardwood pulp had a significantly lower starting DP. The rate of reaction for the hardwood pulp was found to be higher than that of the softwood pulp, which was counter-intuitive due to the higher crystallinity of the hardwood pulp earlier identified. Kinetic analysis showed that the activation energy for the more crystalline hardwood pulp was indeed higher when compared to the softwood pulp, however, the frequency factor of the hardwood pulp was significantly higher and therefore likely to be the main driver in the faster reaction rate. Higher frequency factors may be associated with the morphology of the hardwood pulp, which previous analysis had shown the pulp as having far greater surface area than the other pulps – presenting more opportunity for reaction collisions.

The negative entropy values determined suggested that the reaction mechanism pathway for the given hydrolysis conditions proceeded via protonation of the cyclic (rather than the glycosidic oxyen).

The relevance of the research outlined in **Chapter 5** may be directly applied to the DuPont reaction intensity control method. The 'Reaction Unit' equation generated by the corporation technical department has remained unchanged in many years and uses a single activation energy value irrespective of pulp type. Application of the activation energies for the two pulps determined in the present study revealed large differences in the reaction time predicted by the DuPont equation for a given hydrolysis intensity. This is highly significant to MCC producers who may unwittingly be over or under reacting depending on the pulp type. Furthermore, the DuPont equation does not allow for the impact of frequency factor differences in pulps. The present study revealed these differences as being significant in the reaction rate. A modified version of the DuPont equation was proposed. Opportunity for further work is apparent in the introduction of the modified equation to the operation process.

(v) The FT-IR absorbance peak at around 808 cm^{-1} attributed to silica (Si-O-Si stretching) is not seen in the FT-IR spectrum for standard MCC. This peak was therefore chosen for calibration of silica content in SMCC and samples of SMCC 50 and SMCC 90 grades that were previously tested by the sulphated ash method were used accordingly. Following successful calibration, the method was validated by paired testing of more SMCC samples, and statistical equivalency of results between the two methods was achieved.

A rapid test method for the determination of silica content in SMCC grade products is of high practical use for SMCC producers. Given the lengthy test time for the sulphated ash test, and tight silica specification tolerance, the risk production of out of specification material is high. An accurate indicative rapid test, complimentary to the required sulphated ash test as described in **Chapter 6** is therefore of significant value. It is recommended to further validate the method and introduce in parallel to the production process.

“For I ain’t, you must know,” said Betty, “much of a hand at reading writing-hand, though I can read my Bible and most print. And I do love a newspaper. You mightn’t think it, but Sloppy is a beautiful reader of a newspaper. He do the police in different voices.”

The visitors again considered it a point of politeness to look at Sloppy, who, looking at them, suddenly threw back his head, extended his mouth to its utmost width, and laughed loud and long. At this the two innocents, with their brains in that apparent danger, laughed, and Mrs. Higden laughed, and the orphan laughed, and then the visitors laughed. Which was more cheerful than intelligible.